POLYNOMIAL BASIS FUNCTIONS AND THEIR APPLICATION TO HIERARCHICAL IMAGE PROCESSING

Doctoral Thesis

Amir Badshah

Institute for Automation
Department Product Engineering
University of Leoben
Leoben, Austria

April 2012

Supervisors:

O.Univ.-Prof. Dipl.-Ing. Dr.techn. Paul O'Leary B.A., B.A.I., M.E.E.
University of Leoben, Leoben, Austria

Prof. Dr. Peter Lee B.Sc.
University of Kent, Canterbury, United Kingdom

I declare in lieu of oath, that I wrote this thesis and performed the associated research myself, using only literature cited in this volume.

Leoben, April 2012 Amir Badshah

Acknowledgements

First of all I would like to express my sincere gratitude to my supervisor Professor Paul O'Leary for the continuous support during my stay here in Austria. His encouragement, guidance and support enabled me to complete my Ph.D work successfully. It will be more fitting if I say some people make diamond from stone; this saying really fit to me as Paul O'Leary gave me much time to make me able to gain much knowledge in short time. I really appreciate his moral and social support for which he given when and where I requested from him.

I owe my deepest gratitude to Matthew Harkar who always helped me for solving my difficulties related to my course work or research work. He never hesitated to help me at any time at any position. I thank Richard Neumayr for his help and support for asking countless time help related to academic or non academic problems.

The favorable environment at the institute of automation deserves much appreciation. I would like to thank Gerhard Rath and Gerold Probst for many fruitful discussions, and providing technical facilities. No doubt the evergreen lady Doris Widek deserve many many appreciation for the much help than I deserved; I will never forget her loving laugh specially in the morning time when I used to hear her from my office and which declare that she is arrived.

Many thanks to Higher Education Commission of Pakistan, which provided funding for my higher studies here in Austria. I appreciate the support from Suhail Rahman and Anwar Muzaffar to spare me from my office and sanctioned my study leave.

Many thanks to my father who always thought of my high rank education and mother for always remembering me in her prayers. Finally I will thank my wife and children for being with me here in Austria, although they wished to go Pakistan, I appreciate their sacrifices here only to achieve my PhD degree.

Abstract

The application of Gram polynomial basis functions to hierarchical image processing is presented in this research work. In the early 1960s Ming-kuei Hu used continuous geometrical moments for pattern recognition; since then there has been much research work done on moment invariants in the field of image processing. An accurate set of basis function is required to reconstruct the image of larger order with minimum error. The use of Chebychev moments produces numerical instabilities for moments of large order. The polynomial basis functions used in the method proposed here are discrete orthogonal basis, being unary discrete polynomial basis of order n. These basis functions are numerically better conditioned than discrete cosine transform, which leads us to a new method of image compression.

A new multiresolution image analysis technique is presented based on hierarchies of images. The structure of the hierarchy is adapted to the image information and artefacts of each sequential images are reduced by Gram polynomial decimation. A major improvement is achieved by implementing suitable amount of decimation at each level; this decimation is implemented via Gram polynomial bases. Both global and local polynomial approximation are considered and compared with the Fourier basis. The issue of Gibbs error in polynomial decimation is examined. It is shown that the Gram basis is superior when applied to signals with strong gradient, i.e., a gradient which generated a significant Gibbs error with Fourier basis. The modified functions are used to compute spectra whereby the Gibbs error associated with local gradients in the image are reduced. The present work in the field of image registration also presents the first direct linear solution to weighted tensor product polynomial approximation. This method is used to regularize the patch coordinates, the solution is equivalent to a Galerkin type solution to a partial differential equations. The new solution is applied to published standard data sets and to data acquired in a production environment. The speed of the new solution justifies explicit reference: the present solution, implemented in MATLAB, requires approximately 1.3 s to register an image of size 800 x 500 pixels. This is approximately a factor 10 to 100 time faster than previously published results for the same data set. The proposed algorithm is applied to non-rigid elastic registration of hyper spectral imaging data for the automatic quality control of decorative foils.

Kurzfassung

In dieser Forschungsarbeit wird die Anwendung von Gram-Polynom-Basisfunktionen in der hierarchischen Bildverarbeitung vorgestellt. In den frühen 1960er Jahren verwendete Ming-Kuei Hu kontinuierliche geometrische Momente zur Mustererkennung. Seither wurde viel über Momenteninvarianten im Bereich der Bildverarbeitung geforscht. Eine geeignete Menge von Basisfunktionen ist erforderlich, um ein Bild mit höherer Ordnung und geringerem Fehler zu rekonstruieren. Die Verwendung von Tschebyscheff-Polynomen führt zu numerischen Instabilitäten für Momente höherer Ordnung. Die Polynom-Basisfunktionen, die in dieser Arbeit vorgeschlagen werden, bilden eine unitäre diskrete orthogonale Basis der Ordnung n. Diese Basisfunktionen sind numerisch besser konditioniert als die diskrete Kosinustransformation, was zu einer neuen Methode der Bildkompression führt.
Eine neue Multiskalenanalyse zur Bildverarbeitung basierend auf hierarchischen Strukturen von Bildern wird präsentiert. Die Struktur der Hierarchie wird abhängig gemacht vom Bildinhalt, und die Artefakte der Teilbilder werden reduziert durch Dezimation mit Gram-Polynomen. Eine erhebliche Verbesserung wurde erreicht durch Anpassung der Dezimation auf jeder einzelnen Ebene der Hierarchie. Diese Dezimation erfolgt mit der Gram-Polynom-Basis. Sowohl globale als auch lokale Polynomapproximation werden betrachtet und mit den Ergebnissen der Fourier-Basis verglichen. Auch das Problem des Gibbsschen Phänomens bei der Polynomdezimation wird untersucht. Es wird gezeigt, dass die Gram-Basis bei Anwendung auf Signale mit hohem Gradienten einen geringeren Fehler ergibt als mit der Fourier-Basis. Mit diesen modifizierten Algorithmen werden die Spektren berechnet, wobei der mit dem Gradienten verbundene Gibbs-Fehler in den Bildern reduziert wird. Die vorliegende Arbeit präsentiert weiters die erste direkte lineare Lösung einer gewichteten Tensorprodukt-Polynomapproximation. Diese Methode wird verwendet zur Regularisierung von Patch-Koordinaten. Die Lösung ist äquivalent zur Lösung von partiellen Differentialgleichungen nach dem Galerkin-Ansatz. Die neue Lösungsmethode wird sowohl auf bereits publizierte Daten angewendet, als auch auf Daten, die aus einer aktuellen Industrieanwendung stammen. Besonders hervorzuheben ist der geringe Rechenaufwand, der die Berechnung um einen Faktor 10 bis 100 schneller macht als bei bekannten Lösungen. Der vorgeschlagene Lösungsweg wird angewendet auf nicht-rigide Registrierung von hyperspektralen Bilddaten zur automatischen Qualitätskontrolle bei Dekorfolien.

Table of Contents

List of Figures

List of Tables

Chapter 1

Review of the literature and relationship to the other work

1.1 Literature review

In the field of image processing, computer vision, quality control and image decimation it is very important to represent an image or signal efficiently. For finite set of data Fourier functions are commonly used to reconstruct a desired function. The Fourier bases functions are efficient and suitable if the data is smooth i.e. with neither a gradient nor discontinuities. In case of data with much gradient gives discontinuity. This type of data is challenging for the Fourier basis method to reconstruct. As the Fourier basis functions are suitable for periodic data, and the data with gradients remains no more periodic, Hence the Fourier representation suffer from Gibbs error phenomena. A good explanation is given in [69]. Much has been written on how to reduce the Gibbs error which contaminate the original data[7][21][3].

1. In 1957, G.Forsythe used orthogonal polynomials for least square fitting of data [15], which approximates an arbitrary function by least squares fitting using orthogonal polynomials. It uses a generalization of the three-term relation, generating recursively a system of orthonormal polynomials over arbitrary sets of data points. The main disadvantage of the method is that as the degree of the polynomial increases the condition number of the matrix also increases, the use of orthogonal polynomials is theoretically sound, however their numerical implementation is ill conditioned[18]. The algorithm he proposed could only be used for images or data with limited size.

2. M.K. Hu, for the first time used geometric moments [29] for image demonstration, and at the same time he applied these image moments for pattern recognition. It was a foundational work of the use of the basis function in the field of image processing and was an achievement at the time. However by increasing the degree of the Vandermonde basis functions, errors are generated, therefore the method was limited in the degree of the basis functions. Dudani et al. [11] proceeded the research work for moving objects, and introduced object recognition in 3-D form.

3. Continuous orthogonal moments (e.g. Legendre moments and Zernike moments) can be used to represent an image with the minimum amount of information redundancy. But their computation by a direct method is very time consuming. The use of Legendre polynomials to compute 2D moments of grey level images has been presented in [70]. Yap and Paramesran's [71] work shows reduction of image reconstruction error by Legende polynomial moments. Hosny [28] improved the prescribed research work by presenting a new exact and fast method for computing 2D Legendre moments for gray level images. The Legendre moment values calculated by using the approximated method deviate from the theoretical values.

   Pew-Thian [72] prescribed a new set of orthogonal moments based on the discrete classical Krawtchouk polynomials. Krawtchouk moments are a set of moments formed by using discrete Krawtchouk polynomials as the basis function set. These are used to calculate higher-order Krawtchouk polynomials. It is shown in the prescribed research work that the Krawtchouk polynomials are scaled to ensure numerical stability, thus creating a set of weighted Krawtchouk polynomials. The orthogonality of the moments ensures minimal information redundancy. No numerical approximation is involved in deriving the moments, since the weighted Krawtchouk polynomials are discrete. These properties make the Krawtchouk moments well suited as pattern features in the analysis of two-dimensional images. O'Leary and Harker [52] has rejected the concept that Legendre polynomials causes error, which affects the accuracy of the reconstructed image [72]. It is proved that polynomial basis when properly applied, need only to be complete for correct reconstruction, i.e., it does not need to be orthogonal. Mukundan [49] used discrete Chebichev polynomials as pattern features in the analysis of two-dimensional images. And it is claimed that Chebichev moments are superior to the conventional orthogonal moments such as Legendre moments and Zernike moments.

4. Describing all the above different basis functions used for different purposes in the field of image reconstruction it is concluded by O'Leary and Harker [52] and proved that there is one and only one basis functions for image reconstruction. And explained that the exact Legendre, the Chebichev and the normalized Krawtchouk polynomials are equivalent; and it is presented that they have simply different norms on the individual polynomials, and the polynomials themselves are identical.

5. Digital image compression has great importance in many applications in the field of image processing in the form of signals or images. An image compression technique removes redundant and/or irrelevant information, and efficiently encodes what remains. In the field of machine vision to expedite the data processing the quantity of the data is kept as small as possible but with minimum artefacts. Articles [63][8] give an overview of JPEGs proposed image-compression standard. Hunt and Mukundan [30] have analyzed the reconstruction accuracy when using different orthogonal basis functions as the kernel for a reversible image transform. A comparison has been shown between few transform functions for energy compactness. Mukandan [47] introduced the Chebichev transform as possible alternative to DCT (Discrete Cosine Transform) for applications in image compression. O'Leary and Harker [51]

has introduced a new algebraic framework for discrete basis functions's analysis,it has been shown how to synthesize unitary basis and the concept of anisotropic moments is introduced and applied to 2D seismic data, which is an image processing problem. The new polynomial basis is numerically better conditioned than the discrete cosine transform. This opens the door to new image compression algorithms. A new concept on the orthogonalization of basis is applied to Mukandan's work to properly synthesize perfect basis [46].

6. There are many fields of application of the above mentioned work, in this research work application of these basis functions in the field of image registration has been described generally and non-rigid registration in particular. Goshtasby [19] [20] presented a paper on non-rigid registration, which assumes that a set of corresponding points in two images are known. The task is: given a set of irregularly placed control points, to find the mapping functions $X \approx f(x, y)$ and $Y \approx g(x, y)$ which relate the coordinates in one image to those in a second image. Today this would not be considered registration, it is actually the final step after the required correspondences have been found. Later the concept of hierarchical subdivision was introduced in [40] whereby, mutual information was used to perform the local registration of the small patches. They observed inconsistency in the mutual information during the subdivision process. However, no systematic explanation for the decimation process was given. Xie et al. [73] define the task as given two sets of points. These points are regarded as clouds of points. They implement a subdivided grid using splines, however, assuming that the correspondences between the clouds of points are known.

   Mellor [45] proposed local phase as a measure for registration; it was implemented using Fourier transform methods. There is an implicit assumption here: that the patches are well modeled by periodic basis functions. It is shown in this research work that in general there is a very significant Gibbs error if Fourier bases are used to implement decimation. Further methods based on feature extraction have been presented e.g [26] it is important to note that feature extraction is strongly dependent on the pattern being analyzed.

7. The problem with hierarchical subdivision is that aliasing occurs when an image is decimated to a lower resolution unless appropriate filtering measures are applied. That means, there must also be a consistent hierarchical filtering performed at each layer in the tree structure. Multiresolution [37] pyramids are an attempt to solve this problem. Scale-space filtering [41], i.e., using a Gaussian kernel, has become the most common filtering method in multiresolution pyramids [39]. Indeed, the Gaussian filters deal well with the decimation of additive Gaussian noise; however, it does not address the issue of aliasing adequately.

Chapter 2

Introduction

Hierarchical procedures for image decomposition have been independently proposed by many researchers in computer graphics, scene analysis, architectural design and pattern recognition. The proposed research work is related to the image processing at multiscale resolution, this could be explained as if we see the whole solar system, we can observe few circular objects and can observe only the movements relative to each other by these objects; but what happening inside these objects (planets) will be out of approach; now let's go near to the planet world and see from upper space; then we can see two major parts of the world, i.e. the water and the land; now again if any of these two changes their boundaries we can observe that, but nothing we can see inside; similarly coming further near to the earth then we can see more i.e. plants, rivers, buildings etc. and going further we can travel up to micro and nano scale. In image processing, choosing the correct scale of image for analyzing an image scene is critical for recovering a complete physical interpretation of the objects.

With the help of multiscale image representation it is very easy to analyze any image at multiple scales. An image is decomposed into a set of descriptors, each making explicit image features at a specific scale. The issue of how to best construct such hierarchy of images in coarser to finer is needed to be focused. Representation of this type have been referred to as " pyramids","multiresolution" and "scale-space images".

In this work an alternative interpretation is presented for consistent information decimation during construction of the hierarchial subdivision. The classical design of filters implicitly involve the selection of basis functions; the most common of which are the Fourier basis and polynomials [24] Actually the selection of the best set of basis functions depends on the nature of the data being processed. It is presented that careful attention must be payed to correct decimation procedures.

2.1 Hypothesis

Images with non rigid distortion are better registered by introducing Gram polynomial basis functions for image decimation via multiresolution registration.

2.2 Motivation

The initial motivation for this work was to develop an improved method of image registration for non rigid distortion. Much of it has now been completed and applied on real data images, and is used in the paper industry to find the registration of data and reference images. The second motivation was to facilitate the development of methods for studying image decimation. A new method of image decimation has been generated, i.e., image decimation by Gram polynomial basis.

2.3 Image moments

One of the major tasks of image processing is pattern recognition, in which we get image features and then process those features for pattern recognition. Some moments have the properties invariant and by means of these moment invariants we compare the object to be detected. Various forms of moment descriptors have been extensively employed as pattern features in scene recognition, registration, object matching as well as data compression. There are many fields from applied mechanics to statistics and shape descriptors to image scene analysis. For many years, the concept of mathematical moments have been used. All these different applications start from Hu [29] to the latest present research work trying to improve the applications and get maximum output from these different image moments.

2.4 Discrete Cosine transform and image compression

The more advances in the field of multimedia, the more challenging problems are to be given attention, one of those is to store maximum data in less space. For example, making a web page maximum information is needed in form of images, but by increasing the number of images the cost increase, so it is needed to keep minimal data but with almost the same information. Similarly the present advancement in mobile engineering, a very low data traffic is possible for sending, to send maximum information we are need to compress the data in such a way which at lesser cost but maximum information is transformed. There are many methods to compress data. Lossy and lossless are the two possibilities. The JPEG is a widely used form of lossy image compression which uses Discrete Cosine Transform. The DCT works by separating images into parts of different frequencies. These frequencies are coded and less important and repeatable frequencies are removed, hence the term of lossy is used. Then the only the most important frequencies that remain are used to retrieve the image in the compression space. As a result we get an image with some artifacts, which are supposed to be as minimum as possible. When needed the data is decompressed by the inverse cosine transform.

2.5 Compression artifacts

Storage and retrieval are two stages involved in providing information on a function. To place all the information about a function is to store its expansion coefficients; however, in the case of a discontinuous function one should use more sensitive methods to retrieve this information rather than naively sum up the expansion. Consider the Fourier-Galerkin projection of a piecewise [21] smooth function $f(x)$, $0 \leq x \leq 2\pi$.

$$f_N(x) = \sum_{k=-N}^{N} \hat{f}_k \mathrm{e}^{ikx} \tag{2.1}$$

where the coefficients $\hat{f}_k$ are given by

$$\hat{f}_k = \frac{1}{2\pi} \int_0^{2\pi} f(x) \mathrm{e}^{-ikx} \mathrm{d}x \tag{2.2}$$

The reason for the slow (and nonuniform) convergence of $f_N(x)$ to $f(x)$ can be traced to two facts:

- the slow decay of the Fourier coefficients $\hat{f}_k$
- the global nature of the Fourier series, where the Fourier coefficients are determined by integration over the whole interval, even across discontinuities.

2.6 Scale space filtering

A detailed discussion has been given in [65] about scale space filtering. The extrema in a signal which is calculated by its first derivatives provide a useful general-purpose qualitative description. The signal is first expanded by convolution with Gaussian masks over a continuum of sizes. The actual problem is not so much to eliminate finer-scale noise, to separate events at different scales arising from distinct physical processes and to introduce a parameter of scale by smoothing the signal with a mask of variable size. Scale space filtering begins by continuously varying the scale parameters, in this representation it is possible to track extrema as they move continuously with scale changes and to identify the singular points at which new extrema appear. The scale space image is then collapsed to a tree providing a concise but complete qualitative description of the signal over all scales of observation.

2.7 Gram polynomial basis functions

The eigen values of a matrix could be the roots of a polynomial equation. These polynomial roots are of great importance in the field of numerical analysis. All numerical

analysis depends on the understanding of the polynomials. If the polynomials give us the solution to some problem, the method of analysis could hence be easily found. In 1990 two groups [31] [44], apparently independently, proposed the use of Gram polynomials [4] in place of the Vandermonde basis for Savitzky-Golay smoothing. Meer and Weiss [44] state that the Chebyshev and Gram polynomials are synonymous for the same set of basis functions; this is only partially correct. The modified discrete Chebyshev polynomials [6] [33] do not have a uniform scaling, where as the Gram polynomials do.

2.7.1 Mathematical background

The recurrence relationship [50] for the Gram polynomials is,

$$g_n(x) = 2\ \alpha_{n-1}\ x\ g_{n-1}(x) - \frac{\alpha_{n-1}}{\alpha_{n-2}}\ g_{n-2}(x) \tag{2.3}$$

whereby,

$$\alpha_{n-1} = \frac{m}{n}\ \left(\frac{n^2 - \frac{1}{2}}{m^2 - n^2}\right)^{\frac{1}{2}} \tag{2.4}$$

and

$$g_0(x) = 1,\quad g_{-1}(x) = 0\ \ and\ \ \alpha_{-1} = 1, \tag{2.5}$$

x is computed on equidistance points,

$$x = -1 + \frac{2k-1}{m},\quad 1 \leq k \leq m, \tag{2.6}$$

These points do not span the full range [-1,1].

2.7.2 Fourier basis function

In machine vision image reconstruction typically proceeds by estimating a function from Fourier-transform values. An infinite number of solutions are obtained for finite number of basis function to reconstruct a function. To single out one particular solution, one can require that some functional of the image, such as its entropy, be optimized, or that the solution be closest to some other appropriate prior estimate according to a given distance criterion.

$$F(\omega_n) = \int_{-\infty}^{\infty} f(x)\ \exp\left(-jx\omega_n\right)\mathrm{d}x \tag{2.7}$$

for $n = 1, 2, ..., N$. In many applications, $f(x)$ can be support limited to some region S, and it is typically the case that this function $f(x)$ can be well modelled as the restriction to S of a function, say

$$g(x) = \sum_{N=1}^{N} a_n h_n(x) \tag{2.8}$$

where the $h_n(x)$, for $n = 1, 2, ..., N$, are the basis functions.

$$\hat{f}(x) = \sum_{N=1}^{N} a_n \frac{\sin\left[\sigma(x - x_n)\right]}{\sigma(x - x_n)}, \tag{2.9}$$

$$F(\omega_m) = \sum_{n=1}^{N} a_n A_{mn} \tag{2.10}$$

with

$$A_{mn} = \int_{-x}^{x} \frac{\sin\left[\sigma(x - x_n)\right]}{\sigma(x - x_n)} \exp\left(-jx\omega_m\right) \mathrm{d}x \tag{2.11}$$

The reconstruction procedure is to solve 2.10 for the coefficients a_n for $N = 1, 2, 3, ...N$, and the substitute these coefficients into Eq.2.9.

2.7.3 Generating basis functions

It is explained in detail in [52] that any polynomial basis $P(x)$ which are sum of monomials can be defined by post multiplying the Vandermonde matrix P_V by an upper triangular matrix A, i.e.,

$$P_A \cong P_V A \tag{2.12}$$

whereby the Vandermonde matrix of degree d_x for n_x points in x is defined as,

$$P_V \cong \begin{pmatrix} 1 & x_1^1 & . & . & x_1^{\mathrm{d}x} \\ . & . & . & . & . \\ . & . & . & . & . \\ 1 & x_{nx}^1 & . & . & x_{n_x}^{\mathrm{d}x} \end{pmatrix} \tag{2.13}$$

Hence post multiplying this matrix, which is the result of the coefficients of the polynomial equations with the image data, we get the spectrum of the image. Decreasing the number of rows from the the above basis matrix, and then multiplying we get the resulting image in compressed form.

2.8 Savitzky Golay smoothing

Gram based local polynomial approximation: Both the Fourier and Gram bases are global approaches, i.e., the signal is approximated globally by the respective basis functions over

the full length of the support. They have the advantage of globally averaging the Gaussian noise, which is spread evenly onto the coefficients of all the basis functions. Consequently, they are well suited for application to images which have a high degree of noise. However, the global basis functions requires the signal to be modelled globally; consequently, the Gibbs error from, say, a step function is spread over the complete support. An alternative approach is to use local polynomial approximation (Savitzky-Golay smoothing [56]) to perform decimation. This yields a lower Gibbs error at the cost of reduced noise suppression.

2.9 Quad tree structure

A quad tree hierarchical subdivision is applied to both the reference and data image; this method has been applied in the past by many others [44][1]. A local decimation is performed at each level while ascending the hierarchy, whereby the patch position in the second image is incrementally adjusted by the shift determined from registration at the previous levels. The fundamental problem is that during decimation of the image to lower resolution there are two major sources of error: a Gibbs error which results from the basis function not being able to describe features in the data; the second source of error is aliasing. Commonly aliasing is only considered for periodic basis functions, but the same problem is also present for polynomial basis functions. The issue is further complicated by the presence of Gaussian noise in the image data.

2.10 Image analysis by hierarchies

Hierarchical procedures for picture decomposition have been independently proposed by many researchers in computer graphics, scene analysis, architectural design and pattern recognition. And a very good research outcome has been written in [61]. It discusses methods for solving problems associated with hierarchical image processing systems. The pyramid data structure is one of the simplest hierarchical image data structures. The goal of this application is to segment an image at different resolutions according to its content. The top-down process lies on the fact a pyramid can be seen as a tree from the roots (top to the pyramid) to the leaves. Keeping the level of the pyramids, each region could be split of any level into sub-regions. While the quad-tree is a tree structure with the root corresponding to the whole image. Unless the subimage is homogeneous it is recursively subdivided into four quadrants. The tree growth continues until either a sufficiently fine resolution is reached or all the children nodes correspond to uniform subquadrants.

2.11 Rigid and non-rigid registration

A review of recent as well as classic image registration methods has been described in [75]. Image registration is the process of overlaying images (two or more) of the same scene

taken at different times, from different viewpoints, and/or by different sensors. Registration geometrically aligns two images (the reference and sensed images). The reviewed approaches are classified according to their nature (area based and feature-based) and according to four basic steps of image registration procedure: feature detection, feature matching, mapping function design, and image transformation and sampling. Mainly the registration could be divided in two types. One is area based and the other is feature based. Further, the rigid and non-rigid or elastic registration are subjects of importance.

2.12 Tensor application in image registration

An overview has been written in [36]. A tensor is a multidimensional array. More formally, an N way or Nth-order tensor is an element of the tensor product of N vector spaces, each of which has its own coordinate system. A first-order tensor is a vector, a second-order tensor is a matrix, and tensors of order three or higher are called higher-order tensors. In the last ten years, interest in tensor decompositions has expanded to other fields. Examples include signal processing, numerical linear algebra, data mining, and more.

2.12.1 Tensor approximation

Tensor approximation introduce a lossless hierarchical transformation of multi-dimensional matrices, or tensors. This transformation decomposes the original data into multiple levels and removes the redundancy at each level by exploiting the similarity among different spatial regions. To exploit spatial inhomogeneity of the original data, further lossy approximation (quantization and pruning) is performed on the resulting multilevel data. These two steps together give rise to a very compact representation. An overview to the related work could be found in [68]. In which they show the development of a compact data approximation technique based on a hierarchical tensor-based transformation.

2.12.2 Galerkin's method

Various meshfree particle [42] methods have emerged in the last a few years, and the most basic common feature is that a predefined mesh is not necessary, at least not for field function interpolation. It is focused on the element-free Galerkin method (EFGM) and it is claimed that it is relatively well developed, robust, and has straightforward and obvious links to the finite element methods. In many applications, EFGM has shown superior rate of convergence and high efficiency in modelling moving interfaces.

2.13 Proposed work

The proposed work presents an alternative interpretation for consistent information decimation during construction of the hierarchial subdivision. The classical design of filters

implicitly involve the selection of basis functions; the most common of which are the Fourier basis and polynomials [24]. Actually the selection of the best set of basis functions depends on the nature of the data being processed. It is shown that careful attention must be payed to correct decimation procedures. The use of thin-plate splines has become almost standard [39]. Spline fitting is however numerically time consuming. In this work the use of a global Gram-polynomial tensor product has been introduced for regularization. A new decimation technique is introduced based on Savitzky-Golay smoothing. This technique ensures consistent data and information reduction at each layer in the tree. This is a very important step and has been underestimated in the past. Correct decimation of the image ensures the minimization of the Gibbs error associated with the step, which in turn improves the result of local registration. Furthermore, correct decimation is instrumental in making the registration solution numerically efficient. The research work also presents the first direct linear solution to weighted tensor product polynomial approximation. This method is used to regularize the patch coordinates, the solution is equivalent to a Galerkin type solution to a partial differential equation.

Chapter 3

Moment based approaches in image processing

Real world image analysis for the image recognition is always challenging if these images are acquired in non ideal conditions like in remote sensing, medical images and quality control. Lens aberration, blurring, or improper lens setting can introduce such problems in image acquisition. There are many techniques used for the pattern recognition. In most of them the images are analyzed and the region of interest are segmented. And these are classified for object recognition. There is much research work in moments invariants for object recognition, the approach of invariant features has proved to be the most prominent and efficient. Its basic idea is to describe the objects by a set of features which are not sensitive to particular deformations and which provide enough discrimination power to distinguish among objects from different classes.

In 1957, G.Forsythe [15] used orthogonal polynomials for least square fitting of data. Which approximates an arbitrary function by least squares fitting using orthogonal polynomials. Hu [29] use geometric moments for the pattern recognition. He derived a set of seven moment invariants. And the property of these invariants was that these were unaltered by changing the position either by translation, rotation or scaling. The work was further extended by other researchers for air craft identification [11], ship identification [57] pattern and scene matching [9][67] etc.

These moments invariants briefly described as follow.

3.1 General moments

General definition of moment functions M_{pq} of orders $(p+q)$, of an image intensity $f(x, y)$ can be written as follows:

$$M_{pq} = \int_x \int_y w_{pq}(x, y) f(x, y) \mathrm{d}x \mathrm{d}y \tag{3.1}$$

Table 3.1: Moments Properties

	Noise Sensitivity	Computational Complexity	Reconstruction
Moments of Monomials			
Geometric Moments	High	Low	N/A
Central Moments	High	Low	N/A
Complex Moments	High	Low	N/A
Continuous Moments			
Legendre	Low	High	Medium
Zernike	Low	Very High	High
Pseudo Zernike	Low	Very High	High
Fourier-Mellin moments	Low	Very High	High
Discrete Orthogonal			
Tchebichef	Low	Medium	Very High
Hahn	Low	Medium	Very High

while $w_{pq}(x, y)$ is a weighting function. This generalized form of moment is used to produce image descriptors which are invariant to translation, rotation, scaling and other image deformations. The equation (3.1) could be rewritten in discrete form as follows:

$$M_{pq} = \sum_{x} \sum_{y} w_{pq} f(x, y) \tag{3.2}$$

The image moments could further be divided as in the following.

3.2 Geometric moments

Geometric moments are non-orthogonal moments, used for different purposes in image processing. The two dimensional geometric moment of order $(p + q)$ of a function $f(x, y)$ is defined as follows:

$$M_{pq} = \int_{-\infty}^{+\infty} \int_{-\infty}^{+\infty} x^p y^q f(x, y) \mathrm{d}x \mathrm{d}y \tag{3.3}$$

For discrete data the Geometric moment Equation(3.3) is written as follows:

$$M_{pq} = \sum_{-\infty}^{+\infty} \sum_{-\infty}^{+\infty} x^p y^q f(x, y) \tag{3.4}$$

These moments were used by Hu [29] for pattern recognition. He also proved that the moment sequence is unique. These moment functions were scaled and used by Eden [12] to present images: with the help of these moments functions he obtained the method of approximation and resynthesizing the images. The approaches were theoretically sound, but due to the Vandermonde matrix the methods are very limited. Because it is known that the Vandemonde matrix is ill-conditioned [18] with evenly spaced real nodes.

3.3 Legendre moments

Legendre polynomials are used as basis functions for the Legendre moments. The $(p\ , q)$ order Legendre moment is written as follows,

$$L_{pq} = \frac{(2p+1)(2q+1)}{4} \int_{-1}^{1} \int_{-1}^{1} P_p(x) P_q(y) f(x,y) \mathrm{d}x \mathrm{d}y \tag{3.5}$$

The p^{th} order of Legendre polynomial is as

$$P_p(x) = \frac{1}{2^p p!} \frac{d^p}{d_x^p} (x^2 - 1)^p \tag{3.6}$$

The Legendre polynomial basis is usually computed over the range $x \in [-1, 1]$. The continous Legendre polynomials are orthogonal over the range $[-1, 1]$.

$$\int_{-1}^{1} P_p(x) P_q(x) d_x = \begin{cases} 0 & \text{for } p \neq q \\ \frac{2}{2p+1} & \text{for } p = q \end{cases} \tag{3.7}$$

The recursion relation for Legendre polynomial is written as,

$$n p_n(x) - (2n-1) p_1(x) \circ P_{n-1}(x) + (n-1) p_{n-2}(x) = 0 \tag{3.8}$$

for $n \geq 2$, with $p_0 = 1$ and $p_1 = x$. The norm of the n^{th} Legendre basis function with n_x discrete points can be approximated by,

$$\|p_n\|_2^2 = \sqrt{\frac{2n_x}{2n}} \tag{3.9}$$

3.4 Zernike moments

Geometric moments are computationally inexpensive as we can see in Table (3.1), but due to large dynamic range it creates numerical instabilities; and large sensitivity to noise. Teague [60] applied complex radial polynomials for investigating its results. Zernike moments are rotationally invariant and more robust to noise.

$$Z_{pq} = \frac{p+1}{\pi} \sum_x \sum_y f(x,y) W_{pq}(r, \theta) \tag{3.10}$$

while

$$W_{pq}(r, \theta) = R_{pq} e^{iq\theta} \tag{3.11}$$

and

$$R_{p,\pm q} = \sum_{k=q, p-|-k|=even}^{p} B_{pqk} r^k \tag{3.12}$$

also

$$B_{pqk} = \frac{(-1)^{(p-k)/2} ((p+k)/2)!}{((p-k)/2)! ((q+k)/2)! ((k-q)/2)!} \tag{3.13}$$

We can see that here radius is used while the cartesian coordinates are ignored, thats why zernike moments are invariants to rotation.

3.5 Orthogonal basis proposed by Forsythe

These basis function could be obtained by three term recurrence relationship in the range $x \in [0, N-1]$ as follows:

$$P_n(x) = 2(x - \alpha_n) \circ p_{n-1}(x) - \beta_n p_{n-2}(x) \tag{3.14}$$

With

$$\alpha_n = \frac{\|x \circ p_{n-1}\|_2^2}{\|p_{n-1}\|_2^2} \tag{3.15}$$

$$\beta_n = \frac{\|p_{n-1}\|_2^2}{\|p_{n-2}\|_2^2} \tag{3.16}$$

given $p_{-1} = 0$ and $p_0 = 1$. These polynomial basis are orthogonal but not unitary. More detail could be seen in [52].

3.6 Chebyshev moments

These moment are the outcome of chebyshev polynomials in the range $x \in [0, N-1]$ can be generated from the recurrence relationship as follow.

$$nt_n(x) - (2n-1)t_1(x) \circ t_{n-1}(x) + (n-1)\left\{1 - \frac{(n-1)^2}{N^2}\right\} t_{n-2}(x) = 0 \tag{3.17}$$

While the initial conditions $t_0 = 1$, and $t_1 = (2x + 1 - N)/N$, which form discrete and orthogonal basis. The Chebyshev moments of order $(p+q)$ of an image $f(x, y)$ are defined as follow.

$$T_{nm} = \frac{1}{\rho(m, N)\rho(n, N)} \sum_{x=0}^{N-1} \sum_{y=0}^{N-1} t_m(x) t_n(y) f(x, y) \tag{3.18}$$

while

$$\rho(n, N) = \frac{N(1 - \frac{1}{N^2})(1 - \frac{2^2}{N^2})..(1 - \frac{n^2}{N^2})}{2n + 1} \tag{3.19}$$

Chebyshev moments are not orthonormal. The norm of the i^{th} polynomial basis with n_x discrete points as complemented in [48].

$$\|t_i\|_2^2 = \sqrt{\frac{2n_x}{2(i+1)+1}} \tag{3.20}$$

3.7 Bernstein polynomial basis

The Bernstein polynomials are shown in following equation, which are poorly conditioned polynomial basis. These basis are used for generating Bezier, Spline and NURBS patches.

$$B_{i,n}(x) = \frac{n!}{i!(n-i)!} x^i (1-x)^{n-i} \tag{3.21}$$

for the value of x in the range $x \in [0, 1]$. The Bezier patch is given by the tensor product.

$$S(x, y) = \sum_{i=0}^{n} \sum_{j=0}^{m} B_{i,n}(x) B_{j,m}(y) P_{i,j} \tag{3.22}$$

3.8 A new unitary polynomial basis

O'Leary and Harker [52] proposed a new unitary polynomial basis. It is proved that there is one and only one unitary polynomial basis which can be generated from the sum of monomials. It is stated and proved that unique unitary polynomial basis can be synthesized for N discrete points in the range $[-1, 1]$ directly from the recurrence relationship,

$$p_n = \alpha p_t + \beta p_{n-2} \tag{3.23}$$

while the values in equation (3.23) are given, like $(p_t \cong p_1 \circ p_{n-1})$,$(\alpha = \pm \frac{1}{\sqrt{p_t^T p_t - (p_t^T p_{n-2})^2}})$ and $(\beta = p_t^T p_{n-2} \alpha)$ The initial values are given

$$p_0 = \frac{1}{\sqrt{N}} \tag{3.24}$$

$$p_1 = \sqrt{\frac{3(N-1)}{N(N+1)}} x \tag{3.25}$$

Describing all the above different basis functions used for different purposes in the field of image reconstruction it is concluded by O'Leary and Harker [52] and proved that there is one and only one basis function for image reconstruction. And explained that the exact Legendre, the Tchebichef and the normalized Krawtchouk polynomials are equivalent; and it is shown that they have simply different norms on the individual polynomials, and the polynomials themselves are identical.

3.9 Recursive procedures for sequential calculation of basis coefficients

Linear algebra has solved and made easy many problems in field of image processing. It is known that any polynomial basis $p(x)$ which are sums of monomials can be defined by

post-multiplying the Vandermonde P_v by a matrix A,

$$P_A = P_v A \tag{3.26}$$

While the Vandermonde matrix of degree d_x for n_x points in x is defined as,

$$P_v \cong \begin{pmatrix} 1 & x_1^1 & . & . & x_1^{dx} \\ . & . & . & . & . \\ . & . & . & . & . \\ 1 & x_{nx}^1 & . & . & x_{nx}^{dx} \end{pmatrix} \tag{3.27}$$

3.10 Image representation by moments

A very brief overview of image moments is given in Table (3.1)as described in [38]. Geometric moments have the big advantage of computational cost. The computational cost is much less. These moments are invariant to translation and could be used for pattern recognition; the disadvantage of Geometric moments could be described as they are much sensitive to noise and that image reconstruction is not possible. To overcome the noise sensitivity problem Complex moments are better; these moments also improve the invariance property. But the same problem with these moments is the image reconstruction is not possible. Continuous orthogonal moments, i.e., Legendre, Zernike moments give us much better results in presence of noise. But the computational cost increases on the other hand. Zernike moments are also invariant to rotation. The image reconstruction problem is solved by these moments. They do not remove all the problems, but only some extent. Discrete continuous moments, i.e., Tchebychev moments are better than the above mentioned moments. The results in presence of noise is much better, also the computational cost is not much higher than Zernike moments, the image reconstruction accuracy is very much satisfactory. The only problem with these moments are the invariance properties i.e., these moment are not invariant in nature to any movements.

3.11 Discrete polynomial moments

Legendre polynomial got more interest by researchers due to less noise sensitivity and its image reconstruction property. The computational cost is not as high as for Zernike moments. The major problem pointed out was its non-orthogonal nature in discrete domain. Which is great cause of error propagation when implemented for higher degree. Mukandan [46] for the first time used Chebychev moments for image reconstruction. These polynomials gave efficient results in image reconstruction. Also maintaining the quality and it is lower sensitivity to noise. The only problem with these moments are their invarianct properties. These moments are not invariant to any movements i.e. translation, rotation etc. Also the limitation of the degree of polynomials bounds its application to lower order polynomial. These moments are not orthonormal. For higher degree of polynomials degeneration occurs and errors generate. O'Leary and Harker [51] proposed application of

polynomials for some arbitrary number of degree and their proposed method is efficient to apply for any higher degree polynomial. It is proven that there is one and only one unitary polynomial basis which is complete, that means the polynomial basis for Chebyshev system. By QR decomposition method it is proved that any nonorthogonal matrix could be converted to othonormal matrix, and with the help of this decomposition systematic propagation error is eliminated, which is required for efficient image reconstruction.

3.12 Polynomial approximation and interpolation

The saying "Something for nothing" is much akin to the term interpolation. The behavior of a function of some known data points is first observed, for some missing data we make an assumption and follow the same behavior as given by known functions. The same we do in interpolation process. Polynomials are used for this interpolation. O'Leary and Harker [51] have done work on interpolation for missing Seismic data. Some of the data go missing by geo-phones. 2D anisotropic moments are combined with the interpolation algorithm; an incomplete bases are used to perform the filtering. It is proved that the lower the degree of polynomial used the stronger the filtering i.e. the data is approximated by a polynomial of lower degree.

3.13 Polynomial image decimation

Image decimation may be regarded as transformation from one image to another image. The methods mostly used for image decimation are interpolation, smoothing, compression, enhancement and feature detection. In these image processing applications data images are represented by set of discrete values with uniformly spaced nodes. The coefficients of these polynomials represent a linear transform of the image pixels. For computation these transform matrices are computed by three term relationship. As we get the desired matrix from the polynomial these two dimensional coefficient give us an exact representation, or we can say, an approximation to this rectangular array. The computational cost is decreased by decimating these arrays of polynomials coefficient in the form of interpolation and least square approximation. The proposed research work presents transform properties of Gram polynomials and shows that they can be used for image decimation. The energy compactness of the transform is difficult to calculate directly, we can only approximate it by analyzing the reconstruction error of the transform when the image is reconstructed with fewer basis functions than the total number. Image decimation is done both on a global and local basis. These results are compared with Fourier basis.

General formulation of a discrete equivalent an integeral transorm is

$$s = B_a^+ y \tag{3.28}$$

The spectrum s of the data y is determined by computing the discrete equivalant of an integral transform. The formulation with the Moore-Penrose pseudo inverse B_a^+ has been

chosen as it is the least squares solution for non-orthogonal bases. The synthesis of a signal i.e.,the inverse transform is computed as,

$$\hat{y} = B_s s \tag{3.29}$$

While B_s contains the synthesized functions.

3.13.1 Gram polynomials are polynomial preserving

By comparison of Geometric polynomial; which were used by Hu [29] for pattern recognition, and Gram polynomials basis we can conclude that Gram basis are more flexible for large data size with higher degree of polynomials. Hu used a geometric moment polynomial basis set called the Vandermonde basis. This Vandermonde matrix is poorly conditioned and quickly becomes degenerate as the degree of the polynomial increases. To this degenerate matrix there is no unique inverse so these basis are not perfect for the signal synthesis. Also it is worth to describe that these basis are not orthogonal in the discrete space, and we can say that these polynomials are not polynomial preserving. A detailed discussion has been given in [50], in which a new theoretical framework has been presented for polynomial approximations. A perfect Gram polynomial basis set is synthesized which ensures that the approximations are strictly polynomial preserving. And without any significant error a polynomial of degree $d = 1000$ can be generated.

3.13.2 Artefact free compression of images

Different decimation techniques have been proposed for the image reconstruction accuracy. Discrete Cosine and Fourier transform are the most well known transform in image processing, which are used in many different image processing fields like compression and decimation. The best set of basis functions for image decimation depends on the nature of the image being considered. The Fourier basis is suitable when there are periodic structures in the image. Correspondingly, the Gram basis is suitable when the image is predominantly geometric in nature. To illustrate this consider Figure 3.1, the data corresponds to a surface generated by $z = x + y + x^2 - y^2 + yx$ for the range $x, y \in [-1; 1]$, this is clearly geometric in nature. The residuals resulting from decimation by a factor of 11 with the Gram, Fourier, Cosine, Haar and Savitzky Golay smoothing basis are shown in Figures (3.2,3.3,3.4,3.5,3.6 and 3.7) respectively. Clearly, for this example the Gram basis is superior; not just marginally better but orders of magnitude better.

3.13.3 Decimation is not for visual impression but to avoid aliasing errors

A notable loss in image quality is observed when the image is resamapled i.e decimated. To preserve image quality, the interpolating function used for the resampling should be an ideal low-pass filter. In image processing mostly the aliasing occurs due to the repetitive

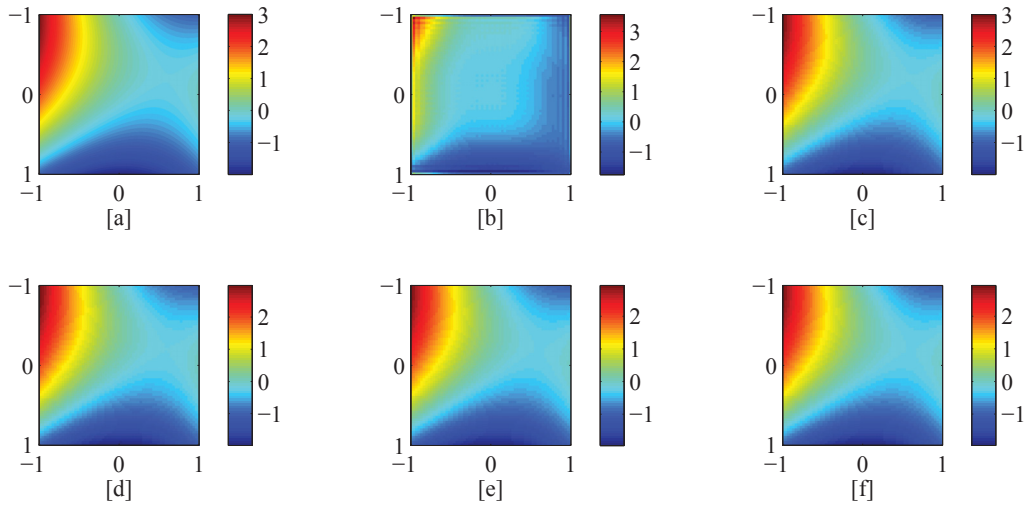

Figure 3.1: Geometric data generated by the function $z = x+y+x^2-y^2+y\,x$ for the range $x, y \in [-1, 1]$. This data set is generated with 550 nodes in both the x and y directions.(a) original surface(b) generated by Fourier basis(c) Gram basis(d) Cosine basis(e) Savitzky Golay Gram smoothing and(f) Sivitzky Golay Cosine smoothing

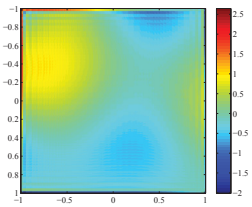

Figure 3.2: Difference between the original surface at the decimation points and the surface decimated using the Fourier basis, the decimation-rate $r_d = 8$.

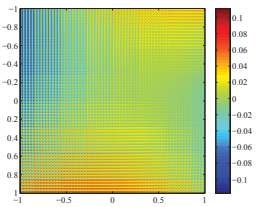

Figure 3.3: Difference between the original surface at the decimation points and the surface decimated using the Gram basis, the decimation-rate $r_d = 8$.

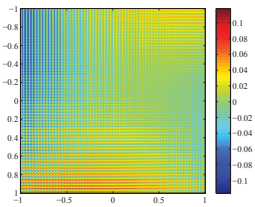

Figure 3.4: Difference between the original surface at the decimation points and the surface decimated using the Cosine basis, the decimation-rate $r_d = 8$.

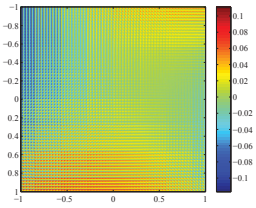

Figure 3.5: Difference between the original surface at the decimation points and the surface decimated using the Haar basis, the decimation-rate $r_d = 8$.

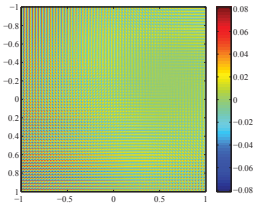

Figure 3.6: Difference between the original surface at the decimation points and the surface decimated using the Gram Savitzky Golay smoothing.

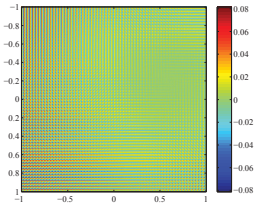

Figure 3.7: Difference between the original surface at the decimation points and the surface decimated using the Cosine Savitzky Golay smoothing, the decimation-rate $r_d = 8$.

structure of the image. An image with repetitive pattern of high spatial frequency when sampled at low resolution, we can observe Moire patterns [32] results on the image. And this happens because the original size is shrunk to a new size. Transformation of discrete image which is defined at certain coordinate location is called sampling. In the sampling process we actually interpolate the discrete image on to a continuous image and then the interpolated image is sampled. A good explantation can be found in [54]. Different interpolating methods have been described and compared. The high frequency artifacts due to gradients at the boundaries could only be decreased by resampling. The interpolating function must be an ideal low pass filter, to remove the replicates of the frequency spectrum caused by the sampling. The sampling of the interpolating function aliases the higher frequencies of the interpolating function into the lower frequencies. To avoid this aliasing generated by this sampling mechanism a perfect basis function is required for particular interpolation. Gram polynomials, we can say, do not introducing any further aliasing in the image, and the final results we get of better quality as compared to other methods like Cosine basis or Fourier basis.

3.13.4 Polynomial antialiasing

A continuous signal is resmapled and it is converted into discrete form, for this discrete signal a discrete function is considered to be an exact representation of a band-limited continuous function. We keep in mind that the original signal can be regenerated exactly from it. An ideal low pass filter is used then for interpolating this discrete signal which give us a new discrete function which is a new representation of the original signal. Similarly the resampled function is resampled back to the original co-ordinate points; then the original discrete function will be exactly reproduced assuming that the different sampling rates are all above the Nyquist sampling rate. This states that the interpolating function which is used for resampling is an ideal low pass filter.

3.13.5 The relationship to the Tchebychev polynomial (functions)

Lengendre and Zernike moments have been explained in detail by Mukundan [48]. And the superiority of the Tchebychev moments to these two, i.e., Legendre and Zernike has been proved. The Tchebychev polynomial [48] in the range $x \in [0, N-1]$ can be generated from the recurrence relationship as in equation 3.17. It is clear that they form a discrete and orthogonal basis but they are not orthonormal. The condition number of the complete Tchebychev polynomial basis shows that these polynomial degenerate more rapidly than Legendre basis. The proposed polynomial basis system is based that there is one and only one unitary polynomial basis which can be generated from the monomials. This has greatly improved the present techniques used. The image reconstructed by these basis functions have less error as compared to the others. These basis functions could be formed from the recursive relationship as shown in equation 3.23. Being orthonormal the matrix containing the polynomials basis generated in this manner having negligible numerical error: Whereby the condition number of this matrix should be unity independent of degree of the basis or number of points used. The recurrence relationship leads to propagation errors for large data sets and polynomial bases of higher degrees. These errors can be eliminated and truly orthogonal polynomial basis generated by applying QR decomposition to the above polynomial basis matrix.

3.13.6 Possible relationship to scale space

The scale space theory: It states that the natural operations perform in a visual front-end are convolutions with Gaussian kernels and their derivatives at different scales. The same technique has been applied in the proposed method, in which the image is decimated on different levels. For filtering on the high scale the image is decimated upto maximum level. As we do the decimation locally we going inside to the image and decreasing the level of decimation on the other hand. On the last level we do not have any decimation. The decimation is variable at variable steps.

Chapter 4

Hierarchical image processing

Data images may be transformed by different linear techniques like rotation, translation, Affine transformation, etc. Scaling is one of these linear techniques for data image alteration. Processing the image at different scale is actually scale space processing. And for this process a hierarchy with different levels is defined for image processing at each level. Specially in the proposed method proper decimation is done at various scale. Scale-space filtering, [41] i.e. using a Gaussian kernel, has become the most common filtering method in multiresolution pyramids. Indeed the Gaussian filters deal well with the decimation of additive Gaussian noise; however, it does not address the issue of aliasing adequately. The basic idea is to embed the original signal into a one parameter family of gradually smoothed signals, in which the fine scale details are successively suppressed. It is shown in [41] that the Gaussian kernel and its derivatives are singled out as the only possible smoothing kernels. The condition that specify the Gaussian kernel are basically, linearity and shift invariance combined with different ways of formalizing the notion that structures at coarse scales should correspond to simplifications of corresponding structures at fine scales. To extract any type of information from data it is necessary to interact with it using certain operators. The type of information that can be obtained is to a large extent determined by the relationships between the size of the actual structures in the data and the size (resolution) of the operators (probes): This research work presents an alternative interpretation for consistent information decimation during construction of the hierarchial subdivision. The classical design of filters implicitly involve the selection of basis functions; the most common of which are the Fourier basis and polynomials. Actually the selection of the best set of basis functions depends on the nature of the data being processed. It is shown that careful attention must be payed to correct decimation procedures.

4.1 Hierarchical subdivision of images.

The hierarchical aspect of subdivision itself leads to a natural hierarchy: the first level of subdivision creates a parent and child relationship between the original image and the resulting four subdivided images, which in turn leads to a hierarchy of subdivision as each

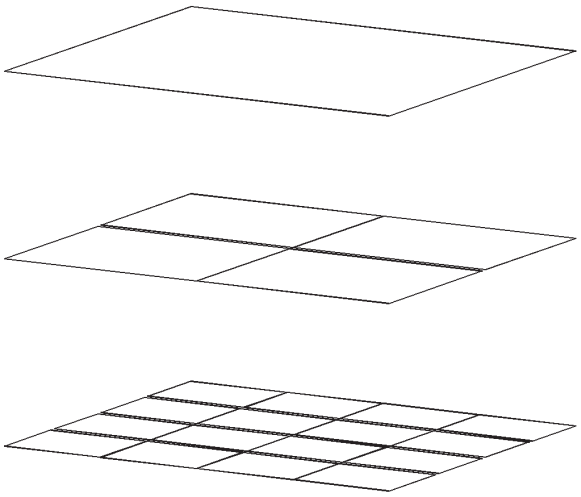

Figure 4.1: decomposition tree, with three layers.

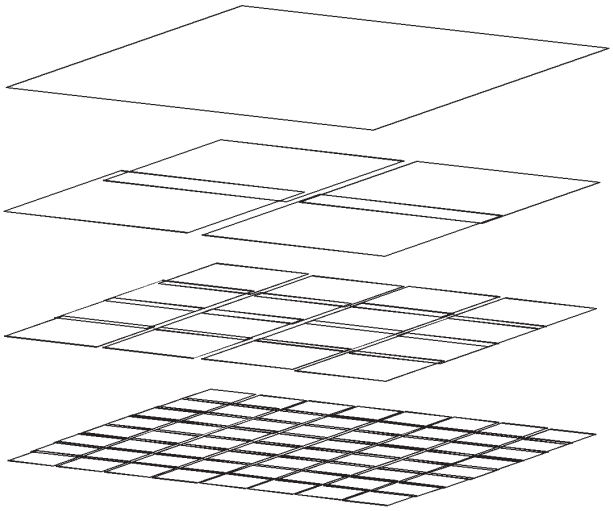

Figure 4.2: decomposition tree, with four layers.

child in turn subdivides. For decimation in any level and any subimage we must have the path to the subdivision, in which we are interested in, excluding of the position of the target cell, means to define a hierarchical path specification for all subimages. For location of any subimage we need information how the subimage are indexed with respect to their root image. We can see in figure(4.1) and (4.2) which shows the multi levels of hierarchy. We see that the base level image has four subimages indexed using the rule, all these subimages have again four subimages and so on. The proposed function generate a vector containing the parent nodes from a quadtree and also return the entry points into each layer. The number of layers in the tree in addition to the root is flexible as shown in figure(4.4), we can give any arbitrary number in forward or reverse direction.

4.1.1 Quad-tree structure

The root-node of the balanced tree as shown in figure (4.4) contains information about the entire image. The root-node is partitioned into four subquadrants. By viewing each descendant node as a father node and repeating the same process, the previously defined quadrants can be further partitioned into four subquadrants up to the level where the nodes contain information obtained by the scanning devices. Every tree node corresponds to a specific area of the original image. By going from top to bottom we go from coarser to finer quality of the image. And decimation is done from global to local. In the proposed method to divide the data and reference image we decide the number of level of quad-tree. The number of layers in the tree in addition to the root is predefined for the process. The main aspect of the proposed quad-tree could be defined and summarized as follows:

1. Number of Layers : Coarser to finer decimation is applied to the image on various scales. The main objective of the research work is to apply the non-rigid registration technique in steps. It is known from the definition of the elastic or non-rigid

registration that the image changes nonlinearly. And the change in image different at different regions. By applying any rigid registration method could not solve the problem exactly. Hence cut and divide rule is applied to the process, and the registration is done from global to local. The same time Gram polynomial decimation is applied at variable level to the image at variable rate.

2. Tree : A row vector is defined which have all the parent node numbers. As in figure 4.4 tree structure shows the parent-child hierarchy. With the help of this row vector any node can be traced. The subdivision starts from the zero level, in the first level division the tree is composed of original image and four equally subdivided images. Similarly in two levels we go further and divide the four subimages in further sixteen subimage, i.e., each subimage is again divided into four equal parts. And the process is repeated till the final level is reached. At this stage each subimage is treated as an independent image. The decimation or registration or both of these processes are applied to all these subimages to get the required results.

3. Entry points: Given a layer number this vector given the entry point into the vector of nodes.

4. Leaves: The leaves of the tree, i.e. the terminal nodes gives the path to the subimge on prescribed level. As we can see in figure (4.4) the number of leaves in each level is described. The main objective of the proposed research work is to consider each leaf at each level as an independent image. The proposed method was mainly used for elastic registration. So both the data and reference images are divided by the prescribed method to the end of the required level. At each level of both the images the leaves are treated independently as a separate image and the pre and post processing techniques are applied i.e. decimation, smoothing and registration to all of them, which could be explained in detail by some real time images and examples in coming sections.

$$P_0 = \quad < 0 > \qquad \text{(Zero level)}$$

$$P_1 = \quad < 1, 2, 3, 4 > \qquad \text{(First level)}$$

$$P_2 = \quad < 5, 6, 7, 8, 9, 10, 11, 12, 13, 14, 15, 16, 17, 18, 19, 20, 21, 22 > \qquad \text{(Second level)}$$

5. Quadrant and layer: The question arises as to why we divide the image in quad tree although all the information already available in the image? Multi scale aspect of the real world image is shown, also to remove all the unwanted information in the image and decrease the processing time of data.

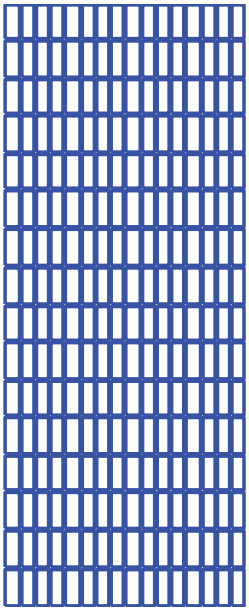

Figure 4.3: decomposed image, with four layers.

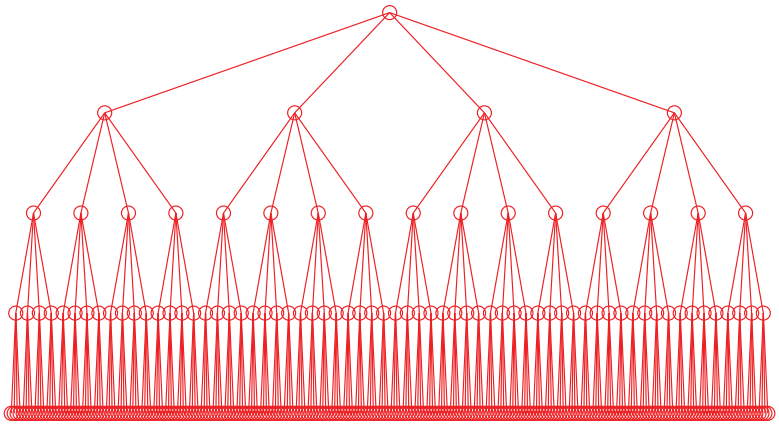

Figure 4.4: decomposition tree, with four layers.

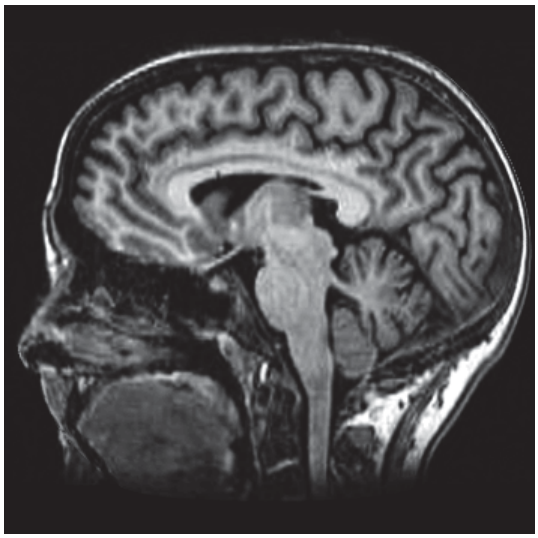

Figure 4.5: Target image to be decomposed.

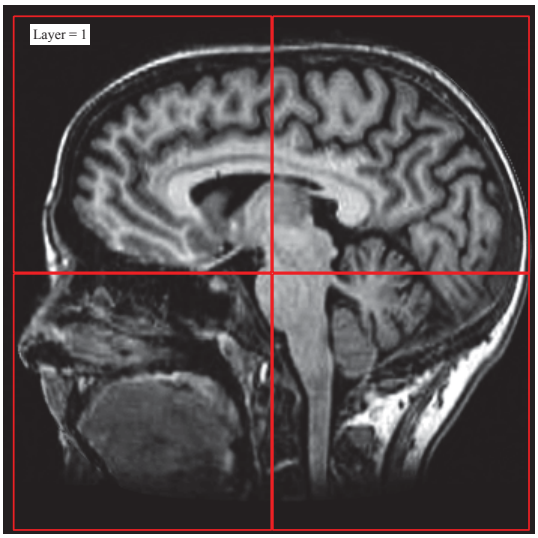

Figure 4.6: decomposition tree, first layer.

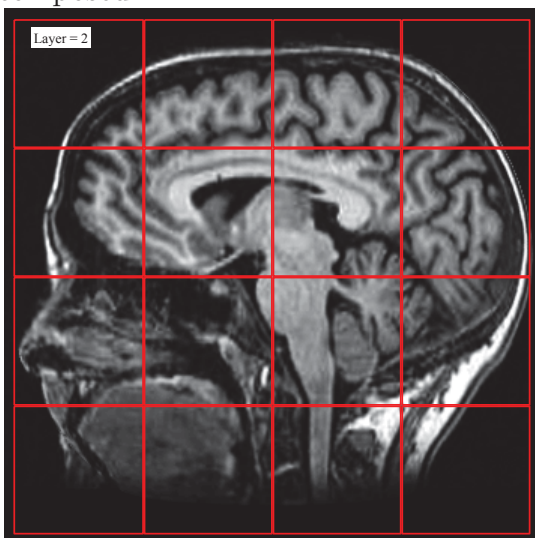

Figure 4.7: decomposition tree, second layer.

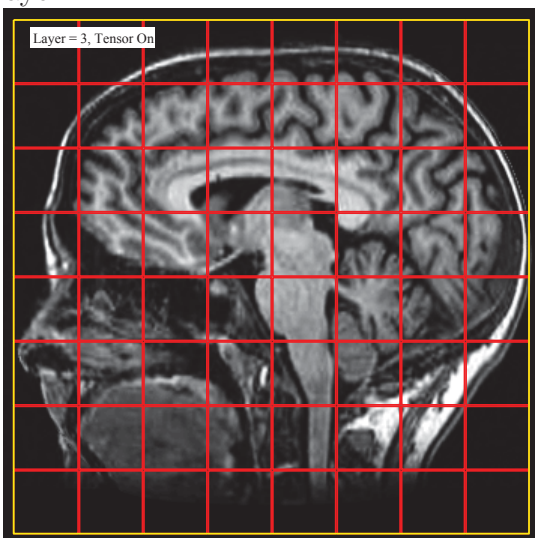

Figure 4.8: decomposition tree, third layer.

4.1.2 Multiresolution decomposition

Multiscale image decomposition is used for analyzing image features at multiscales. An image is decomposed in different levels and each level is set at various scales. In this way going upwards or downwards in the process, the image is processed at various scales. We can say that during the process we go from coarser to finer forms. In the proposed research work two processes at a time are applied to the image on one level i.e. the image is first cut and divided in quad tree structure and then each sub image is decimated at certain decimation rate. These decimation rates vary for all the levels. To get exact registration first we do global registration on zero level and then going inside the image by moving from global to local. And similarly we are cutting and dividing the image. But the rate of decimation we decrease as we go inside the image. At the last level we have no decimation.

4.1.3 Implementing a suitable decimation at each level

It is explained in detail earlier that cut and division, decimation and registration of the images are done in levels. During the testing of the proposed algorithm on real data images exact results were not obtained by keeping the decimation rate constant at each level. Because when decimation is applied at the same time the image scale also changes. The process is a multiscale process. From zero level up to the last level the number of quadrants increases, therefore at the same time the unit size of the image also decreases. As the size of the unit image decreases we also decrease the decimation rate. It could be concluded that as we keep maximum decimation rate at the top or zero level, in this position the size of the image is maximum which is at its original position. Going inside the image the unit size of the image decreases while we reaches the last level. Here the decimation rate we keep minimum or zero decimation because here the size of the unit image is too small to operate by applying more decimation rate we loose much information from the image and it is difficult then to register with the target image. This could be understood by figure (4.9,4.10,4.11,4.12) in detail.

4.1.4 Proposed decimation algorithm based on QT decomposition

The main objective of the proposed research work is to register two or more images with non-rigid or elastic distortion. There are many linear or rigid registration techniques like translation, rotation, scaling ,etc., used by many researchers. The main challenging task was to register the non linear images consuming very small time for execution of the data. Many other techniques like used by [59] [58], but in all those process the execution time was much longer. It was decided to cut and divide the images in quadtrees, and then decimate each unit image. Keeping maximum decimation at zero level saves much processing time. And similarly going inside the image in quad tree the time consumption increases.

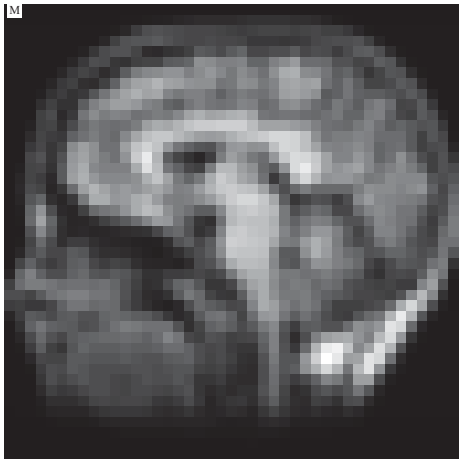

Figure 4.9: Maximum decimation rate 8 at zero level.

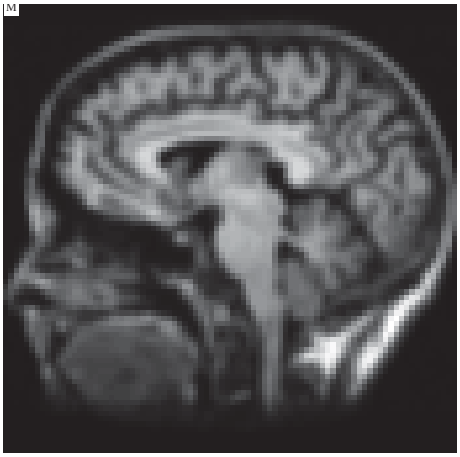

Figure 4.10: Decimation rate 4 at intermediate level .

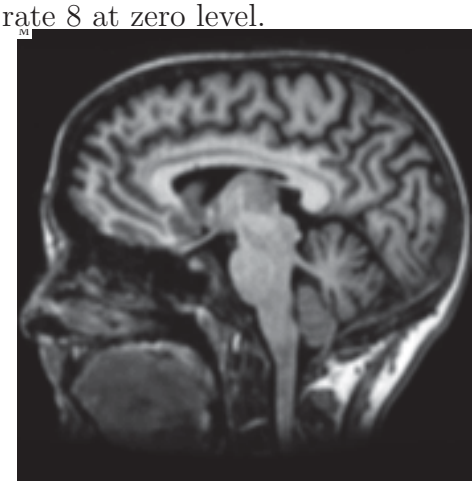

Figure 4.11: Decimation rate 2 at intermediate level .

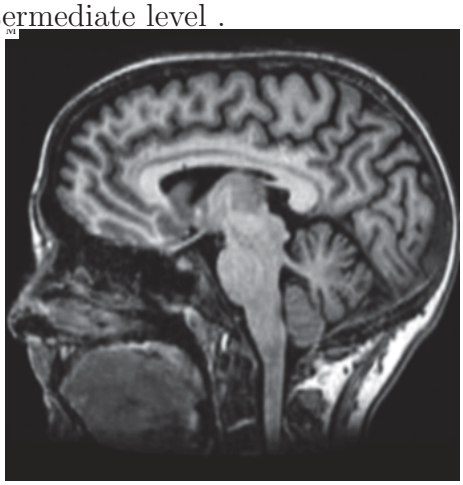

Figure 4.12: Decimation rate 1 at last level .

Chapter 5

Application of the proposed algorithm for global registration

Very much has been written on non-rigid registration; an overview of techniques in biomedical applications is given in [14] and a general review of non-rigid registration can be found in Zitova [75] and Lester [39]. It is virtually impossible to reference all past research work in an introduction: for this reason it restrict the references to the research work most pertinent to the issues dealt with in this proposed research work. Goshtasby [19] [20] presented a paper on non-rigid registration, which assumes that a set of corresponding points in two images are known. The task is: given a set of irregularly placed control points, to find the mapping functions $X \approx f(x, y)$ and $Y \approx g(x, y)$ which relate the coordinates in one image to those in a second image. Today this would not be considered registration, it is actually the final step after the required correspondences have been found. Later the concept of hierarchical subdivision was introduced; [40] whereby, mutual information was used to perform the local registration of the small patches. Likar observed inconsistency in the mutual information during the subdivision process. However, no systematic explanation for the decimation process was given. Xie et al. [73] define the task as given two sets of points. These points are regarded as clouds of points. They implement a subdivided grid using splines, however, assuming that the correspondences between the clouds of points are known.

Mellor [45] proposed local phase as a measure for registration; it was implemented using Fourier transform methods. There is an implicit assumption here: that the patches are well modeled by periodic basis functions. It is shown in the proposed work that in general there is a very significant Gibbs error if Fourier basis are used to implement decimation. Further methods based on feature extraction have been presented [26]; it is important to note that feature extraction is strongly dependent on the pattern being analysed. There are, however, thousands of different decorative patterns which are produced on one and the same printing machine, effectively making feature extraction based methods impractical. Andronache [1] suggests using mutual information (MI) and cross-correlation to perform non-rigid registration. They observe : . the loss of MI's statistical consistancy along the hierarchical subdivision . . . ", Information theoretical measures are proposed to identify

regions in which such problems occur. Their method identifies such regions, but cannot truly solve the problem.

The problem with hierarchical subdivision is that aliasing occurs when an image is decimated to a lower resolution unless appropriate filtering measures are applied. That is, there must also be a consistent hierarchical filtering performed at each layer in the tree structure. Multiresolution [37] pyramids are an attempt to solve this problem. Scale-space filtering, [41]i.e., using a Gaussian kernel, has become the most common filtering method in multiresolution pyramids [39]. Indeed, the Gaussian filters deal well with the decimation of additive Gaussian noise; however, it does not address the issue of aliasing adequately. This work present an alternative interpretation for consistent information decimation during construction of the hierarchial subdivision. The classical design of filters implicitly involve the selection of basis functions; the most common of which are the Fourier basis and polynomials [24]. Actually the selection of the best set of basis functions depends on the nature of the data being processed. In the proposed work it is shown that careful attention must be payed to correct decimation procedures.

5.1 Data filtering by proper basis functions

The very first step to design a filter is to examine the nature of the data being processed. The selection of basis functions are then finalized for the filter. Fourier and polynomial basis functions are commonly used for these filter design. Three signals of different nature have been presented in the figure (5.1). It is difficult for both Fourier and polynomial basis functions to reconstruct all these three signals separately. But it is easy for Fourier basis to analyze the periodic signal but not to reconstruct the other two, i.e., the polynomial and stepped signal will have some error. Similarly for the polynomial basis functions, the polynomial signal is reconstructed with minimum error, but the other two will have more error.

5.1.1 Periodic signal

A test signal of periodic nature has been generated by 128 points as shown in figure (5.3). First the Gram basis functions are applied to reconstruct the signal by keeping order 11 decimation ratio. The result is shown by the red line; which does not show exact signal reconstruction. As it is already described earlier the nature of data is of more importance for signal reconstruction. The given data signal is of periodic nature, therefore it is regenerated by Gram basis function with some error. Then Fourier basis functions are applied for the same data keeping the same decimation rate and the results are shown by the green line. Which describe the accuracy of the Fourier function; because the signal is of periodic nature so the Fourier basis give exact signal representation.

5.1.2 Polynomial signal

Here we try to apply the two basis functions i.e. Fourier and Gram basis on a data signal of polynomial nature. In the figure (5.4) a polynomial data signal is presented. After applying the Fourier basis function, keeping the decimation rate 11 we get the results as shown by the green line. Because the data is of polynomial nature we have some error for Fourier basis functions. But on the other hand by application of polynomial basis functions the results are more accurate; as shown by the red line.

5.1.3 Stepped signal

Here we have a stepped data signal as shown in figure (5.5). Results with error are obtained after applying both of the basis functions. The result of Fourier basis functions are shown by green line and the red line show the result of polynomial basis functions. This concludes that for both of the basis functions either Fourier or Gram we will have some error if we want to reconstruct a stepped signal.

5.1.4 Mixed signal

All the three signal are combined and presented by one signal as shown in figure (5.6). Fourier basis function being suitable for periodic data have problem at starting and at the end. The outcome is presented by green line. While due to gradient or stepped nature of the signal the polynomial basis are also not well suited for the signal representation. Fluctuations are observed when there is abrupt changes in signal. And this is the major

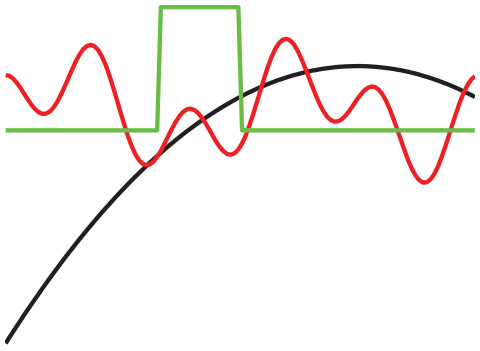

Figure 5.1: The test function shows three different signals,(a) black color shows polynomial signal (b) red color shows periodic (c) Green color shows stepped signal

Figure 5.2: Combining all these three signal we have signal with all these properties.

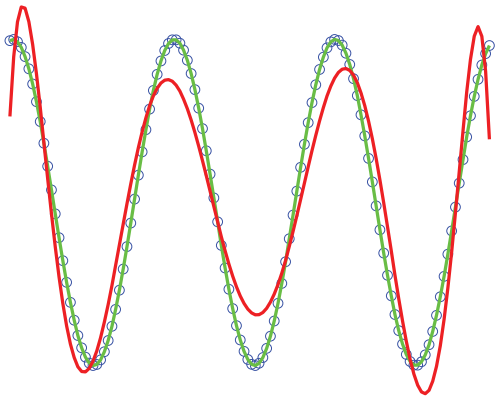

Figure 5.3: The periodic signal generated by Fourier and Gram basis functions , (a) original data “small circle”(b) Gram basis “red line” (c) Fourier basis “Green line”.

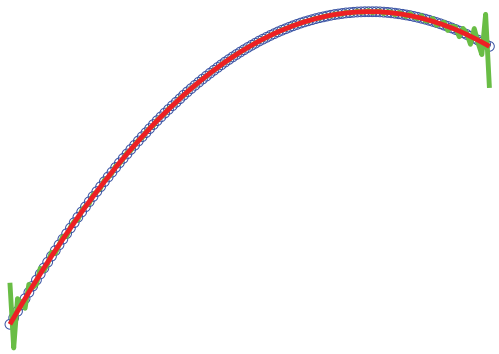

Figure 5.4: The polynomial signal generated by Fourier and Gram basis functions , (a)original data “small circle” (b) Gram basis “red line” (c) Fourier basis “Green line”.

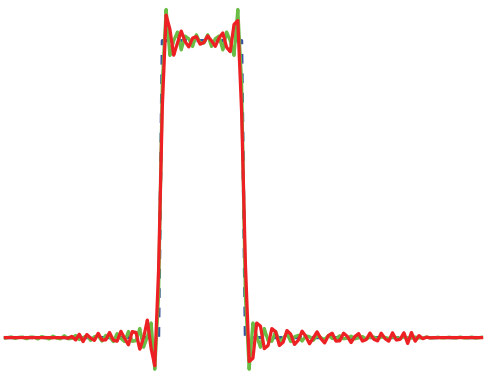

Figure 5.5: The stepped signal generated by Fourier and Gram basis functions ,(a) Gram basis “red line” (b) Fourier basis “Green line”.

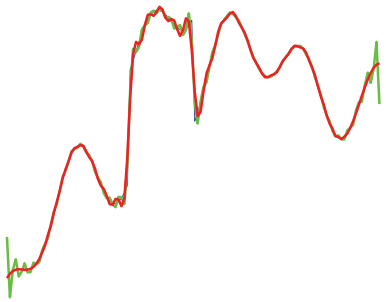

Figure 5.6: All the three signals are combined (a) green line present Fourier and (b) red line present Gram basis functions

cause of the well known Gibbs error [33].

5.2 Reduction of the Gibbs energy

During decimation of the image to lower resolution there are two major sources of error: a Gibbs error which results from the basis function not being able to describe features in the data; the second source of error is aliasing. Commonly aliasing is only considered for periodic basis functions, but the same problem is also present for polynomial basis functions. The issue is further complicated by the presence of Gaussian noise in the image data. Consider a signal y with n data points, to find the spectrum s for this signal we have a set of k discrete orthonormal basis functions $[b_0...b_{k-1}]$, which form the columns of the matrix $B = [b_0...b_{k-1}]$.

$$s = B^T\ y \tag{5.1}$$

and the inverse transform as,

$$\hat{y} = Bs \tag{5.2}$$

If the basis are complete,i.e., any set of basis functions,B, where $BB^T = I$, can represent a discrete signal without error, since from equation 5.1 and 5.2, $\hat{y} = BB^T y$. Similarly the Gibbs error is not principally associated with specific basis, but with approximating a signal by truncated set of basis functions, or by weighting the basis functions. This could be formulated generally as follow,

$$\hat{y} = BHB^T\ y \tag{5.3}$$

where the element H weight the respective spectral components, in the case Fourier basis H is traditionally diagonal ; however, with polynomials more general structures are encountered. This could be explained for one and two dimensional data as follows:

5.2.1 One dimensional problem

It is instructive to consider the decimation of a one-dimensional signal before proceeding to 2D data sets representing images. Consider the simple example shown in Figure (5.7) and (5.8): the data consists of a ramp with a slope of 0.5 in the support range $x \in [-1, 1]$ and a superimposed unit step function, the signal has been computed for $n = 100$ points. The decimation-rate of $k = 4$ is simulated for two different cases:

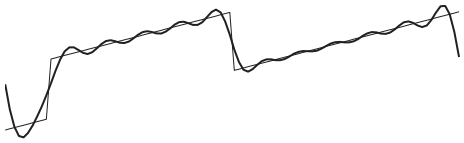

Figure 5.7: The test function is a linear ramp in the range $x \in [-1, 1]$ with a slope of 0.5 with the addition of a unit step. Decimation-rate of four is performed using 25 Fourier basis functions.

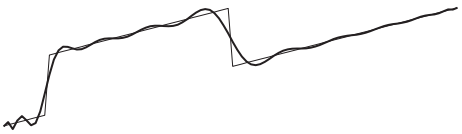

Figure 5.8: Decimation-rate of four is performed using the first 25 Gram polynomial basis functions.

1. the Fourier basis functions. The result of approximating the test signal by the first $m = 25$ Fourier basis functions is shown in Figure 5.7. There are two sources of Gibbs error in this signal: the step function and the ramp. The error associated with the ramp is usually dealt with using windowing; this however modifies the signal spectrum and with this influences the phase correlation;

2. Gram polynomial basis. The recent introduction of polynomial basis [51] which are virtually free from errors, enable new decimation procedures. The result of decimating the signal with the first $m = 25$ Gram basis functions is shown in Figure 5.8, there is no Gibbs error associated with the ramp, since the basis function of degree 1 can model the linear portion of the signal exactly; however, a Gibbs error is still associated with the step function. As can be seen there is significantly lower distortion in the decimated signal than using the Fourier basis;

To summarize: general images are poorly modelled by Fourier basis functions. This explains why Mellor [45] did not achieve the desired results. In general Gram polynomial basis functions offer a better solution.

5.2.2 Two dimensional problem

The best set of basis functions for image decimation depends on the nature of the image being considered. The Fourier basis is suitable when there are periodic structures in the image. Correspondingly, the Gram basis is suitable when the image is predominantly geometric in nature. To illustrate this consider Figure (5.9), the data corresponds to a

surface generated by $z = x + y + x^2 - y^2 + y\,x$ for the range $x, y \in [-1, 1]$, this is clearly geometric in nature. The residuals resulting from decimation by a factor of 8 with the Fourier and Gram basis are shown in Figures (5.10) and (5.11) respectively. Clearly, for this example the Gram basis is superior; not just marginally better but orders of magnitude better.

5.2.3 Comparison of Fourier and Gram basis functions for image analysis

A common approach for accessing image quality is to determine one of a wide variety of figures of merit including values such as signal to noise ratio, bias, contrast levels, etc.

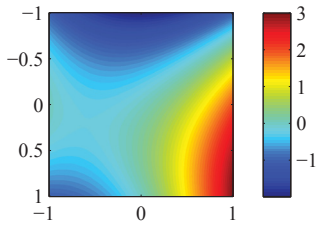

Figure 5.9: Geometric data generated by the function $z = x + y + x^2 - y^2 + yx$ for the range $x; y \in [-1; 1]$. This data set is generated with 550 nodes in both the x and y directions.

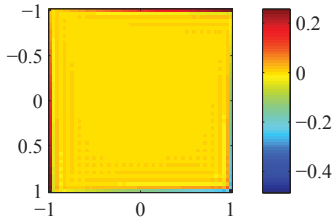

Figure 5.10: Difference between the original surface at the decimation points and the surface decimated using the Fourier basis, the decimation-rate $r_d = 11$.

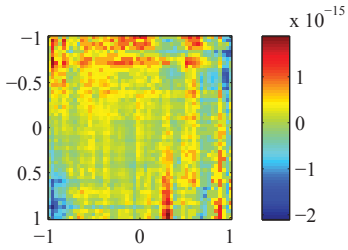

Figure 5.11: Difference between the original surface at the decimation points and the surface decimated using the Gram polynomial, the decimation-rate $r_d = 11$.

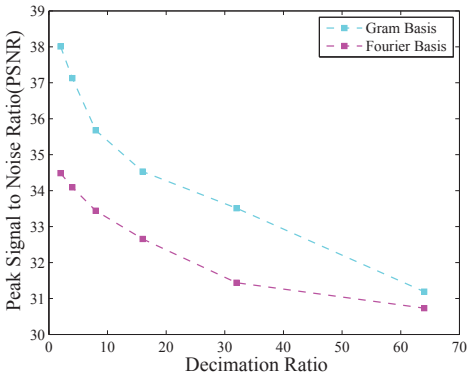

Figure 5.12: Variation in the peak signal to noise ratio(PSNR) with respect to variation in decimation ratio for Gram and Fourier basis functions.

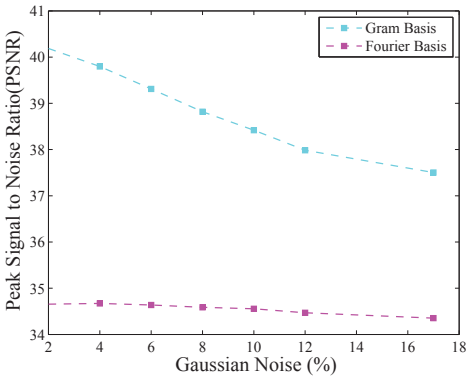

Figure 5.13: Variation in the peak signal to noise ratio(PSNR) with respect to variation in Gaussian noise for Gram and Fourier basis functions.

Figure 5.14: Lenna original image.

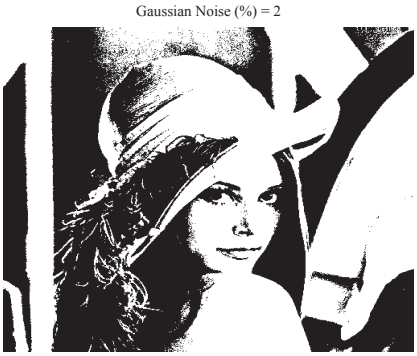

Figure 5.15: Lenna image with 2 percent noise.

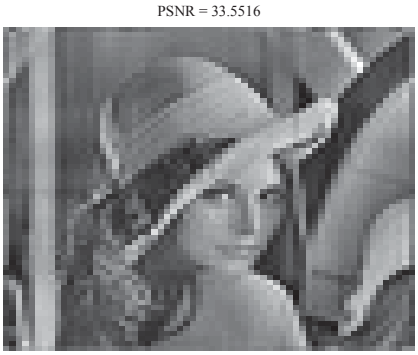

Figure 5.16: Reconstructed Lenna image by Fourier basis keeping decimation rate of 4.

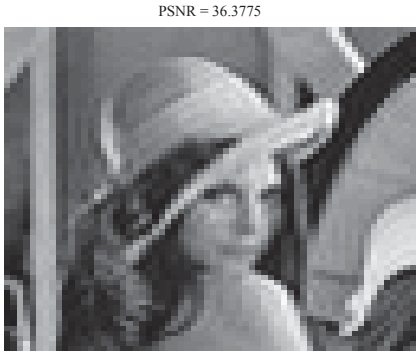

Figure 5.17: Reconstructed Lenna image by Gram basis keeping decimation rate of 4.

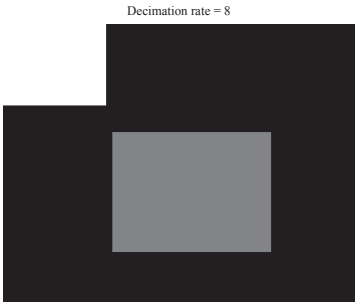

Figure 5.18: Synthetic stepped image.

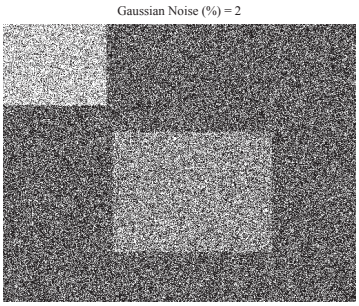

Figure 5.19: Image with 2 percent noise.

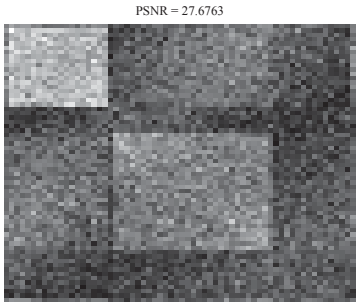

Figure 5.20: Reconstructed image by Fourier basis keeping decimation rate of 4.

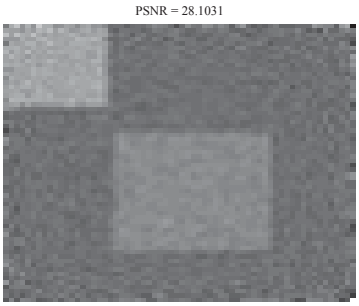

Figure 5.21: Reconstructed image by Gram basis keeping decimation rate of 4.

The commonly used is the signal to noise ratio, to use this method first the signal to noise ratio is calculated for the reference image and then similarly signal to noise ratio is found for the reconstructed image either by Fourier or Gram basis functions. The maximum value for any of the method provide the better quality of the image. In the proposed work different test has been done for both the basis functions at various decimation rate, and a graph is plotted as shown in figure 5.12. The testing is also done for additional Gaussian noise i.e. in the presence of different amount of noise how the peak signal to noise ratio changes. The results are shown in the figure 5.13.

5.2.4 Peak signal to noise ratio and change in decimation rate

As long as we increase the decimation ratio we are removing information from the original data image. This means by increasing the decimation ratio the peak signal to noise ratio ($PSNR$) is going to decrease. It is desired in most of the cases to keep maximum quality with maximum decimation rate. In figure 5.12 it is shown that how Peak Signal to Noise Ratio ($PSNR$) value changes for changing the decimation ratio. This Graph is generated by decimating Lenna image at different decimation ratio and then finding the peak signal to noise ratio at consecutive decimation points. The graph shows the comparison of

the Fourier and Gram basis image reconstruction quality. Gram polynomial basis method shows better result than Fourier basis. The target of the research work is to investigate the trends of changing behavior with changes in the decimation rate, and conclude with the best method for image decimation with maximum peak signal to noise ratio. Applying suitable decimation at each level of the hierarchy during non-rigid registration, implemented using the Gram basis, eliminates the statistical inconsistencies.

5.2.5 Peak signal to noise ratio and change in Gaussian noise

Looking at the figure (5.13) the graph showing the change in the *Peak Signal to Noise Ratio* with respect to change in the Gaussian noise. The test has been done on the well known Lenna image for both Fourier and Gram basis. The results show that Gram bases are better than Fourier basis for same Gaussian noise. The resultant image after reconstruction by both Fourier and Gram basis could also be seen in figure (5.16) and (5.17). These tests are also applied on a $2D$ stepped data image as shown in figure (5.20) and (5.21). And the relative signal to noise ratio after reconstruction is presented. Here also the Gram basis are superior than Fourier basis for reconstruction, because the signal to noise ratio for Gram basis is better than Fourier basis functions.

5.3 Covariance propagation

This problem is further explained in the field of statistics by considering its covariance. If we have a signal y of n data points, the covariance propagation could be achieved by first obtaining its covariance matrix. As we know that Fourier basis are orthogonal, therefore the independent and identical distributed Gaussian noise is distributed these equally spaced places in the Fourier spectrum. Three possible modification type of covariance propagation has been described in [25]. The linear transformation could be found as following,

$$\Lambda_{y_m} = \frac{\partial y_m}{\partial y}\ \Lambda_y\ \left(\frac{\partial y_m}{\partial_y}\right)^T \tag{5.4}$$

where Λ_y is the covariance matrix of the signal y. Since windowing and the least squares projections are linear operators, in each case the Jacobian matrix $\frac{\partial y_m}{\partial y}$ is simply the coefficient matrix effecting the linear operator.

5.3.1 Windowing application for possible modification

Application of the windowing function can be written as,

$$y_m = Wy \tag{5.5}$$

where,

$$W = \text{diag}\{w_1, ..., w_n\}. \tag{5.6}$$

The covariance of the windowed signal is therefore,

$$\Lambda_{y_m} = W\Lambda_y W^T \tag{5.7}$$

In the case Fourier basis i.e i.i.d (independent and identical distributed) Gaussian noise with variance σ^2, i.e., $\Lambda_y = \sigma^2 I$, the covariance matrix is then,

$$\Lambda y_w = \sigma^2 W^2 = \sigma^2 \text{diag}\{w_1^2, ..., w_n^2\} \tag{5.8}$$

5.3.2 Subtraction of the aperiodic part

A common method eliminating the aperiodic part of a signal is to simply subtract the linear component connecting the end points. This amounts to subtracting the linear function,

$$l = [l_1 ... l_n]^T \tag{5.9}$$

where $l_k = y_1 + \frac{(k-1)}{(n-1)}(y_n - y_1)$. In matrix form, the k^{th} element of this linear function can be written as,

$$l_k = [1 - \frac{(k-1)}{(n-1)} \quad 0 ... \ 0 \quad \frac{(k-1)}{(n-1)}] \begin{pmatrix} y_1 \\ y_2 \\ . \\ . \\ . \\ \\ y_{n-1} \\ y_n \end{pmatrix} \tag{5.10}$$

we can write it more concisely as,

$$l = Ty \tag{5.11}$$

Thus, subtracting this component from the original signal yields,

$$y_l = (I - T)y \tag{5.12}$$

The covariance matrix of this operation is hence,

$$\Lambda_{yl} = (I - T) \quad \Lambda_y \quad (I - T)^T \tag{5.13}$$

In the case of i.i.d. Gaussian noise with variance σ^2, i.e. ,$\Lambda_y = \sigma^2 I$ the covariance matrix is then,

$$\Lambda_{yl} = \sigma^2 (I - T)(I - T)^T \tag{5.14}$$

The entries of the matrix can be shown to be,

$$\sigma^{-2}\Lambda_{yl}(i, j) = \delta_{ij} + \frac{(n-i)(n-j)}{(n-1)^2} + \frac{(i-1)(j-1)}{(n-1)^2} - \delta_{i1}\frac{n-j}{n-1} \tag{5.15}$$

$$-\delta_{1j}\frac{n-i}{n-1} - \delta_{(n-i+1)1}\frac{j-1}{n-1} - \delta_{1(n-j+1)}\frac{i-1}{n-1} \tag{5.16}$$

where δ_{ij} is the Kronecker delta. The diagonal entries of the matrix, i.e., the variances, are,

$$\Lambda_{yl}(k,k) = \begin{cases} 0 \quad \text{for } k = 1, n \\ \sigma^2(1 + \frac{(n-k)^2}{(n-1)^2} + \frac{(k-1)^2}{(n-1)^2}) \quad \text{for } k = 2, ..., n-1 \end{cases} \tag{5.17}$$

With the exception of the end points, all the diagonal entries are clearly greater than 1, in fact, reaching a minimum value of 3/2. The maximum variance occur at $k = 2$ and $k = n - 1$, where the variance is,

$$\sigma^2_{max}(n) = 2\frac{n^2 - 3n + 3}{(n-1)^2}\sigma^2 \tag{5.18}$$

As n increases, the maximum variance tends asymptotically to 2.

5.3.3 Polynomial approximation

Removal of the low degree polynomial approximation can be written as,

$$y_g = \tilde{G}_d\tilde{G}_d^T y \tag{5.19}$$

where the matrix $\tilde{G}_d$ is the orthogonal complement of G_d, that is,

$$G = [G_d \quad \tilde{G}_d] \tag{5.20}$$

is a complete set of Gram polynomials. Thus, the covariance of the modified signal is,

$$\Lambda_{yg} = \tilde{G}_d\tilde{G}_d^T\Lambda_y\tilde{G}_d\tilde{G}_d^T \tag{5.21}$$

In this case, when the input noise is i.i.d. Gaussian noise, the covariance becomes,

$$\Lambda_{yg} = \tilde{G}_d\tilde{G}_d^T(\sigma^2 I)\tilde{G}_d\tilde{G}_d^T \tag{5.22}$$

$$\Lambda_{y_g} = \sigma^2\tilde{G}_d\tilde{G}_d^T \tag{5.23}$$

The significance of this result can be seen in the fact that the Moore-Penrose pseudo-inverse of $\tilde{G}_d$ is its transpose,i.e.

$$\tilde{G}_d^+ = \tilde{G}_d^T \tag{5.24}$$

The pseudo-inverse, however, is a minimizer in the sense that the term $\tilde{G}_d\tilde{G}_d^+$ is as close to an identity in the least-squares sense.

$$\tilde{G}_d^+ = \min_X ||\tilde{G}_d X - I||_F \tag{5.25}$$

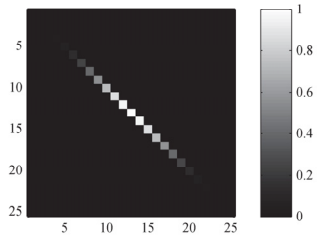

Figure 5.22: Covariance matrix of pre-processing step of Hanning windowing function

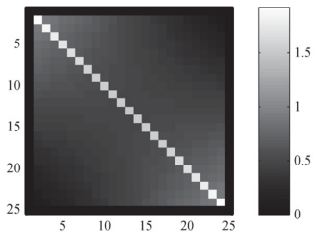

Figure 5.23: Covariance matrix of pre-processing step of subtraction of the aperiodic portion.

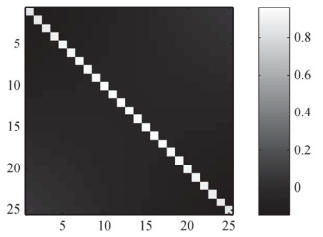

Figure 5.24: Covariance matrix of pre-processing step of Gram polynomial approximation of degree 1.

This means that for a given set of basis functions G_d, the covariance of the modified signal y_g is that which is closest to an identity matrix in the least squares sense. Specially, given G_d, the signal y_g is the signal whereby,

$$\Lambda_{yg} = \min_X ||X - I||_F \tag{5.26}$$

and X is a covariance matrix. The matrix Λ_{y_g} is then generally symmetric and positive semi-definit.

5.3.4 Comparative results

In the case of windowing functions a large variation in gain across the signal is observed, because the covariance matrix of the windowing function is diagonal and the square of the windowing function. While the second method i.e. simple subtraction of the aperiodic portion has all non-zero variances are greater or equal to 3/2, and thus the gain in general is more than unity. For the least squares approximations the variances are generally slightly less than unity. These comparisons could bee seen in detail in the figure (5.22)(5.23)(5.24). The diagonals of the corresponding covariance matrices are shown in Figures (5.25)(5.26)(5.27).

5.4 Improved normalized phase correlation by modified Fourier basis functions

A modified normalized phase correlation method is introduced to perform registration. The Fourier basis is modified by projection onto the orthogonal complement of a degree $d = 1$ Gram-polynomial. This eliminates the effects of intensity and intensity gradients within a patch. This modification is an alternative to windowing in Fourier analysis [53]

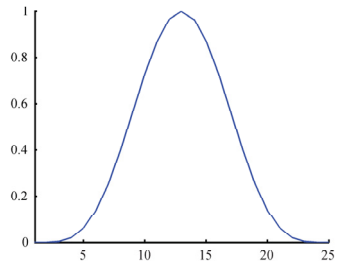

Figure 5.25: A Hanning windowing function

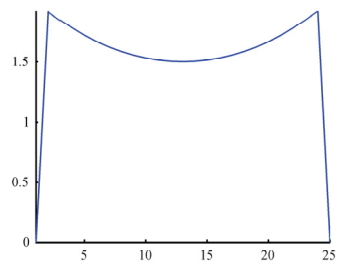

Figure 5.26: Subtraction of the aperiodic portion.

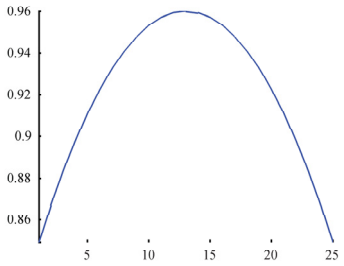

Figure 5.27: Gram polynomial approximation of degree 1.

$$P(n) = F^{-1}\left\{\frac{R(\omega)M^T(\omega)}{\|R(\omega)M^T(\omega)\|_2}\right\} \tag{5.27}$$

where $R(\omega)$ and $M(\omega)$ are the $2D$ Fourier spectra of the reference image and measurement image respectively. Mellor [45] proposed local phase, i.e. computing the phase correlation for each patch individually, as a measure for registration in non-rigid registration. As mentioned earlier: Andronache [1] observed . . . the loss of MIs statistical consistency along the hierarchical subdivision . . . . Indeed the main loss of consistency is due to aliasing and/or Gibbs error during the decimation and Fourier based registration processes. Aliasing leads to a shifting of peaks in the frequency domain; while ringing associated with the Gibbs error leads to spurious peaks in the spectrum as in figure (5.34). These additional peaks are not properties of the image, they are errors associated with mathematical processing. The Fourier basis functions are,

$$f(k) = e^{-\frac{2\pi k}{N}j} \tag{5.28}$$

clearly these basis functions can not model a simple gradient. However, the image patches regularly have strong slope. Consequently, the Fourier transform will have significant Gibbs errors and associated spurious peaks in the spectrum which can lead to errors in the registration: this phenomena is well known and documented in [33]. In classical signal processing windowing is used [24] to reduce the Gibbs error. However, windowing is not appropriate in image registration, since it would modify the signal significantly and preclude a correct registration. For this reason a modified Fourier transform [53] is introduced here for the computation of the image spectrum.

5.4.1 Orthogonal residualization of the Fourier basis

Prior to computing the $2D$ Fourier spectrum, the image patch D is projected onto the orthogonal complement of a set of truncated Gram polynomials,

$$D_{pg} = D - G_y G_y^T D G_x G_x^T \tag{5.29}$$

where the columns of Gx and Gy contain the Gram basis functions for the x and y directions respectively. This process removes, to a large degree, the subharmonic components

in the patch (for more detailed description see [53]); reducing the Gibbs error associate with this portion of the data. This computation can be performed as either a two step task, as presented above, or a modified set of basis functions can be computed a-priory and applied at run-time. The spectrum of D_{pg} is computed as,

$$S_{pg} = F_y^T D_{pg} F_x, \tag{5.30}$$

where Fx and Fy are the matrices containing the Fourier basis functions for the x and y directions respectively. The fast Fourier transform is only a numerically efficient method of performing this computation. Now substituting Equation(5.29) into Equation(5.30) yields,

$$S_{pg} = F_y^T \{D - G_y G_y^T D G_x G_x^T\} F_x \tag{5.31}$$

Expanding this equation yields,

$$S_{pg} = F_y^T \{I - G_y G_y^T\} D \{I - G_x G_x^T\} F_x \tag{5.32}$$

Now defining the modified basis functions as by $B_y = F_y^T \{I - G_y G_y^T\}$ and $B_x = \{I - G_x G_x^T\} F_x$. The modified Fourier transform is now computed as,

$$S_{pg} = B_y D B_x \tag{5.33}$$

and the modified spectrum is used for the computation of the normalized phase correlation. This computation is numerically efficient than the two step process for small patches.

5.4.2 Numerical testing

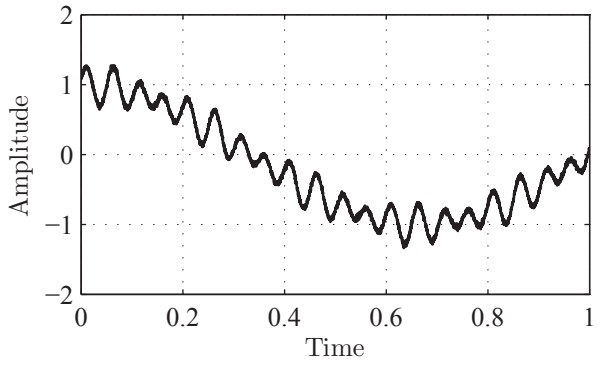

Figure 5.28: A test signal generated with a subharmonic component $s_h = \cos(0.75\phi)$, a purely periodic component $f_p = 0.1\cos(15\phi) + 0.2\sin(20\phi)$ and a additive Gaussian noise with standard deviation $\sigma = 0.02$. The data set has $n = 2048$ points.

Numerically this could be demonstrated by considering the signals shown in the figure 5.28. The signal has been generated by superposition of subharmonic component $s_h = \cos(0.75\phi)$, to a purely periodic component $f_p = 0.1\cos(15\phi) + 0.2\sin(20\phi)$ and with additive Gaussian noise with standard deviation $\sigma = 0.02$. Five different spectra have been computed for comparison purposes, Figures (5.29)(5.30).

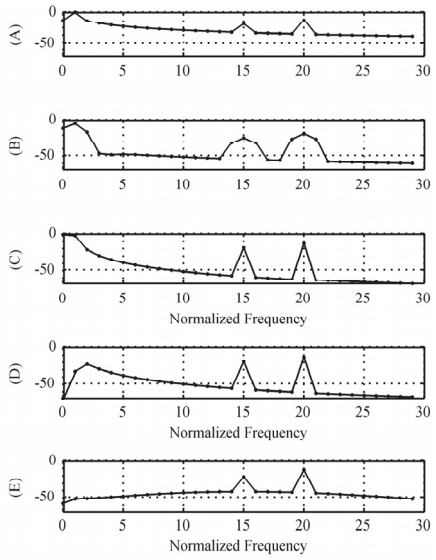

Figure 5.29: Without additional noise Fourier spectra(dB) derived from the test signal shown in Figure 5.28.

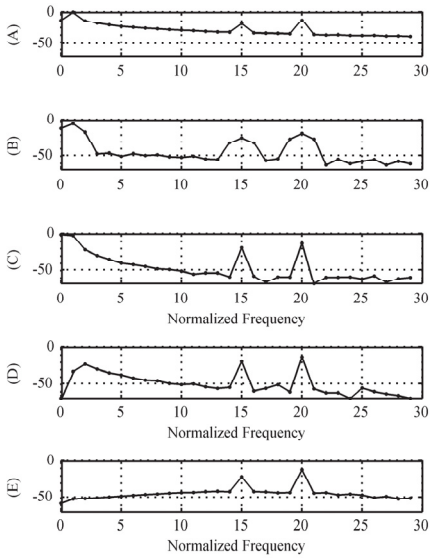

Figure 5.30: With additional Gaussian noise. Fourier spectra(dB) derived from the test signal shown in Figure 5.28.

- The image (5.29)(5.30)A presents the spectra of the signal without any modifications.
- Figure (5.29)(5.30)B show that spectra of the signal after applying the Blackman windowing function.
- The method of subtracting the linear aperiodic portion, is presented in the figure (5.29)(5.30)C.
- The proposed method of projection onto a truncated gram polynomial basis, in this example of degree $d = 2$, as shown in figure (5.29)(5.30)D.
- The new method of the removal of local Gram polynomial approximation with $p = 11$ and degree $d = 1$ as in figure (5.29)(5.30)E.

The target of the research work is to estimate the signal frequency and amplitude more accurately. From the results shown above it could be clearly concluded that Hanning window spreads the signal energy over number of frequencies which we can see in figure (5.29)(5.30)B. But in comparison of this result the proposed method shows more accurate result as shown in figure (5.29)(5.30)E. The proposed work is majorally used for image registration. For which the concentration of the signal energy on narrow peaks is particularly important when performing normalized phase correlation. The work is further analyzed by a test signal explained in following section.

5.4.3 Testing of the modified phase correlation method

The improvement in the registration associated with the modified Fourier basis set is demonstrated with a one dimensional data example. This is an operation commonly used when determining displacements. Given two discrete signals, $\mathrm{d}_1 x$ and $\mathrm{d}_2 x$,together with their corresponding discrete Foureir spectra, $D_1(w)$ and $D_2(w)$ computed via FFT, the normalized phase correlation is computed as,

$$c(n) = IFFT\left(\frac{D_1(w)D_2(w)^*}{|D_1(w)D_2(w)^*|_2}\right) \tag{5.34}$$

A synthetic data signal $d(n)$ has been generated for this test, see Figure 5.31. Two subsets $d_1(n)$ and $d_2(n)$ are cut from $d(n)$ with a shift of 55 samples. These two data sets, with known time shift, are used to test the normalized phase correlation with (see Figure 5.33) and without projection onto the orthogonal complement of a truncated Gram polynomial of degree $d = 2$ (see Figure 5.32). It can be seen that the shift by 55 samples can be clearly identified, if the projection onto the truncated Gram polynomials is performed prior to computing the correlation. The signal to noise ratio is significantly better than with the conventional computation.

Considering in two dimensional case lets see figure 5.34. The image has been modified with known shift. The two images before and after shift are registered by proposed method. Phase correlation is used to find the shift in the images. To register two images by phase correlation, we calculate the discrete 2D Fourier transform of both images. The cross power spectrum is calculated by taking the complex conjugate of the shifted image. The result is normalized element wise as in equation 5.34. Taking the inverse Fourier transform of the calculation we get the required shift in the two images. We get a false result by this method due to the false peak value in the cross power spectrum, and this leads us to an incorrect registration. In figure 5.34(left) we observe many peaks, due to covariance propagation by fourier basis functions. The proposed work reduce those peaks to a single peak as shown in the figure 5.34(middle). So the false peaks are removed and as a result

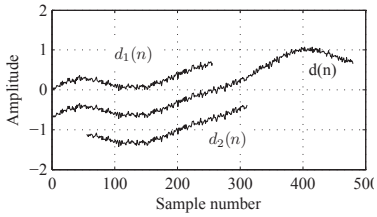

Figure 5.31: A synthetic data set $\boldsymbol{d}(n)$, with two data subsets $\boldsymbol{d}_1(n)$, and $\boldsymbol{d}_2(n)$. Both data subsets have a length of 256 samples and are cut from $\boldsymbol{d}(n)$ with a relative shift of 55 samples.

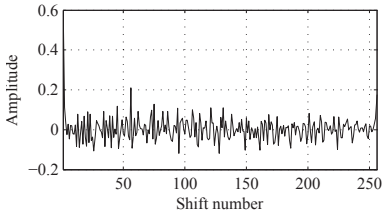

Figure 5.32: Normalized phase correlation of the signals $\boldsymbol{d}_1(n)$ and $\boldsymbol{d}_2(n)$ computed using Equation 5.42

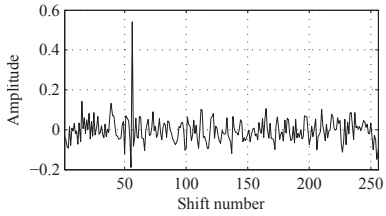

Figure 5.33: Normalized phase correlation of the signals $\boldsymbol{d}_1(n)$ and $\boldsymbol{d}_2(n)$, after projection onto the orthogonal complement of a truncated Gram polynomial basis of degree $d = 2$.

we have the exact shift of the data image from the reference image. Figure 5.34(right) shows the difference in the two patches produced by the two methods.

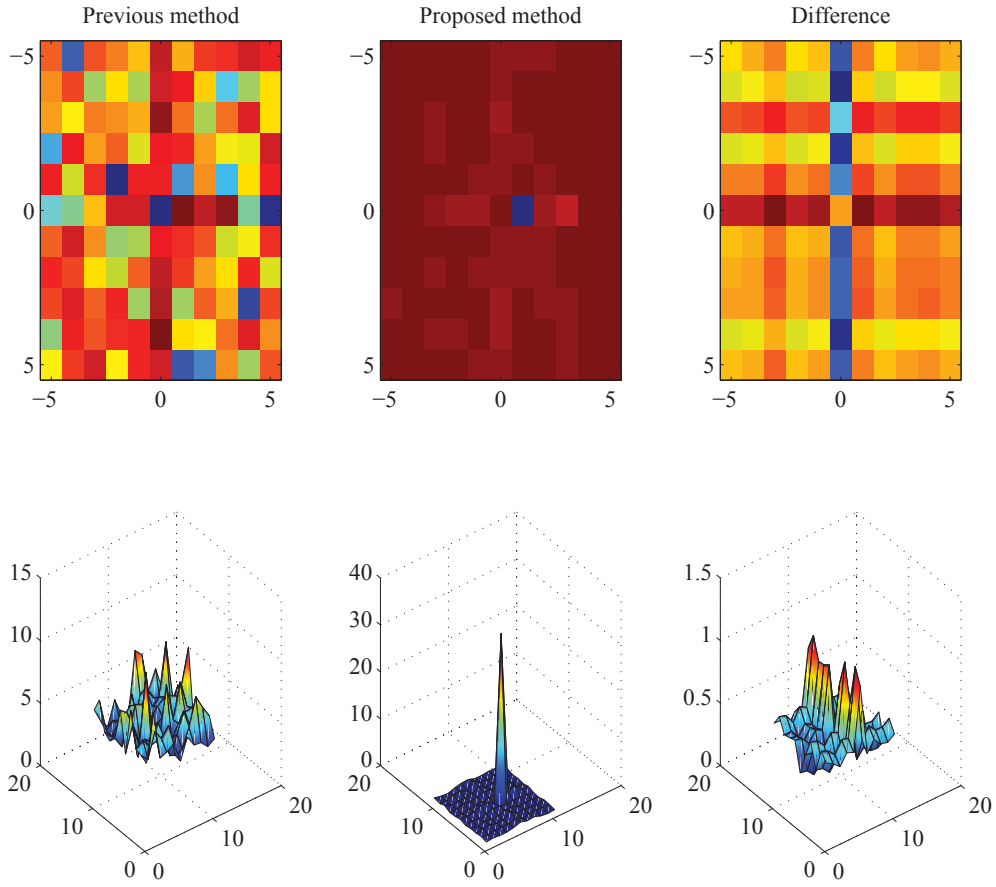

Figure 5.34: (left) the cross power spectrum produced by the older method, this showing many peaks. (Middle) the cross power spectrum produced by the proposed method, this showing single peak. (right)the difference in the two patches produced by the two methods

5.5 Image registration

A detailed introduction of image registration can be found in [75]. It is described that image registration is the process of overlaying two or more images of the same scene taken at different times, from different viewpoints, and/or by different sensors. Image registration geometrically aligns two images - the reference and data images. The present differences between images are introduced due to different imaging conditions. Image registration is a crucial step in all image analysis tasks in which the final information is gained from the combination of various data sources like in image fusion, change detection, and multichannel image restoration. Typically, registration is required in remote

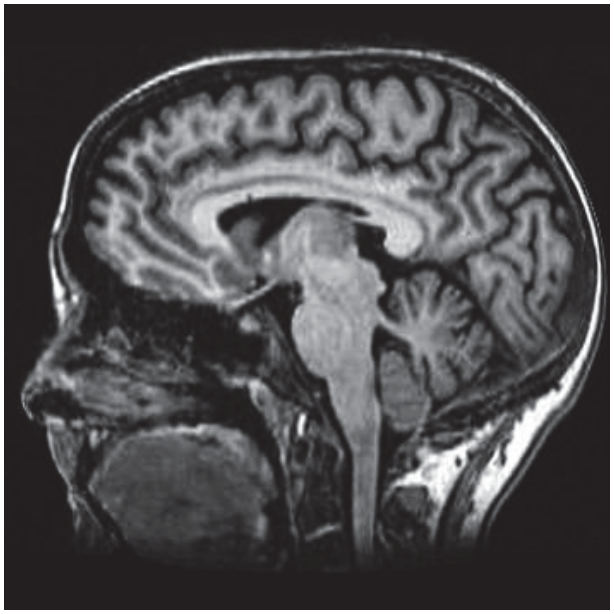

Figure 5.35: Example of a biomedical image requiring registration. This image has 353×354 pixels. This image has been published online and enables the comparison with other implementations[10].

Figure 5.36: Example of a decorative laminate (imitation wood). This image has 800×500 pixels.

sensing (multispectral classification, environmental monitoring, change detection, image mosaicing, weather forecasting, creating super-resolution images, integrating information into geographic information systems - GIS), in medicine (combining CT and NMR data to obtain more complete information about the patient, monitoring tumor growth, treatment verification, comparison of the patients data with anatomical atlases), in cartography (map updating), and in computer vision (target localization, automatic quality control).

5.6 Non rigid or elastic registration

Non-rigid or elastic registration is a major area of research in biomedical applications of image processing; see for example. [14] The biological material, which is not rigid, may deform in the time between the acquisition of two images. Consequently, an automatic comparison of the images is only possible when the two images are non- rigidly registered to each other. A further area of application is emerging in quality control of printed surfaces which are subject to deformation. Two examples of typical images requiring non-rigid registration can be found in Figure (5.35) and (5.36).

5.7 Image registration by proposed method

The proposed work presents a new approach to non-rigid registration. A hierarchical subdivision approach is applied, with local normalized phase correlation for patch registration. The major improvement is achieved by implementing a suitable decimation at each level. The decimation is implemented via a Gram polynomial basis. Both global and local polynomial approximation are considered and compared with the use of a Fourier basis. The issue of Gibbs error in polynomial decimation is examined. It is shown that the Gram basis is superior when applied to signals with strong gradient, i.e., a gradient which generates a significant Gibbs error with a Fourier basis. A bivariate Gram polynomial tensor product approximation is used to implement regularization. It is demonstrated that the new method performs well on both synthetic and real image data. The procedure requires approximately 1.3 sec. to register an image with 800×500 pixels

5.8 Application of algorithm on rotation, translation and scaling distortion

The linear transformation of images results in linear registration, which is not too difficult to compute. In these transformations the most important are translation, rotation, scaling and Affine transformation. The proposed algorithm is applied for all of these transformations and the image are registered as shown in figure (5.37, 5.38, 5.39 and 5.40).

5.8.1 Application on Affine distortion

Complete non-rigid registration applied to an image with Affine distortion is shown in figure(5.41). The green blue line show the original position of the image, while the grid shows the final position of the image after applying Affine distortion.

5.8.2 Application on non rigid and elastic distortion

Now returning to the reference data from paper industry application: the registered images are shown in Figure (5.42 and 5.43), the image which is known to be subject to Pin cushion distortion is shown in Figure (5.42) the registered grid shows the distortion in the data image. The distortion required to map the reference image to the registered image is shown in Figure (5.46) . The new procedure has performed well on the reference data set. The speed of the new solution is worth explicit reference: Suarez et al. have published two different techniques for registration: the first [59] required 7 mins, the second [58] required 15 mins. In contrast, the solution presented here required approximately 1 sec. to perform the complete registration including the regularization. This is an improvement of at least 2 orders of magnitude.

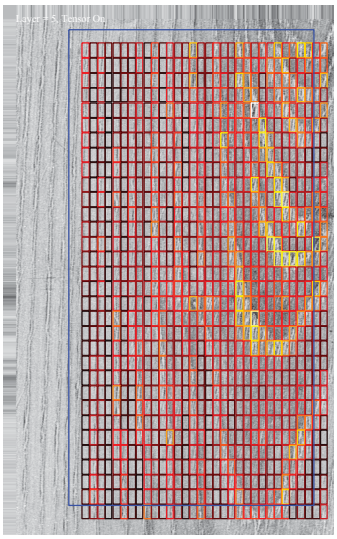

Figure 5.37: Application of the method on translation. The blue line shows the original position while the grids shows final position of the the image.

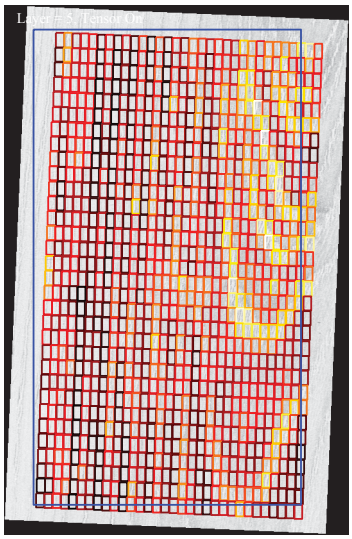

Figure 5.38: Application of the method on rotation. The blue line shows the original position while the grids shows final position of the the image

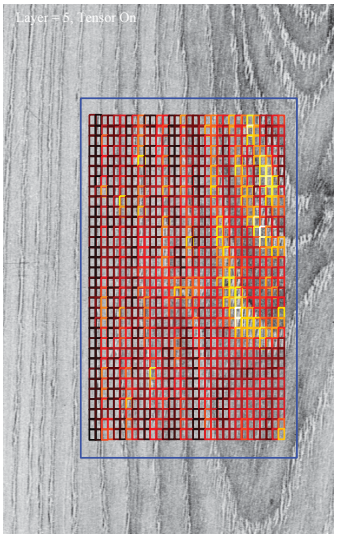

Figure 5.39: Application of the method on scaling. The blue line shows the original position while the grids shows final position of the the image

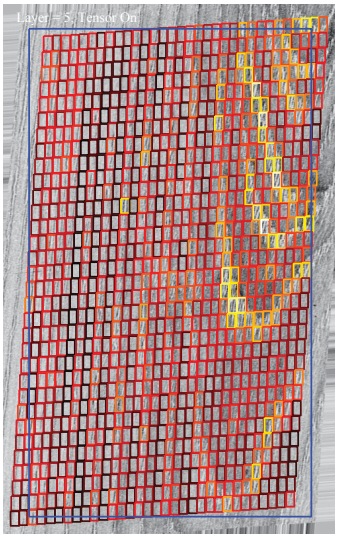

Figure 5.40: Application of the method on combination of all the three i.e. translation, rotation and scaling. The blue line shows the original position while the grids shows final position of the the image

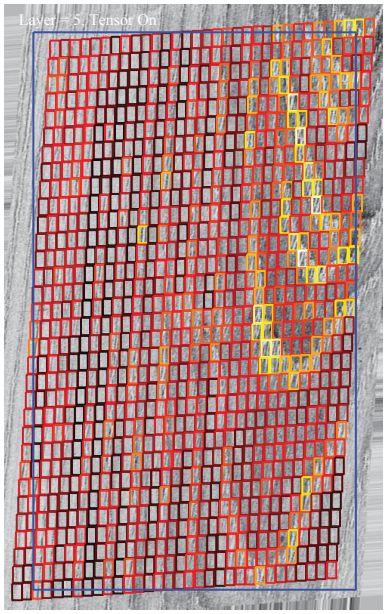

Figure 5.41: Application of the method on Affine distortion. The blue line shows the original position while the grids shows final position of the the image

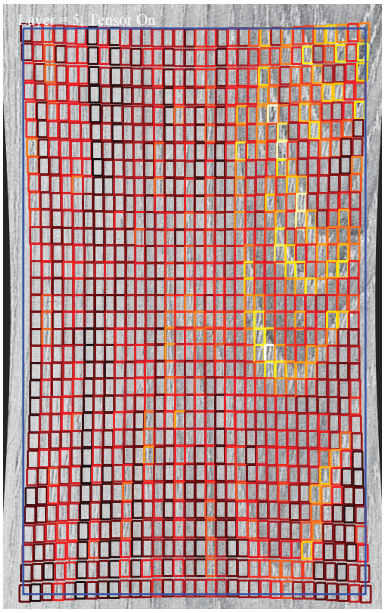

Figure 5.42: Application of the method on Pin and cushion distortion. The blue line shows the original position while the grids shows final position of the the image

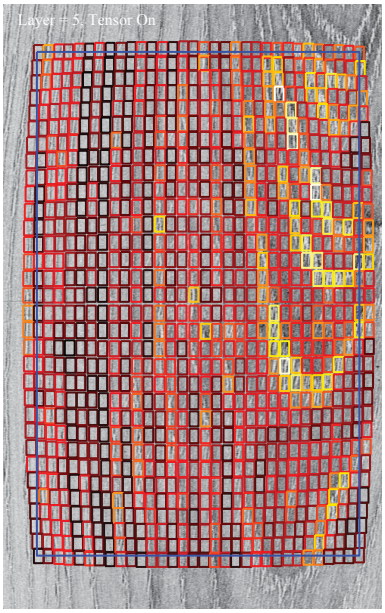

Figure 5.43: Application of the method on Barrel distortion. The blue line shows the original position while the grids shows final position of the the image

5.8.3 Behavior in the presence of noise

The Gram polynomial basis is unitary; consequently, Gaussian noise in data is evenly spread onto all spectral components. The polynomial decimation and tensor regularization serve to reduce the noise power significantly, resulting in a registration which is not susceptible to noise. In Figure (5.44 and 5.45) the registration is shown for images with a signal to noise ratio of $SNR = 0 : 442$,i.e., the noise power is larger than the signal power; also non rigid distortion of both types i.e., Pin cushion and Barrel type has been applied to the data images, Applying the proposed algorithm the result is correct. The present

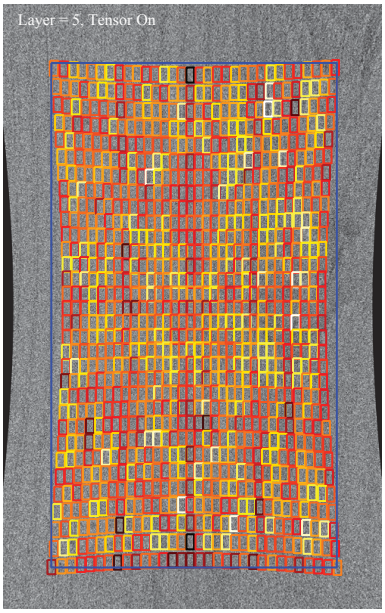

Figure 5.44: Application of the method on Pin and cushion distortion in presence of Gaussian noise. The blue line shows the original position while the grids shows final position of the the image

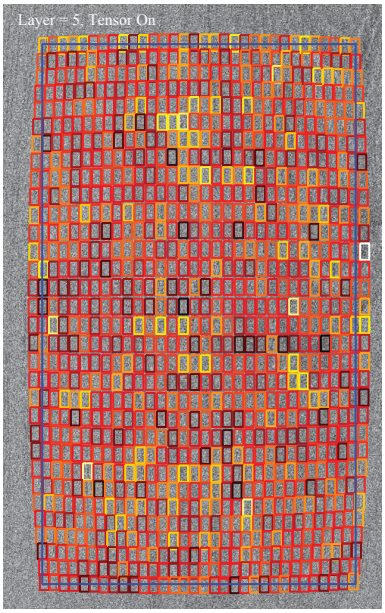

Figure 5.45: Application of the method on Barrel distortion in presence of Gaussian noise. The blue line shows the original position while the grids shows final position of the the image

techniques used for registration are using image intensity for processing, and most of them are sensitive to noise, but the proposed method is an area based phase correlation type of image registration which is quite rigid in the presence of a high amplitude Gaussian noise. In the given tested example a huge Gaussian noise has been added to the data images, It looks like difficult to recognize the distortion for human beings but very fine results are achieved by the proposed method. So the outcome shows that no matter what the amount of Gaussian noise present in data or reference image the distortion or registration could be achieved accurately by the method proposed. A detailed discussion has been given in chapter (6), how the signal to noise ratio changes by changing the amount of Gaussian noise. And a comparison has been presented for different basis functions i.e. Fourier, Gram, Haar, Cosine, and Savitzky Golay smoothing.

5.8.4 Registration with and without decimation

The result of registration using local normalized phase correlation is shown in Figure 5.47, this is basically equivalent to Mellor's method [45]. Considering the results shown in Figure 5.47: the local phase correlation has failed in the upper left corner of the image. Andronache [1] observed a similar effect and considered it to be a loss of statistical consistency in the hierarchical subdivision. Mellor [45] used Fourier based decimation to try and obtain the desired results. However, they failed to observe that the Fourier basis is not well suited to perform aliasing and Gibbs-error free decimation on data representing typical images. Also multiresolution pyramids [39], [37] which use scale-space filtering [41] cannot fully solve this problem. The fundamental problem is that during decimation of the image to lower resolution there are two major sources of error: a Gibbs error which results from the basis function not being able to describe features in the data; the second source of error is aliasing. Commonly aliasing is only considered for periodic basis functions, but the same problem is also present for polynomial basis functions. The issue is further complicated by the presence of Gaussian noise in the image data.

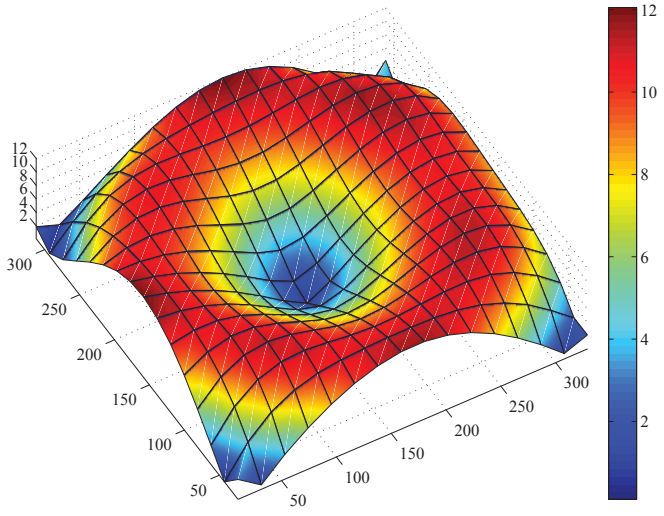

Figure 5.46: The distortion relating the reference image to the registered image, i.e. how far has a patch moved (the dimension is in pixels) from its original position .

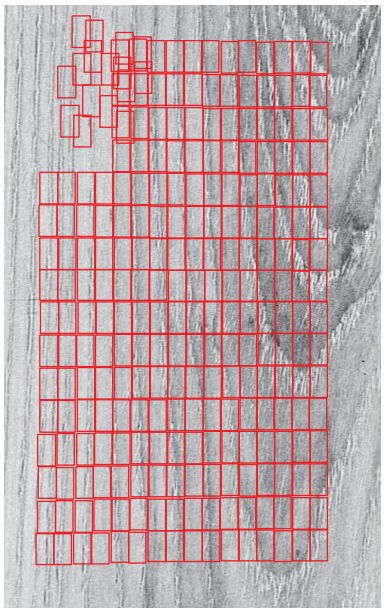

Figure 5.47: Example of image registration without compression during subdivision.

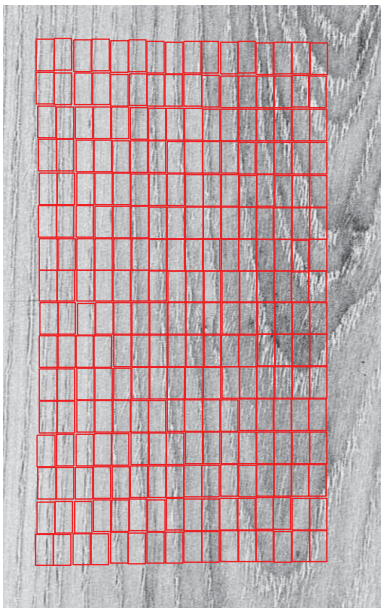

Figure 5.48: The same example as shown in (Figure 5.47) but with consistent Gram polynomial compression.

Chapter 6

Local registration and modified normalized phase correlation

This section presents a new approach to non-rigid elastic registration. A new image decimation procedure based on Savitzky-Golay smoothing is presented and applied in a multiresolution pyramid. Modified Fourier basis functions implemented by projection onto the orthogonal complement of a truncated Gram polynomial basis are presented. The modified functions are used to compute spectra whereby the Gibbs error associated with local gradients in the image are reduced. The new method also presents the first direct linear solution to weighted tensor product polynomial approximation. This method is used to regularize the patch coordinates, the solution is equivalent to a Galerkin type solution to a partial differential equations. The new solution is applied to published standard data set and to data acquired in a production environment.

Numerical testing demonstrations shows that the method provides a good alternative to windowing for signals with significant sub-harmomics components. Further, it is showed that the normalized phase correlation (NPC) can be significantly improved using the new method. The speed of the new solution justifies explicit reference: the present solution implemented in MATLAB requires approximately 1.3 second to register an image of size 800×500 pixels. This is approximately a factor 10 *to* 100 times faster than previously published results for the same data set.

6.1 Decimation and Savitzky-Golay smoothing

Multi-resolution pyramids [40] [37] require that the resolution of the image be reduced as the tree is traversed. This requires a consistent filtering prior to decimation if aliasing and/or Gibbs errors are to be avoided. A Gibbs error would lead to an artificial ringing at edges in the image. This ringing would contribute to peaks in the Fourier spectrum, result is a perturbation of the registration process.

Scale-space filtering [41] i.e. using a Gaussian kernel, has become a common technique to implement filtering in multiresolution pyramids. The problem with Gaussian kernels

is that they are neither periodic nor polynomial and a consistent decimation cannot be achieved in an optimal manner. Andronache [1] observed ". . . the loss of MIs statistical consistency along the hierarchical subdivision . . . ", and proposed information theoretical measures to identify regions in which such errors occur. However, they provided no explanation for the source of this inconsistency.

The classical design of filters implicitly involve the implicit selection of basis functions; the most common of which are the Fourier basis and polynomials [24]. Actually the selection of the best set of basis functions depends on the nature of the data being processed. Images are clearly not periodic and consequently generate a significant error when filtered and decimated using Fourier basis functions.

The use of Gram polynomials for filtering prior to decimation has been proposed by the author in the previous chapter; the Gram polynomials are global basis functions and lead to Gibbs ringing at discontinuities [33] in the image. In this chapter a new decimation process is implemented to perform simultaneous low-pass polynomial filtering and decimation, which is based on Savitzky-Golay filtering [56] [50]. The Gram polynomials are applied as basis functions in local approximation. Filters with monotonic step response can be implemented by correct selection of the support length and local polynomial degree. In this manner Gibbs ringing is avoided. The new process enables the implementation of arbitrary decimation factors. The Savitzky-Golay filtering can be implemented as a linear matrix operation [50] the filtered image D_{sg} is generated by pre- and post-multiplying the unfiltered data D by matrices S_y and S_x^T respectively,

$$D_{sg} = S_y D S_x^T \tag{6.1}$$

The rows of the matrices S_x and S_y contain the coefficients required to implement the desired Savitzky-Golay filter, details can be found in [50]. Given a data matrix D of size $n \times m$ then S_y is $m \times m$ and S_x is $m \times m$. Equation (6.1) implements the Savitzky-Golay filtering without decimation. Given the desired size of the decimated image $p \times q$ then a decimation rate of $\mathrm{d}y = m/p$ is required in the y direction. An indices vector i_y is generated in the range $i_y(k)\ \epsilon\ [1, n]$ with p equidistant nodes. For integer indices the decimating matrix is extracted from S_y directly,

$$S_{y,d} = S_y(i_y, :) \tag{6.2}$$

yielding a $p \times n$ matrix. Linear interpolation between the two adjacent rows S_y is used for non-integer indices. The resulting filtering and decimation process is,

$$D_{sg,d} = S_{y,d} D S_{x,d}^T \tag{6.3}$$

The matrices $S_{x,d}$ and $S_{y,d}$ can be computed a-priory, so that only matrix multiplications are required at run-time. This enables a numerically highly efficient implementation of the required filtering and decimation.

Global Gram polynomial decimation

The concept of of a unitary polynomial basis and their application to least squares approximation has been introduced by Gram in [22]. The Gram-Schmidt orthogonalization process is used to synthesize the polynomials by a three term relationship. But this process is unstable with respect to numerical roundoff errors, so that previously a complete set of discrete polynomials with small enough errors could not be generated for a large number of nodes. These difficulties could only be overcome by new synthesis procedures derived in [51]. And with help of the proposed procedures it is possible to generate a complete set of Gram polynomial basis of the same accuracy as the Fourier basis.

Consider G_d a truncated Gram basis of degree d, whereby the basis is synthesized using the procedure presented in [51]. The least square approximation of the signal y by the basis functions is computed as the orthogonal projection onto the basis functions, i.e.

$$y_g = G_d G_d^T y. \tag{6.4}$$

This component is then removed from the input data,

$$y_r = y - y_g = (I - G_d G_d^T) y \tag{6.5}$$

This residulization process is the projection onto the orthogonal complement of the basis functions. The frequency spectrum S_r is then computed by taking the Fourier transform of the residualization data y_r, i.e.,

$$s_r = F^T y_r, \tag{6.6}$$

$$s_r = F^T (I - G_d G_d^T) y, \tag{6.7}$$

In this case $F_{G,d} = F^T(I - G_d G_d^T)$ can be considered to be modified Fourier basis functions. There are two approaches to perform this computation.

1. It is numerically more efficient to perform a two stage computation, i.e., residualzation followed by an FFT, for a single computation of the spectrum and resiualization on a polynomial of low degree.

2. If computing many spectra, e.g., as is the case when computing power spectral densities, it may be numerically more efficient to compute the modified basis and then apply it multiple times.

Local Gram polynomial decimation

It is also possible to apply local aproximation rather than applying a global approximation to the entire signal y. This method of approximation was introduced by Savitzky and

Golay [56]. Their method was later improved by incorporating Gram polynomials and by addition of end-point computations.

Decimation by local method reduces Gibbs error effects in reconstruction of stepped signal. Comparing the reconstruction of a signal by global method which is described in details in previous chapter and signal reconstruction by local method i.e. Savitzky Golay smoothing, we have less reconstruction error by the local method. An example of a synthetic signal as shown in figure(6.4). In which the test function is a linear ramp in the range $x \in [-1; 1]$ with a slope of 0.5 with the addition of a unit step. First the signal is reconstructed by Fourier method which is a general method and belong to the global type of decimation. Decimation-rate of four is performed using 25 Fourier basis functions. We can see the reconstruction error on the image clearly. Then Gram basis method which also belong to the global type of decimation is applied [3]. The results shows some improvement to the Fourier basis method, but there still error exists. Now finally applying the proposed method which belongs to the local decimation method category, this method is explained in detail in [2]. The results shows much improvements. Showing minimum error as compared to the Fourier and Gram basis methods. So this shows that the local way of decimation reduces the Gibbs error effects and results in more accurate reconstructed signal.

6.2 Generating Savitzky Golay matrix

Consider an input signal y with n data points and a subinterval of this data $y_p(k) = y(k - m : k + m)$ for $p = 2m + 1$ sequential data points, whereby p is called the support length. The points $y_p(k)$ can be regarded as a sliding window, centered at the location k in y. For each position k one output value $z(k)$ is computed from $y_p(k)$. Generalized polynomial spectral filtering can be formulated as,

$$z_p(k) = GHG^T y_p(k) \tag{6.8}$$

Where G is complete Gram basis with p nodes and H is a weighting matrix. Defining $M = GHG^T$ yields,

$$z_p(k) = My_p(k) \tag{6.9}$$

The matrix M is a $p \times p$ matrix where p is an odd number. The matrix M can be partitioned as follow,

$$M = \begin{bmatrix} M(1 : m, :) \\ M(m + 1, :) \\ M(m + 2 : p, :) \end{bmatrix} \tag{6.10}$$

$$M = \begin{bmatrix} M_u \\ M_c \\ M_l \end{bmatrix} \tag{6.11}$$

The center point formula for $z(k)$ is,

$$z(k) = z_p(m+1) \tag{6.12}$$

$$z(k) = M(m+1,:)y_p(k) \tag{6.13}$$

In term of the full signal y,

$$z(k) = M_c y(k-m:k+m). \tag{6.14}$$

This point is centered in the support and the computation is valid for all positions k such that $m < k < (n-m)$. End points formulas are required for the start of and end of the data sequence. These are provided by M_u and M_l, such that,

$$z(1:m) = M_u y(1:m) \tag{6.15}$$

$$z(n-m:n) = M_l y(n-m+1:n). \tag{6.16}$$

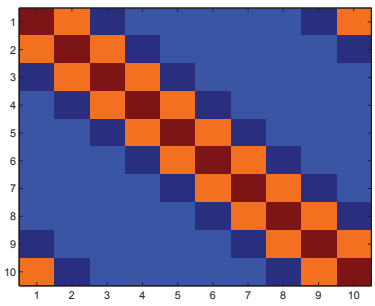

Figure 6.1: structure of the linear transformation for Savitzky Golay smoothing,support length $l_s = 5$, degree $d = 3$ and $n = 10$.

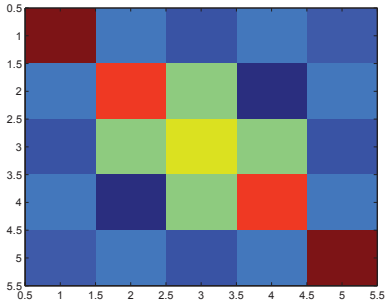

Figure 6.2: sliding window and the points can be regarded as sliding window.

End point formulas are neglected in FIR filtering; indeed for small p the consequences may be negligible. However, in this application the support has a significant length and determines the length of the signal for which the local approximations are computed. In this case the endpoint formulas are essential: The complete local approximation process can now be formulated in a matrix algebraic form by defining the matrix S as,

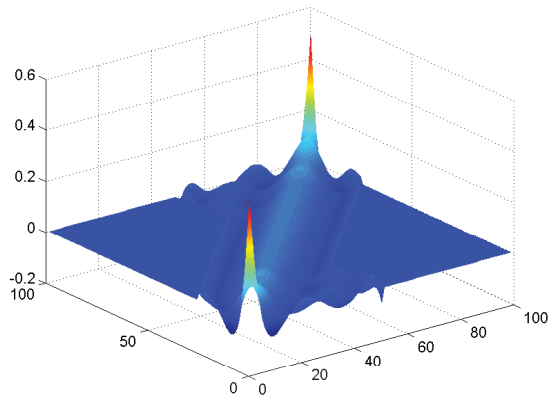

Figure 6.3: Example of transformation matirx with the parameters $l_s = 51$, of degree $d = 5$, and $n = 100$ points

$$S = \begin{bmatrix} \hat{M}_u \\ I_{n-p+1} * M_c \\ \hat{M}_l \end{bmatrix} \tag{6.17}$$

Where $\hat{M}_u$ and $\hat{M}_l$ correspond to post- and pre- augmenting M_u and M_l with the necessary number of zeros, I_{n-p+1} is an $(n-p+1)\times(n-p+1)$ identity matrix as shown in figure 6.1. The local approximation is now computed as,

$$y_l = Sy \tag{6.18}$$

and the residualizatiion, i.e removing the local polynomial estimate for the signal is computed as,

$$y_r = (I - S)y \tag{6.19}$$

This is the proposed local approximation alternative to windowing. We are, however, not proposing to compute the filtering in this manner, since there are numerically more efficient solutions, The advantage of formulating the process as a linear matrix operator $(I - S)$ is that it enables the algebraic analysis of the performance, e.g the covaraince propagation can be computed explicitly.

6.3 Gibbs error problem

It is instructive to consider the decimation of a one-dimensional signal before proceeding to 2D data sets representing images. Consider the simple example shown in Figures 6.4, 6.5, and 6.6: the data consists of a ramp with a slope of 0.5 in the support range $x \in [-1, 1]$ and a superimposed unit step function, the signal has been computed for $n = 100$ points. The decimation-rate of $k = 4$ is simulated for three different cases:

1. the Fourier basis functions. The result of approximating the test signal by the first $m = 25$ Fourier basis functions is shown in Figure 6.4. There are two sources of Gibbs error in this signal: the step function and the ramp. The error associated with the ramp is usually dealt with using windowing; this however modifies the signal spectrum and with this influences the phase correlation;

2. Gram polynomial basis. The recent introduction of polynomial basis [51] which are virtually free from errors, enable new decimation procedures. The result of decimating the signal with the first $m = 25$ Gram basis functions is shown in Figure 6.5, there is no Gibbs error associated with the ramp, since the basis function of degree 1 can model the linear portion of the signal exactly; however, a Gibbs error is still associated with the step function. As can be seen there is significantly lower distortion in the decimated signal than using the Fourier basis;

3. Gram based local polynomial approximation. Both the Fourier and Gram bases are global approaches, i.e., the signal is approximated globally by the respective basis functions over the full length of the support. They have the advantage of globally averaging the Gaussian noise, which is spread evenly onto the coefficients of all the basis functions. Consequently, they are well suited for application to images which have a high degree of noise. However, the global basis functions requires the signal to be modelled globally; consequently, the Gibbs error from the step function is spread over the complete support. An alternative approach is to use local polynomial approximation (Savitzky-Golay smoothing [56]) to perform decimation (see Figure 6.6). This yielded the lowest Gibbs error at the cost of reduced noise suppression.

6.4 Frequency response

The method is further investigated by its frequency and impulse response. Consider a set of n measurement values $y(i)$ which are concatenated to form a column vector y. The output of the linear process is also in the form of vector x. The input to output mapping is effected through multiplication by a matrix A, i.e.,

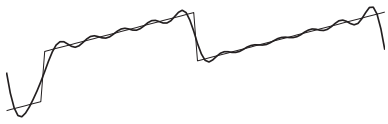

Figure 6.4: The test function is a linear ramp in the range $x \in [-1, 1]$ with a slope of 0.5 with the addition of a unit step. Decimation-rate of four is performed using 25 Fourier basis functions.

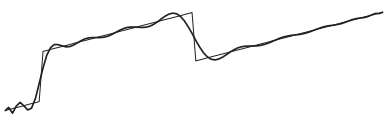

Figure 6.5: Decimation-rate of four is performed using the first 25 Gram polynomial basis functions.

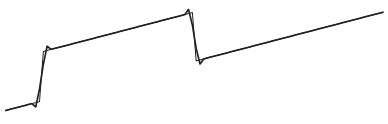

Figure 6.6: Decimation-rate of four is performed so as to prevent aliasing, the resulting Gibbs error is shown for: Savitzky-Golay smoothing with $l_s = 5$ and $d = 2$.

$$y = Ay \tag{6.20}$$

The i^{th} output value is obtained by multiplying the i^{th} row $r_i^T = A(i,:)$ of the matrix A by complete input vector y,

$$x(i) = r_i^T y = \sum_{j=1}^{n} r_i(j)y(j) \tag{6.21}$$

This is the same computation associated with as FIR filter; whereby,r_i can be considered to contain the coefficients of the the filter. Given the coefficients of an FIR filter it is a simple task to compute the frequency response.

Now consider an input vector y of zeros with a single 1 at the location $y(i)$; the output vector x then corresponds to the i^{th} column $c_i = A(:,i)$ of A. Consequently, the i^{th} column c_i of the matrix A defines the impulse response of the linear system to an impulse at the i^{th} input position. Consequently, an invariant frequency and an impulse response of the linear system is only given when the matrix A is circulant [23].

6.5 Frequency response of the residualization process

The process of global and local polynomial approximation can be interpreted as the difference of two independent $FFTs$, for the global case it is formulated as,

$$\begin{aligned} s_r &= F^T(I - G_d G_d^T)y, & (6.22)\\ &= FFT(y) - FFT(G_d G_d^T y). & (6.23) \end{aligned}$$

Given n data points, the matrix $P_{G,d} = G_d G_d^T$ is of size $n \times n$. The matrix $P_{G,d}$ is not circulant; consequently, the frequency response of the residualization process varies across the range of the support, it is not the same for each output value. This can be seen in figure 6.7 where the frequency response of the projection onto degree-1 polynomial basis is shown. The variation of the frequency response across the support is not surprising; this is characteristic of polynomial approximations. However, it can be computed analytically. In the case of windowing, the end points are suppressed very strongly and also have different frequency response. The frequency response for polynomial filter at the center of the support is shown in figure 6.8 for degree 1,3 and 5.

6.6 Savitzky Golay decimation and comparative results

The above discussion concludes that if the Gram polynomial basis functions are applied locally to reconstruct a signal then it give more accurate result.

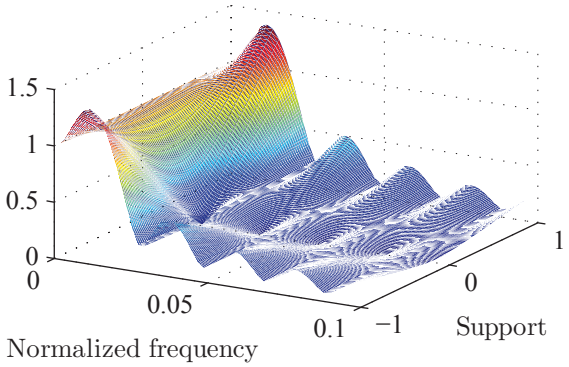

Figure 6.7: Frequency response for the polynomial filters $P_{G,d}$ of degree 1. Each row of the matrix has a particular frequency response as an FIR filter

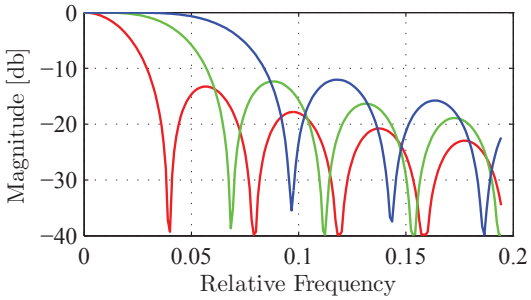

Figure 6.8: Frequency response for the polynomial filters $P_{G,d}$ of degree 1,3 and 5. This computation has been performed at the center of the support, that is shown in figure 6.7.

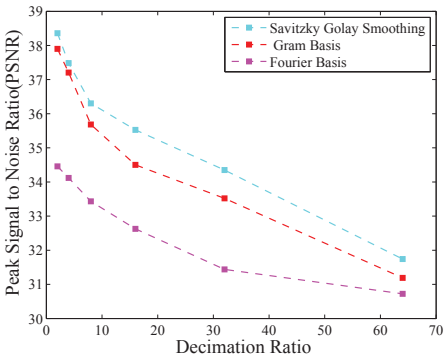

Figure 6.9: Variation in the peak signal to noise ratio(PSNR) with respect to variation in decimation ratio for Gram global, Fourier and Gram local basis functions.

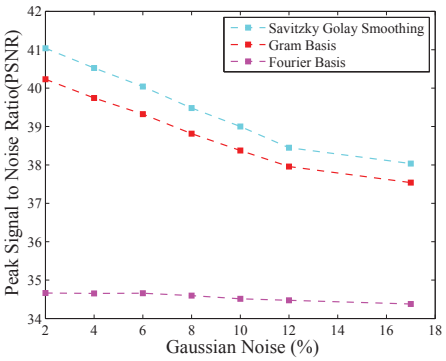

Figure 6.10: Variation in the peak signal to noise ratio(PSNR) with respect to variation in Gaussian noise for Gram global, Fourier and Gram local basis functions.

By replacing the Fourier basis function to Gram basis improve to some extent but Gram basis are globally applied, which results with some error at the gradients. Savitzky and Golay [56] applied the basis function for data smoothing or regression locally, similarly applying the Gram basis locally we achieve some satisfactory result. These three methods are applied on the well known Lenna image for different decimation ratio and additional Gaussian noise and a graph is plotted for these results as shown in figure 6.9 and 6.10. Signal to noise ratio is the one method through which the quality of an image could be calculated. The Lenna image is reconstructed by the three methods,i.e., Fourier basis,

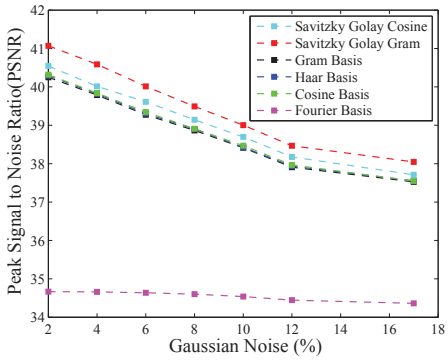

Figure 6.11: Variation in the peak signal to noise ratio(PSNR) with respect to variation in decimation ratio for Gram and Fourier basis functions

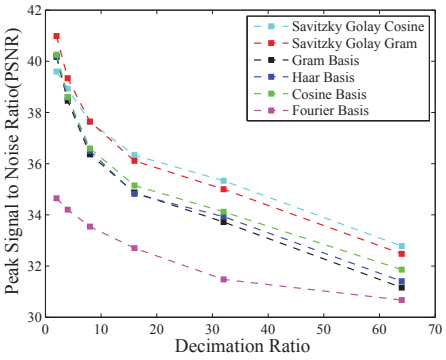

Figure 6.12: Variation in the peak signal to noise ratio(PSNR) with respect to variation in decimation ratio for Gram and Fourier basis functions.

Gram basis global and Gram basis local at different decimation rates, and consecutively the peak signal to noise ratio are determined. The pink line present the change in peak signal to noise ratio for Fourier basis, the red line presents Gram basis and the cynic color line presents Gram basis applied locally. This leads us to the conclusion that if the Gram basis is applied locally like Savitzky Golay smoothing then the results are better for minimum decimation ratio as compared to Fourier basis or Gram basis globally. The tests are also done for changing the additional Gaussian noise and the results are presented in figure (6.10). For changes in additional Gaussian noise again the Gram polynomial decimation locally outclass the other two approaches. This further proves the quality of the proposed method which also satisfactory in presence of any additional Gaussian noise.

All the basis functions i.e. Fourier, Gram basis globally, Gram basis locally, Cosine and Haar basis are applied for the same test; the results are presented in figure 6.11 for change in decimation ratio and similarly for change in the additional Gaussian noise as in figure 6.12. In the whole test it is proved that local decimation outclass the all other basis functions either changing the decimation factor or the additional Gaussian noise. It is further tested on a mixed signal reconstruction as shown in figure 6.13, and we can say that in this case also the local basis better synthesize the mixed signal as by the other basis functions.

6.7 Image registration by local method

The proposed method of local decimation has already been applied on all major type of rigid and non-rigid registration. These further improve the results obtained by the Gram polynomial decimation registration method which is applied globally. The challenging task was to accurately register non-rigid and elastic distortion with minimum processing time. Hence on one side if the proposed method remove the Gibbs error problem which enhance the exact registration, on the other side the decimation on each layer decrease the processing time. And some data image like 1200×1500 of size is processed just in few seconds. A significant speed improvement has been achieved. Using the same data as presented by Suarez et al. [59], the proposed method requires approximately 1 sec. to perform registration. In comparison, Suarez et al. required 7 mins, and their alternative method [58] required 15 mins. This is an improvement in the range of 2 to 3 orders of magnitude.

The proposed method of local decimation and then registration is further tested on a porous compressible medium, which is compressed to find the properties of the material, see Figure 6.14, 6.15 and 6.16. The typical barrel distortion with flat tops and bottoms can be observed. The area of the original grid can be compared with the area of the compressed grid to determine the volumetric compression of the material. Figure 6.14 shows the block position before distortion, figure 6.15 and 6.16 presents the final position

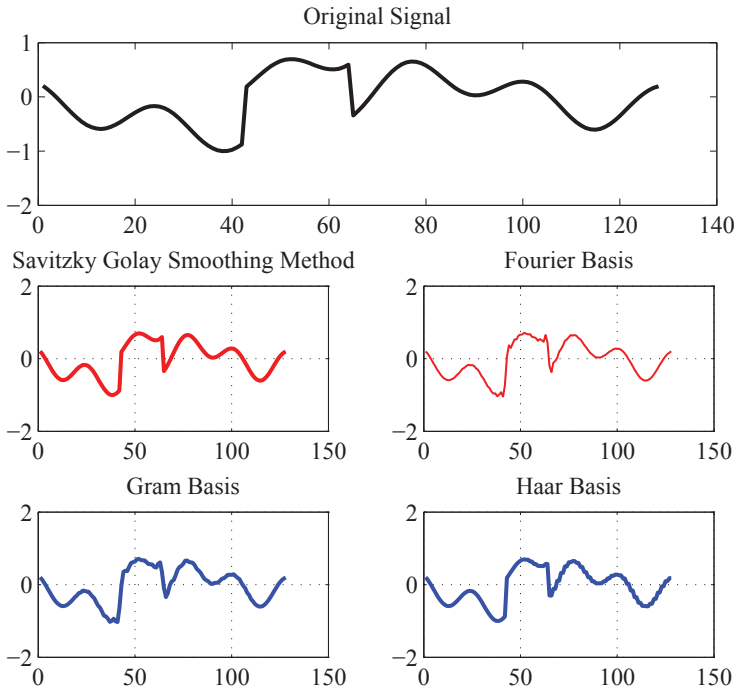

Figure 6.13: Comparison of the Fourier, Gram basis global, Haar basis and Gram basis local. A signal is reconstructed by all these methods and the results are shown.

after distortion. The grid shows the non-rigid registration. Gram polynomial basis are applied globally, but distortion is not properly registered as shown in figure 6.15. When the Gram basis are applied locally for decimation, the results are accuratelly achieved which are shown in figure 6.16.

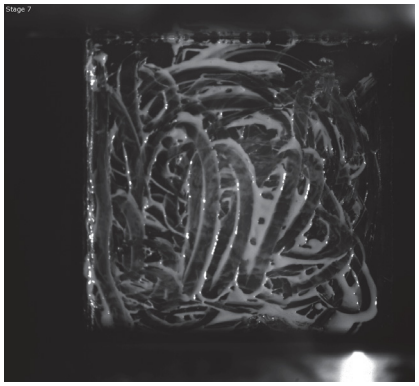

Figure 6.14: Test specimen for compression testing. This is a porous compressible medium.

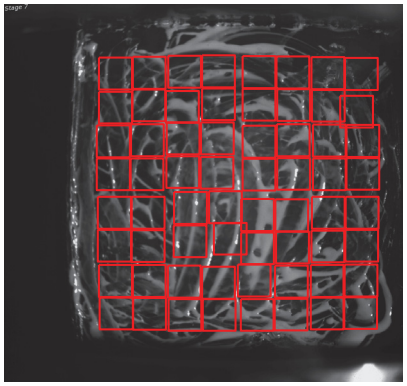

Figure 6.15: The sample under compression, and the compression distortion is found by the grid. The Gram basis failed globally to find the exact registration

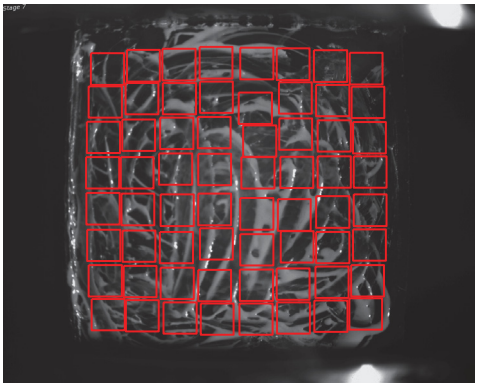

Figure 6.16: Applying the Gram basis locally the compression distortion is found accurately as shown by the grid.

Chapter 7

Registration enhancement by regularization

Normalized phase correlation delivers the coordinates for each shifted patch. The shifted positions are also affected by noise in the image, and numerical errors associated with the computation. There is no guarantee that the coordinates of the patches lie on a grid which corresponds to an elastic deformation. Regularization of the coordinates onto a grid which is consistent with the solutions of a partial differential equations for elastic deformation can be achieved by approximation by a tensor product of global polynomial basis functions.

Here we propose the alternative approach of using a bivariate Gram-polynomial tensor product for regularization. Given the matrices X and Y containing the coordinates of the original points, i.e. the reference point, of the patches and G_r the Gram polynomial basis functions of degree r, the least squares tensor product approximation for the coordinates can be computed as follows,

$$X_r = G_r\{G_r^T X G_r\}G_r^T \quad \text{and} \tag{7.1}$$

$$Y_r = G_r\{G_r^T Y G_r\}G_r^T \tag{7.2}$$

This approach is significantly faster than using spline approximations.

7.1 Image registration by splines

Modelling of machine's parts by bending long wood or metal strips is termed as "splines". The desired model is obtained by attaching some weights at certain positions or bending these strips by some other ways. The same method is used in image processing to model certain spatial transformations. If we have two surfaces, i.e., reference and data, then certain points are selected in these two surfaces and a $2D$ transformation is used to

compare or register these two surfaces. Registration of reference and data images by splines works on the principle that some points are selected in reference image and these points are then identified in the data image. These points are called as control points. Spline-based transformations either interpolate or approximate the distances at these points. Between these control points a smooth varying displacement is achieved. The interpolation condition for both data and reference surface is modelled as follows:

$$T(\phi_i) = \phi_i^{'} \tag{7.3}$$

Where ϕ_i indicates the location of selected control points in data image and $\phi_i^{'}$ shows the location of the corresponding selected points in the reference image. There are many different techniques used to find these control points. Intensity based and Geometric based registration are commonly used. Intensity-based registrations match intensity patterns over the whole image but do not use anatomical knowledge. Geometric registration uses anatomical information but usually sparsely distributed throughout the images. Combining geometric features and intensity features in registration should result in more robust methods. Hybrid algorithms are therefore of particular current interest, combining intensity-based and model-based criteria to establish more accurate correspondences in difficult registration problems, of the these the one is geometrical method which could be recognized in data and reference image by spline- based transformation mapping functions.

7.2 Regularization by Gram basis

The position of the individual patches is subject to some error. Thin-plate splines have been applied to regularize the coordinates of the patches; [39] unfortunately, their computation is numerically intensive. The functional for such a tensor product approximation [35] [43] [74] is,

$$E = ||G_y S G_x^T - D||_F \tag{7.4}$$

The aim is to determine the values of the entries in the matrix S which minimize the functional. Given the Gram polynomials as global basis functions a linear solution to the minimization of the functional is known, to be the projection onto the orthogonal complement,

7.2.1 Bivariate Gram-polynomial tensor product regularization

Looking at figure 7.1 and 7.2 we can see the original problem during registration. An image is distorted with 12 *percent* pin cushion distortion. Non rigid registration technique is applied to register this image with the image before distortion i.e reference image, but the image could not be registered accurately and we can see the wrong registered grid at the center of the image as in figure 7.1. In this test no regularization was applied. Now Some extra distortion i.e. 15 *percent* is applied to the same image and again try to register the

image and find the distortion. This time the bivariate Gram-polynomial tensor product regularization is applied along with the registration method. An accurate registration is achieved after applying the proposed method as in figure 7.2. The application of Gram-

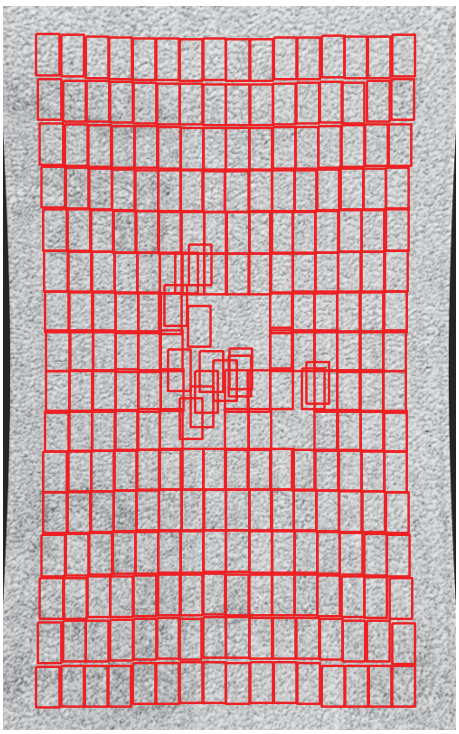

Figure 7.1: The image is distorted with 12 *percent* pin and cushion distortion. The method is failed to register the image without applying the tensor approximation.

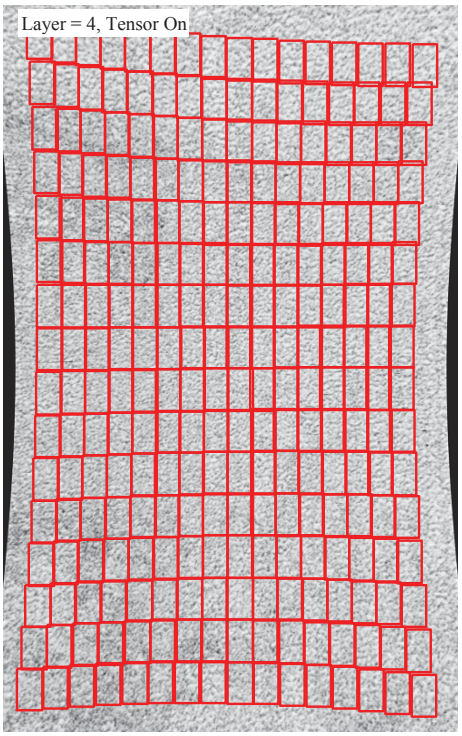

Figure 7.2: The image is distorted with 15 *percent* pin and cushion distortion. Registration is achieved after applying the tensor approximation.

polynomial tensor product regularization further enhances the non-rigid registration. And the proposed method is the replacement of the spline methods, which are mostly used for the tensor approximation purposes, they also take more time for data computation.

7.2.2 Proposed tensor approximation and Galerkin's method

One of the most important weighted residual methods was invented by the Russian mathematician Boris Grigoryevich Galerkin (February 20, 1871 - July 12, 1945). Galerkin's method selects the weight functions in a special way: they are chosen from the basis functions, i.e. $w(x) \in \{\phi_i(x)\}_{i=1}^{n}$. It is required that the following equations hold true

$$\int_a^b \phi_i(x)\ (L[u(x)]\ + f(x))\mathrm{d}x = 0 \qquad \text{for} \quad i = 1, 2, 3....., n \tag{7.5}$$

The proposed work presents the first direct linear solution to weighted tensor product

polynomial approximation. This method is used to regularize the patch coordinates, the solution is equivalent to a Galerkin type solution to a partial differential equation. The boundary condition at the border has been removed and replaced with the constraint that the mean distance of all patch positions to the solution of the partial differential is zero. The new solution is applied to test samples and compare with other methods. The speed of the new solution justifies explicit reference: the present solution implemented in MATLAB requires approximately 1.3 s to register an image of size 800×500 pixels. This is approximately a factor 10 to 100 faster than previously published results for the same data set.

Regularization of the coordinates onto a grid for elastic deformation can be achieved by approximation by a tensor product of global polynomial basis functions. The functional for such a tensor product approximation is,

$$E = ||G_y S G_x^T - D||_F \tag{7.6}$$

The aim is to determine the values of the entries in the matrix S which minimize the functional. Given the Gram polynomials as global basis functions a linear solution to the minimization of the functional is known, to be the projection onto the orthogonal complement,

$$S = D - G_y G_y^T D G_x G_x^T \tag{7.7}$$

A further issue which needs to be considered is that not all patches have the same information content. It is desirable to weight the coordinates of a patch by the information contained in the patch, i.e. patches with a higher information content are given more significance during the least squares approximation process. Given the matrix of weights W, the functional for the weighted tensor product approximation can be formulated as,

$$E_w = ||W^{o\frac{1}{2}} \circ \{G_y S G_x^T - D||_F \tag{7.8}$$

7.3 Entropy-weighted tensor polynomial regularization

Without weighting the least squares with ordinary polynomials will have wrong average interpolation over all the surface if the images have local geometric differences or the control points in a local neighborhood are inaccurate. The resultaning approximated registration will not find the exact distortion produced in the data image. In the proposed method the information available in the image is kept as weighting function. In some area of the images there will be very less information available and will be difficult for the phase correlation to find the exact registration. Therefore entropy plays its role in this regards, and the approximated value is allotted to those portions having no information. The solution for S which minimizes the functional Ew has been considered a non-linear task in the past. This work presents the first direct linear solution to this task based on the Kronecker product. The coordinates of the registered patches are regularized by weighted

least squares approximation by a sum of a tensor products of Gram polynomials. [22] [51]. The weighted tensor product of two sets of truncated Gram polynomial basis functions of maximum degree n ensures that the solution lies on a $C(n)$ continuous grid. This is consistent with the elastic deformations of the sample which are also $C(n)$ continuous up to the end point. The entropy of the data contained in each patch is used as a weighting factor during the least squares tensor approximation. This ensures that patches with low information content do not contribute so strongly to the functional as do the patches with a strong information content. There are three specific cases which need to be considered for a general solution:

7.3.1 The matrix W is rank one and positive semi-definite

If rank $W = 1$ then the matrix can be computed from two vectors, a left w_l and right w_r singular vector respectively,

$$W^{\circ\frac{1}{2}} = w_l w_r^T = w_l \otimes w_r \tag{7.9}$$

The left w_l and right w_r singular vectors are determined by applying singular value decomposition to $W^{\circ\frac{1}{2}}$. Now substituting into equation 7.8 yields,

$$E_w = \|\text{diag}\{w_l\} G_y S G_x^T \text{diag}\{w_r\} - W^{\circ\frac{1}{2}} D\|_F \tag{7.10}$$

The normal equations associated with the above functional can be solved directly and linearly for S yielding,

$$S = (\text{diag}\{w_l\} G_y)^+ \; W^{\circ\frac{1}{2}} D \; (G_x^T \; \text{diag}\{w_r\})^+ \tag{7.11}$$

7.3.2 The matrix W is rank one and is strictly positive definite

If w_l and w_r are strictly positive the problem can be solved directly using weighted polynomial basis functions.

7.3.3 The matrix W is full rank and strictly positive definite

If the matrix W is full rank and strictly positive definite, then the functional (7.8) must be vectorized. Consider the properties of the Kronecker product,

$$\text{vec}\{AXB\} = (B^T \otimes A)\text{vec}\{X\} \tag{7.12}$$

The vec {X} corresponds directly to the MATLAB operator X(:). Now consider,

$$\text{vec}\{G_y S G_x^T\} = G_x \otimes G_y \; \text{vec}\{S\} \tag{7.13}$$

Before proceeding further it is helpful to define some succinct notations,

$$s = \text{vec}\{S\}, \quad d = \text{vec}\{D\} \quad , \quad A = G_x \otimes G_y, \quad \text{and} \quad V = \text{diag vec}\{W^{\circ\frac{1}{2}}\}\} \tag{7.14}$$

Now vectorizing Equation 7.8 using this notation yields,

$$E_w = \|V\{As - d\}\|_2^2 \tag{7.15}$$

This is the cost function for a weighted vector approximation, the solution for s which minimized E_w is well known $s = \{VA\}^+ Vd$. For numerical reasons it is more efficient to compute,

$$s = \{VA\}^+ \ \text{vec}\{W^{\circ\frac{1}{2}} \ \circ \ D\} \tag{7.16}$$

This is a direct linear solution and is non-iterative. Consequently, the number of computations required can be determined a-priori making this solution suitable for real-time applications. In this application the entropy of the data contained in each patch is used as the corresponding weight. Since all images contain some noise the entropy will be strictly positive and it must be assumed that the matrix W is full rank. The coordinates of each patch are reformed to generate a matrix of X and of Y coordinates. Both matrices are regularized using the above procedure.

7.3.4 Improvement of Galerkin's method

The new method, whereby the solution is generated from a tensor product of Gram basis functions, is fundamentally equivalent to the Galerkin method of solving partial differential equations. However, its implementation is considerably better in its numerical efficiency. The boundary condition at the border has been removed and replaced with the constraint that the mean distance of all patch positions to the solution of the partial differential is zero.

7.3.5 Comparison of the two methods

It is known that in the area of numerical analysis, Galerkin methods belongs to the class of methods for converting a continuous operator problem i.e. a differential equation to a discrete problem. In principle, it is the equivalent of applying the method of variation of parameters to a function space, by converting the equation to a weak formulation. Some constraints on the function space are applied to characterize the space with a finite set of some basis functions. Solving differential equations in which the solution is assumed to be well approximated by these function of a particular form having a finite set of degree and then any one of a theoretically infinite set of methods of weighted residuals are applied in an attempt to find which precise value each of these degrees of freedom should take in order to minimize these residuals in some way the residue function. The Galerkin method, which uses the basis functions themselves as test functions or in the more general case of a nonlinear assumed form (where the nonlinearity is in the degrees of freedom) of the

solution the Galerkin method uses the test functions. For all these approximating testing we have the Governing equation a very basic equation, which is written as follows;

$$f(u) = 0 \tag{7.17}$$

For load application on a beam,

$$f(u) = P \tag{7.18}$$

This equation sates as we apply load on a beam then the stress produced is equal to the load P applied. There are many approximation methods to find the stress produced in the beam, which is not the exact solution of the problem to find load. For the approximated guess we will have,

$$f(\bar{u}) - P = e \tag{7.19}$$

This presents that the approximated value $\bar{u}$ will have some error being not the exact solution. But our target is to keep this error as minimum as possible. Most of the cases basis functions are used to find these approximation i.e. $\bar{u} = a_0 + a_1 x + a_2 x^2$. Galerkin proposed a test to find the solution with minimum error by introducing a weighted function multiplication to the approximated value with some boundary condition.

$$\int_x \; w \;\; e \; \mathrm{d}x = 0 \tag{7.20}$$

Putting equation 7.19 in 7.20 we will have.

$$\int_x \; w \;\; (f(\bar{u}) - P) \; \mathrm{d}x = 0 \tag{7.21}$$

Equation 7.21 is a typical Galerken equation for one dimensional case. Looking at the proposed functional for such a tensor product approximation is,

$$E = ||G_y S G_x^T - D||_F \tag{7.22}$$

In which the aim is to determine the values of the entries in the matrix S which minimize the functional. Given the Gram polynomials as global basis functions a linear solution to the minimization of the functional is known, to be the projection onto the orthogonal complement, the patch coordinates are weighted by the information contained in the patch, i.e. patches with a higher information content are given more significant during the least squares approximation process. Given the matrix of weights W, the functional for the weighted tensor product approximation can be formulated as,

$$E_w = ||W^{o\frac{1}{2}} \circ \{G_y S G_x^T - D||_F \tag{7.23}$$

Comparing equation 7.21 and 7.23 looks exactly same equation. Both are calculating the approximated solution by using the basis functions and the result is then weighted for minimizing the error. In the proposed method the Gram polynomial are used as basis functions being unitary basis and there solution is complete. On the other hand the Gibbs error problem is minimized by local application of the basis functions.

7.3.6 Behavior in the presence of noise

There are some factors which lead to a wrong non-rigid registration, one common factor is the noise arising from the processes of image acquisition and feature extraction. The resulting feature points cannot be exactly matched if there is noise present in the data or reference or both images. Another factor is the existence of outliers i.e many point features may exist in an image that have no corresponding points in the reference image and hence need to be rejected during the matching process. Finally, the geometric transformations may need to incorporate high dimensional non-rigid mappings in order to account for deformations of the point-sets. It should be possible to solve for the correspondences between selected area in the data and reference images and reject outliers and determine a good non-rigid transformation that can map a data image to a reference image.

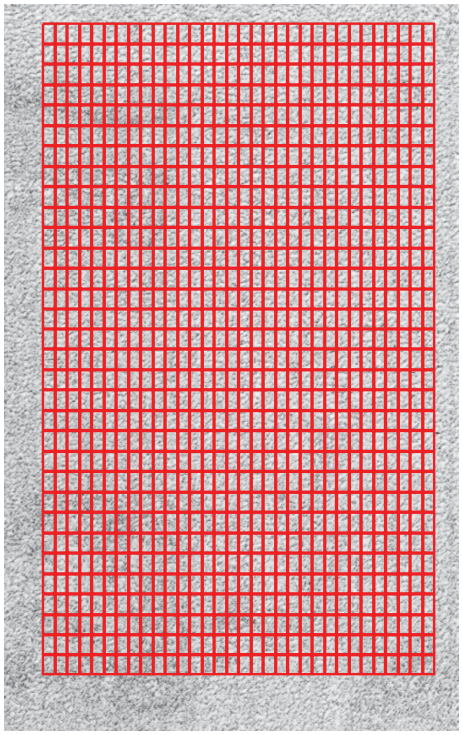

Figure 7.3: The original stochastic image to be registered after some addition of Gaussian noise

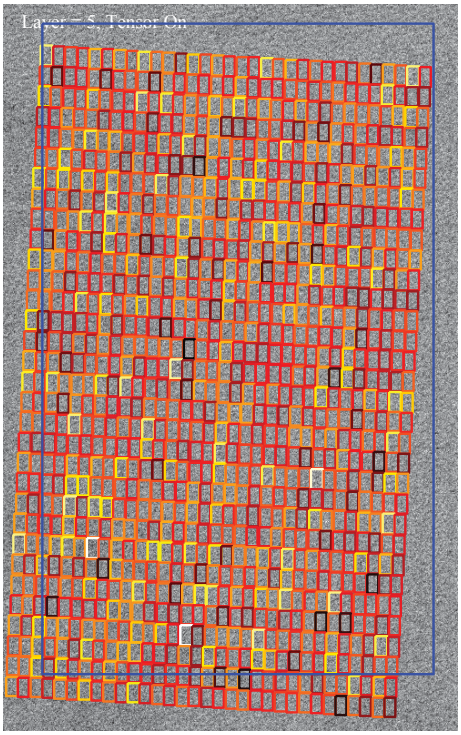

Figure 7.4: 15 percent Gaussian noise added to the image and the registered image is shown. The blue line presents the original image position and the colored grid presents the deformation in the image

This could be explained by the example presented in the figure 7.3 and 7.4. A stochastic image has rotational deformation and an additional 15 *percent* Gaussian noise has been added to the data image. The proposed algorithm of non-rigid registration with bivariate tensor approximation is applied to register the two images. The results are shown, as, the blue line presents the position of the reference image, and the grids shows the image after deformation.

Chapter 8

Published Papers

Non-Rigid Registration for Quality Control of Printed Materials[1]

Amir Badshah[1], Paul O'Leary[1], Matthew Harker[1] and Christian Sallinger[2]
[1] University of Leoben, A-8700 Leoben, Austria
[2] IPAC Improve Process Analytics and Control GmbH, Europastrasse 8, A-9524 Villach, Austria

Abstract

This paper presents a new approach to non-rigid elastic registration. The method is applied to hyper spectral imaging data for the automatic quality control of decorative foils which are subject to deformation during lamination. A new image decimation procedure based on Savitzky-Golay smoothing is presented and applied in a multiresolution pyramid. Modified Fourier basis functions implemented by projection onto the orthogonal complement of a truncated Gram polynomial basis are presented. The modified functions are used to compute spectra whereby the Gibbs error associated with local gradients in the image are reduced. The paper also presents the first direct linear solution to weighted tensor product polynomial approximation. This method is used to regularize the patch coordinates, the solution is equivalent to a Galerkin type solution to a partial differential equations. The new solution is applied to published standard data set and to data acquired in a production environment. The speed of the new solution justifies explicit reference: the present solution implemented in MATLAB requires approximately 1.3 s to register an image of size 800 500 pixels. This is approximately a factor 10 to 100 faster than previously published results for the same data set.

1 Introduction

Many products and most modern furniture are given their final optical finish by laminating or gluing decorative foils onto the surface. The self adhesive foils and laminates are printed with decorative patterns, some examples of which are shown in Figures 1 to 4. There are many thousands of patterns, whereby the characteristic features vary strongly. Some of the patterns have a strong geometric content, e.g. Figure 1, some imitate natural structures, e.g. Figures 2 and 3, while yet others are almost purely stochastic as can be seen in Figure 4. In particular for the production of furniture, it is important that the decorative patterns can be reproduced with the same optical quality over a period of many

[1]This paper presented in QCAV'2011 conference, 28-30 june Saint-Etienne, France

years, i.e., a piece of office furniture bought years later should generate the same optical impression. This requires a stringent quality control, of both the spatial pattern and its spectral properties. Furthermore, the decorative foils are subject to deformations during the lamination process. The laminating press exerts a force on the foil which tends to stretch before the layer of glue hardens. These deformations have in the past precluded an automatic quality control, since simple registration is not sufficient to enable comparison of the patterns properties. This paper presents a new solution to non-rigid registration which is used in conjunction with an Advanced Colour Measurement System (ACMS).

Figure 1: Example of a decorative laminate with a strong geometric design. The pattern is both partially and globally repetitive.

Figure 2: Imitation wood laminate.

Figure 3: Imitation stone laminate.

Figure 4: Example of a laminate with an almost purely stochastic pattern.

The two survey papers [28, 13] and the workshop dedicated to biomedical image registration [5] show the vast extent of material published on non-rigid registration. Two major techniques have evolved as reliable solutions to nonrigid registration:

1. Feature based registration, see Zitova [28]. In this technique specific features are identified in both the reference and measurement images. The matched features are used to determine a mapping between the two images. This techniques is well suited to images where features are unique and evenly distributed across the image. The method can deal with discontinuities in the deformation, since the features are individually matched. However, some of the patterns in this application, e.g. the pattern in Figure 4, are almost purely stochastic and will not deliver reliable features. Furthermore, the techniques only uses a discrete set of features and as such does not take advantage of all the information in the image, this has detrimental consequences for the signal to noise ratio. For these reasons this approach was deemed to be unsuitable in this application;

2. elastic registration which is most commonly implemented using some form of hierarchical subdivision, also called pyramid processing, see Lester [13] for a survey of such techniques. The distortions generated during the lamination process are indeed elastic in nature, suggesting that an elastic registration approach is suitable. However, the techniques suffered from a speed problem which would make their present implementations unsuitable for real time non-rigid registration.

A good overview of non-rigid or elastic registration can be gained from studying the review articles [13, 28] and the present state of the art in medical imaging can be found in [5]. The solution presented here falls into the general class of hierarchical subdivision[2]; whereby, three new and major contributions are made:

1. a new decimation techniques is introduced based on Savitzky-Golay smoothing. This technique ensures consistent data and information reduction at each layer in the tree. This is a very important step and has been underestimated in the past. Correct decimation of the image ensures the minimization of the Gibbs error associated with the step, which in turn improves the result of local registration. Furthermore, correct decimation is instrumental in making the registration solution numerically efficient;

2. a modified normalized phase correlation method is introduced to perform local registration. The Fourier basis is modified by projection onto the orthogonal complement of a degree $d = 1$ Gram-polynomial. This eliminates the effects of intensity and intensity gradients within a patch. This modification is an alternative to windowing in Fourier analysis [18];

3. a new direct, i.e. non iterative, solution to least squares approximation via weighted bivariate Gram polynomial tensor product is presented. The least squares weighted tensor product is used to regularize the positions of the patches at each level in the tree structure, whereby the entropy of the patch is used as weight. This new approach is numerically efficient and optimal in terms of finding a least squares solution in the presence of Gaussian perturbations;

4. the new solution can be computed in real-time and is suitable for in-line quality control. Presently the algorithm requires approximately 1 second to register an image with 500×800 pixels. This is significantly faster than other reported solutions, Suarez et. al [22] require and with a "Fast entropy" method [21] they require 15 minutes .

2 Data Acquisition: Advance Color Measurement System

The Advance Color Measurement System (ACMS) is a new industrial scanner which performs spatially resolved color measurements of decorative and multi-colored patterned

[2]The literature pertinent to the new issues is reviewed in the relevant section of the paper.

surfaces. The system uses hyper-spectral [4] imaging to scan an area of maximum $8 \times 20\ cm$ with a spatial resolution of $125 \mu m$. Each pixel is measured with 81 spectral windows within the CIE-specified [10] wavelength range $380 \ldots 780 \mu m$ yielding a spectral resolution of $5 \mu m$. The measurement result is stored in a 3-dimensional data-cube of size $640 \times 160 \times 81$.

The aim of the measurement is to determine if the spatial distribution of the spectral properties on the newly produced foil corresponds to the desired reference. The task is further complicated by the elastic deformation of the foil which may occur during the lamination process. The deformation is the same for all spectral layers, since the foil is produced from a single printed layer. The 81 spectral layers are summed-up to generate a single image I_m of size 640×160. This image is used to perform registration prior to comparing the spectral properties at each layer.

3 Elastic registration

The deformations of the decorative layer which occurs during the lamination process is a true elastic deformation. The flow of the foil — a 3D viscous material — results from anisotropic forces during the lamination process, which are the result of irregularities in the surface onto which the foil is being laminated and due to nonuniform distribution of the glue. This is in strong contrast to the general case in non-rigid registration, e.g. in medical imaging tissue[3] growth plays a major role — this is a non-conservative process. Computational techniques based on partial differential equations for fluid dynamics [25, 19, 26] have become popular as a means of implementing elastic registration. Most commonly the Navier-Stokes equation is used to describe the motion of the viscous fluid,

$$\frac{\partial \boldsymbol{u}}{\partial t} + \boldsymbol{u} \cdot \nabla \boldsymbol{u} = \frac{\nabla \boldsymbol{P}}{\rho} + v \nabla^2 \boldsymbol{u} \tag{1}$$

whereby, $\boldsymbol{u}$ is the velocity vector, $\boldsymbol{P}$ is the pressure vector, ρ the fluid density and v is the kinematic viscosity. However, there are a number of unsolved problems associated with this approach:

1. the measurement is a 2D observation of a 3D deformation. Wang and Staib [24] deal with this issue by modifying the Navier-Stokes equation to remove the constraint that the volume of the fluid is invariant and proceed to solve the modified equation. An alternative is to assume that the thickness of the film remains unchanged, so that the flow is characterized by the 2D observation. In this case the Navier-Stokes equation can be simplified to 2D field. This may be a valid approximation for films where thickness is small with respect to the local deformations;

2. it is assumed that the force is applied over the boundary of the image. Consequently the forces at the boundary and the corresponding deformation would yield a valid boundary condition of the solution of the differential equation within the field. This

[3] This image is used during method testing and comparison of methods since it is freely available online and results from other research groups are available for this image pair.

assumption is not true for the application at hand. The lamination press together with the irregularities in the surface and thickness of the layer of glue yield a distribution of forces over the field of observation.

3. the solution of the differential equation corresponding to the observation is determined via iterative approaches [25], both boundary element methods and finite element methods have been investigated [6]. The solutions are computationally prohibitive if they are to be applied in a real-time quality control application.

The aim of using a specific partial differential equation is to introduce regularization into the solution, i.e. the motion within the registration process is forced to lie on a path corresponding to a solution of the partial differential equation. This improves the quality of the solution by reducing the influence of perturbations, if the partial differential equation truly describes the system being observed.

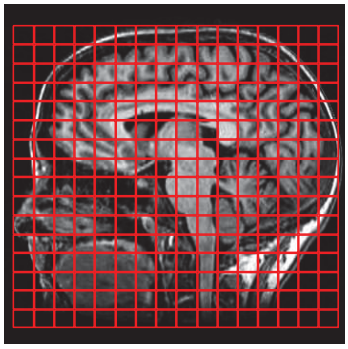

Figure 5: Reference image with the final layer reference patches .

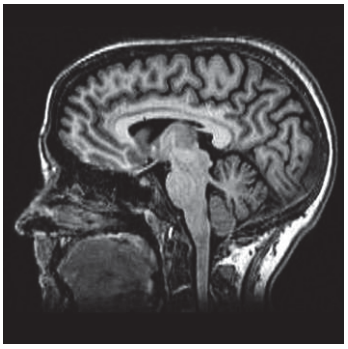

Figure 6: Image which is to be registered.

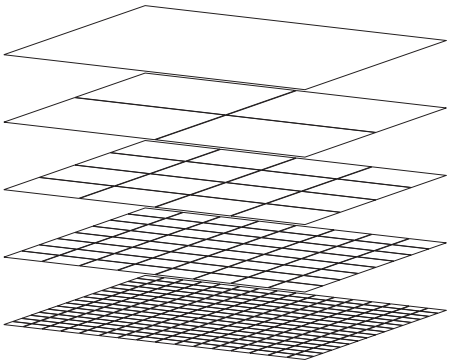

Figure 7: Reference decomposition tree, with five layers

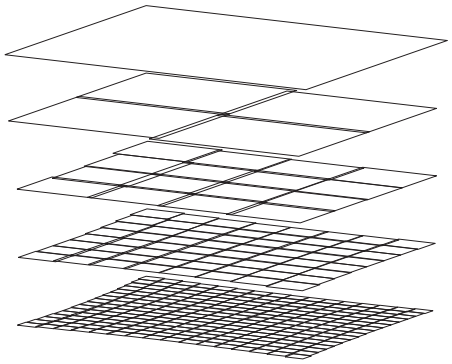

Figure 8: Registered decomposition tree, with five layers, the modified position of each patch can be seen.

The new method, whereby the solution is generated from a tensor product of Gram basis functions, is fundamentally equivalent to the Galerkin method of solving partial differential equations. However, its implementation is considerably better in its numerical

efficiency. The boundary condition at the border has been removed and replaced with the constraint that the mean distance of all patch positions to the solution of the partial differential is zero.

3.1 Decimation and Savitzky-Golay smoothing

Multi-resolution pyramids [12, 14] require that the resolution of the image be reduced as the tree is traversed. This requires a consistent filtering prior to decimation if aliasing and/or Gibbs errors are to be avoided. A Gibbs error would lead to an artificial ringing at edges in the image. This ringing would contribute to peaks in the Fourier spectrum, resulting is a perturbation of the registration process.

Scale-space filtering [15], i.e. using a Gaussian kernel, has become a common technique to implement filtering in multi-resolution pyramids. The problem with Gaussian kernel is that they are neither periodic nor polynomial and a consistent decimation can not be achieved in an optimal manner. Andronache [2] observed "...the loss of MI's statistical consistency along the hierarchical subdivision ...", and proposed information theoretical measures to identify regions in which such errors occur. However, they provided no explanation for the source of this inconsistency.

The classical design of filters implicitly involve the implicit selection of basis functions; the most common of which are the Fourier basis and polynomials [7]. Actually the selection of the best set of basis functions depends on the nature of the data being processed. Images are clearly not periodic and consequently generate a significant error when filtered and decimated using Fourier basis functions. The authors previously proposed the use of

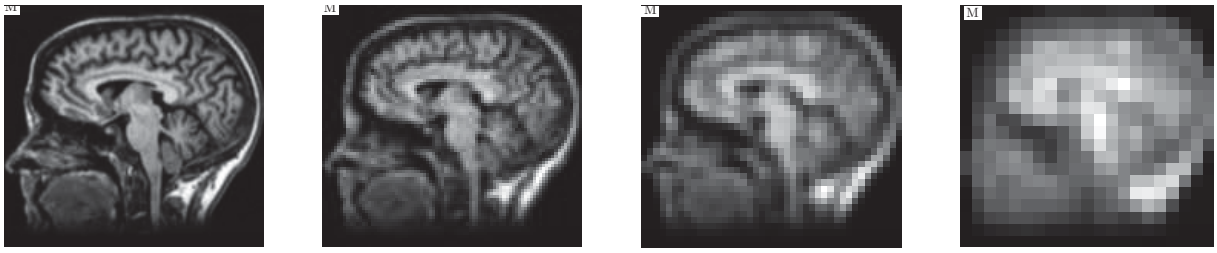

Figure 9: Results of the Savitzky-Golay smoothing and decimation across the multi-resolution pyramid. The decimation rate, from left to right are 2, 4, 8 and 16.

Gram polynomial for filtering prior to decimation [3]. However, the Gram polynomials are global basis functions and lead to Gibbs ringing at discontinuities [9] in the image. In this paper a new decimation process is implemented to perform simultaneous low-pass polynomial filtering and decimation, which is based on Savitzky-Golay filtering [20, 17]. The Gram polynomials are applied as basis functions in local approximation. Filters with monotonic step response can be implemented by correct selection of the support length and local polynomial degree. In this manner Gibbs ringing is avoided. The new process enables the implementation of arbitrary decimation factors. The Savitzky-Golay filtering can be implemented as a linear matrix operation [17], the filtered image D_{sg} is generated

by pre- and post-multiplying the unfiltered data D by matrices S_y and $\mathsf{S}_x^{\mathrm{T}}$ respectively,

$$\mathsf{D}_{sg} = \mathsf{S}_y \, \mathsf{D} \, \mathsf{S}_x^{\mathrm{T}}. \tag{2}$$

The rows of the matrices S_x and S_y contain the coefficients required to implement the desired Savitzky-Golay filter, details can be found in [17]. Given a data matrix D of size $n \times m$ then S_y is $m \times m$ and S_x is $m \times m$. Equation 4 implements the Savitzky-Golay filtering without decimation. Given the desired size of the decimated image $p \times q$ then a decimation rate of $d_y = m/p$ is required in the y direction[4]. An indices vector i_y is generated in the range $i_y(k) \in [1, n]$ with p equidistant nodes. For integer indices the decimating matrix is extracted from S_y directly,

$$\mathsf{S}_{y,d} = \mathsf{S}_y(i_y, :), \tag{3}$$

yielding a $p \times n$ matrix. Linear interpolation between the two adjacent rows S_y is used for non-integer indices. The resulting filtering and decimation process is,

$$\mathsf{D}_{sg,d} = \mathsf{S}_{y,d} \, \mathsf{D} \, \mathsf{S}_{x,d}^{\mathrm{T}}. \tag{4}$$

The matrices $\mathsf{S}_{x,d}$ and $\mathsf{S}_{y,d}$ can be computed a-priory, so that only matrix multiplications are required at run-time. This enables a numerically highly efficient implementation of the required filtering and decimation.

3.2 Modified Fourier Basis Functions for Improved Normalized Phase Correlation

Normalized phase correlation $\mathsf{P}(n)$ computed via the FFT is well known for image registration of two images where only translations need to be determined,

$$\mathsf{P}(n) = \mathcal{F}^{-1} \left\{ \frac{\mathsf{R}(\omega) \, \mathsf{M}^{\mathrm{T}}(\omega)}{\|\mathsf{R}(\omega) \, \mathsf{M}^{\mathrm{T}}(\omega)\|_2} \right\}, \tag{5}$$

where $\mathsf{R}(\omega)$ and $\mathsf{M}(\omega)$ are the 2D Fourier spectra of the reference image and measurement image respectively. Mellor [16] proposed local phase, i.e. computing the phase correlation for each patch individually, as a measure for registration in non-rigid registration. As mentioned above: Andronache [2] observed "...the loss of MI's statistical consistency along the hierarchical subdivision ...". Indeed the main loss of consistency is due to aliasing and/or Gibbs error during the decimation and Fourier based registration processes. Aliasing leads to a shifting of peaks in the frequency domain; while ringing associated with the Gibbs error leads to spurious peaks in the spectrum. These additional peaks are not properties of the image, they are errors associated with mathematical processing.

The Fourier basis functions are,

$$\boldsymbol{f}(k) = \mathrm{e}^{-\frac{2\pi k}{N} j} \tag{6}$$

[4]The same procedure is applied in the x direction with the respective parameters.

clearly these basis functions can not model a simple gradient. However, the image patches regularly have strong gradients. Consequently, the Fourier transform will have significant Gibbs errors and associated spurious peaks in the spectrum which can lead to errors in the registration: this phenomena is well known and documented [9]. In classical signal processing windowing is used [7] to reduce the Gibbs error. However, windowing is not appropriate in image registration, since it would modify the signal significantly and preclude a correct registration. For this reason a modified Fourier transform [18] is introduced here for the computation of the image spectrum.

Prior to computing the 2D Fourier spectrum, the image patch D is projected onto the orthogonal complement of a set of truncated Gram polynomials,

$$\mathsf{D}_{pg} = \mathsf{D} - \mathsf{G}_y \, \mathsf{G}_y^{\mathrm{T}} \, \mathsf{D} \, \mathsf{G}_x \, \mathsf{G}_x^{\mathrm{T}}, \tag{7}$$

where the columns of G_x and G_y contain the Gram basis functions for the x and y directions respectively. This process removes, to a large degree, the subharmonic components in the patch (for more detailed description see [18]); reducing the Gibbs error associate with this portion of the data. This computation can be performed as either a two step task, as presented above, or a modified set of basis functions can be computed a-priory and applied at run-time. The spectrum of D_{pg} is computed as,

$$\mathsf{S}_{pg} = \mathsf{F}_y^{\mathrm{T}} \, \mathsf{D}_{pg} \, \mathsf{F}_x, \tag{8}$$

where F_x and F_y are the matrices containing the Fourier basis functions for the x and y directions respectively. The Fast Fourier Transform is only a numerical efficient method of performing this computation. Now substituting Equation 7 into Equation 8 yields,

$$\mathsf{S}_{pg} = \mathsf{F}_y^{\mathrm{T}} \, \left\{ \mathsf{D} - \mathsf{G}_y \, \mathsf{G}_y^{\mathrm{T}} \, \mathsf{D} \, \mathsf{G}_x \, \mathsf{G}_x^{\mathrm{T}} \right\} \, \mathsf{F}_x. \tag{9}$$

Expanding this equation yields,

$$\mathsf{S}_{pg} = \mathsf{F}_y^{\mathrm{T}} \, \left\{ \mathsf{I} - \mathsf{G}_y \, \mathsf{G}_y^{\mathrm{T}} \right\} \, \mathsf{D} \, \left\{ \mathsf{I} - \mathsf{G}_x \, \mathsf{G}_x^{\mathrm{T}} \right\} \, \mathsf{F}_x. \tag{10}$$

Now defining the modified basis functions as $\mathsf{B}_y \triangleq \mathsf{F}_y^{\mathrm{T}} \, \left\{ \mathsf{I} - \mathsf{G}_y \, \mathsf{G}_y^{\mathrm{T}} \right\}$ and $\left\{ \mathsf{I} - \mathsf{G}_x \, \mathsf{G}_x^{\mathrm{T}} \right\} \, \mathsf{F}_x$. The modified Fourier transform is now computed as,

$$\mathsf{S}_{pg} = \mathsf{B}_y \, \mathsf{D} \, \mathsf{B}_x, \tag{11}$$

and the modified spectrum is used for the computation of the normalized phase correlation. This computation is numerically efficient than the two step process for small patches.

3.3 Entropy-Weighted Tensor Polynomial Regularization

The normalized phase correlation delivers the coordinates for each shifted patch. The shifted positions are also affected by noise in the image, and numerical errors associated with the computation. There is no guarantee that the coordinates of the patches lie on a grid which corresponds to an elastic deformation. Regularization of the coordinates onto

a grid which is consistent with the solutions of a partial differential equations for elastic deformation can be achieved by approximation by a tensor product of global polynomial basis functions. The functional for such a tensor product approximation [11][23][27][8] is,

$$E = \left\| \mathsf{G}_y \, \mathsf{S} \, \mathsf{G}_x^{\mathrm{T}} - \mathsf{D} \right\|_F . \tag{12}$$

The aim is to determine the values of the entries in the matrix S which minimize the functional. Given the Gram polynomials as global basis functions a linear solution to the minimization of the functional is known, to be the projection onto the orthogonal complement,

$$\mathsf{S} = \mathsf{D} - \mathsf{G}_y \, \mathsf{G}_y^{\mathrm{T}} \, \mathsf{D} \, \mathsf{G}_x \, \mathsf{G}_x^{\mathrm{T}} \tag{13}$$

A further issue which needs to be considered is that not all patches have the same information content. It is desirable to weight the coordinates of a patch by the information contained in the patch, i.e. patches with a higher information content are given more significant during the least squares approximation process. Given the matrix of weights W, the functional for the weighted tensor product approximation can be formulated as[5],

$$E_w = \left\| \mathsf{W}^{\circ \frac{1}{2}} \circ \left\{ \mathsf{G}_y \, \mathsf{S} \, \mathsf{G}_x^{\mathrm{T}} - \mathsf{D} \right\} \right\|_F . \tag{14}$$

The solution for S which minimizes the functional E_w has been considered a non-linear

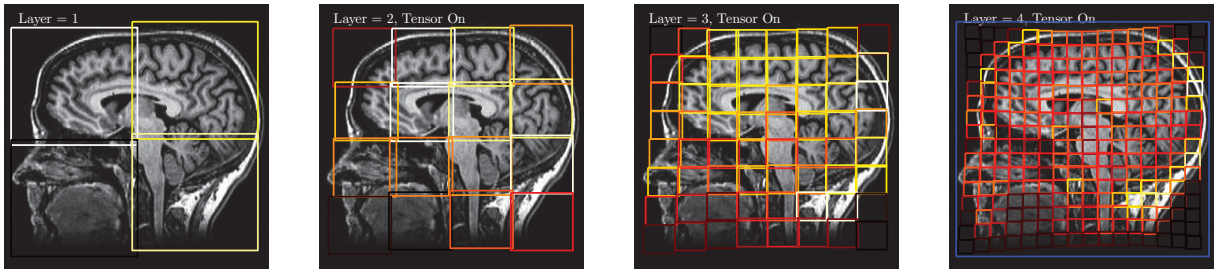

Figure 10: The above figures show the registration at each of the four sublayers in the multi-resolution pyramid. The color of the patch is proportional to the entropy of the data contained within the patch. This is used as the relative weighting in the tensor polynomial approximation.

task in the past. This paper presents the first direct linear solution to this task based on the Kroneker product. There are three specific cases which need to be considered for a general solution:

The matrix W is rank one and positive semi-definite

If $\mathrm{rank}\{W\} = 1$ then the matrix can be computed from two vectors, a left $\boldsymbol{w}_l$ and right $\boldsymbol{w}_r$ singular vector respectively,

$$\mathsf{W}^{\circ \frac{1}{2}} = \boldsymbol{w}_l \, \boldsymbol{w}_r^{\mathrm{T}} = \boldsymbol{w}_l \otimes \boldsymbol{w}_r . \tag{15}$$

[5]The notation $\mathsf{W}^{\circ \frac{1}{2}}$ indicates a Hadamard operator with respect to the square root, i.e. the square root of each entry in W.

The left $\boldsymbol{w}_l$ and right $\boldsymbol{w}_r$ singular vectors are determined by applying singular value decomposition to $\mathsf{W}^{\circ\frac{1}{2}}$. Now substituting into Equation 14 yields,

$$E_w = \left\| \operatorname{diag}(\boldsymbol{w}_l)\ \mathsf{G}_y\, \mathsf{S}\, \mathsf{G}_x^{\mathrm{T}}\ \operatorname{diag}(\boldsymbol{w}_r) - \mathsf{W}^{\circ\frac{1}{2}}\, \mathsf{D} \right\|_F . \tag{16}$$

The normal equations associated with the above functional can be solved directly and linearly for S yielding,

$$\mathsf{S} = \left(\operatorname{diag}(\boldsymbol{w}_l)\ \mathsf{G}_y\right)^{+}\ \mathsf{W}^{\circ\frac{1}{2}}\, \mathsf{D}\ \left(\mathsf{G}_x^{\mathrm{T}}\ \operatorname{diag}(\boldsymbol{w}_r)\right)^{+} . \tag{17}$$

The matrix W is rank one and is strictly positive definite

If $\boldsymbol{w}_l$ and $\boldsymbol{w}_r$ are strictly positive the problem can be solved directly using weighted polynomial basis functions.

The matrix W is full rank and strictly positive definite

If the matrix W is full rank and strictly positive definite, then the functional (Equation 14) must be vectorized. Consider the properties of the Kronecker product,

$$\mathsf{A}\, \vec{\mathsf{X}}\, \mathsf{B} = \left(\mathsf{B}^{\mathrm{T}} \otimes \mathsf{A}\right)\ \vec{X} \tag{18}$$

The $\vec{\mathsf{X}}$ corresponds directly to the MATLAB operator $\mathsf{X}(:)$. Now consider,

$$\mathsf{G}_y\, \vec{\mathsf{S}}\, \mathsf{G}_x^{\mathrm{T}} = \mathsf{G}_x \otimes \mathsf{G}_y\, \vec{\mathsf{S}}. \tag{19}$$

Before proceeding further it is helpful to define some succinct notations,

$$\boldsymbol{s} \triangleq \vec{\mathsf{S}}, \quad \boldsymbol{d} \triangleq \vec{\mathsf{D}}, \quad \mathsf{A} \triangleq \mathsf{G}_x \otimes \mathsf{G}_y, \quad \text{and} \quad \mathsf{V} \triangleq \operatorname{diag}\left(\vec{\mathsf{W}^{\circ\frac{1}{2}}}\right). \tag{20}$$

Now vectorizing Equation 14 using this notation yields,

$$E_w = \|\mathsf{V}\ \{\mathsf{A}\, \boldsymbol{s} - \boldsymbol{d}\}\|_2^2 . \tag{21}$$

This is the cost function for a weighted vector approximation, the solution for $\boldsymbol{s}$ which minimized E_w is well known $\boldsymbol{s} = \{\mathsf{V}\, \mathsf{A}\}^{+}\ \mathsf{V}\, \boldsymbol{d}$. For numerical reasons it is more efficient to compute,

$$\boldsymbol{s} = \{\mathsf{V}\, \mathsf{A}\}^{+}\ \vec{\mathsf{W}^{\circ\frac{1}{2}}} \circ \mathsf{D}. \tag{22}$$

This is a direct linear solution and is non-iterative. Consequently, the number of computations required can be determined a-priori making this solution suitable for real-time applications.

In this application the entropy of the data contained in each patch is used as the corresponding weight. Since all images contain some noise the entropy will be strictly positive and it must be assumed that the matrix W is full rank. The coordinates of each patch are reformed to generate a matrix of X and of Y coordinates. Both matrices are regularized using the above procedure.

4 Testing

The improvement in the registration associated with the modified Fourier basis set is demonstrated with a one dimensional data example. A synthetic data signal $\boldsymbol{d}(n)$ has been generated for this test, see Figure 11. Two subsets $\boldsymbol{d}_1(n)$ and $\boldsymbol{d}_2(n)$ are cut from $\boldsymbol{d}(n)$ with a shift of 55 samples. These two data sets, with known time shift, are used to test the normalized phase correlation with (see Figure 13) and without projection onto the orthogonal complement of a truncated Gram polynomial od degree $d = 2$ (see Figure 12). It can be seen that the shift by 55 samples can be clearly identified, if the projection onto the truncated Gram polynomials is performed prior to computing the correlation. The signal to noise ratio is significantly better than with the conventional computation.

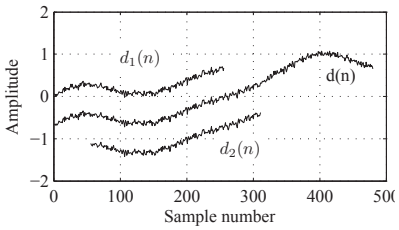

Figure 11: A synthetic data set $\boldsymbol{d}(n)$, with two data subsets $\boldsymbol{d}_1(n)$, and $\boldsymbol{d}_2(n)$. Both data subsets have a length of 256 samples and are cut from $\boldsymbol{d}(n)$ with a relative shift of 55 samples.

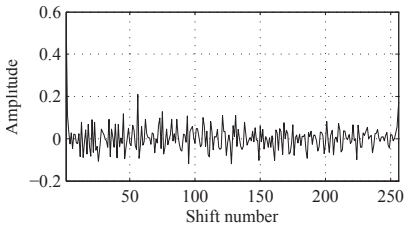

Figure 12: Normalized phase correlation of the signals $\boldsymbol{d}_1(n)$ and $\boldsymbol{d}_2(n)$ computed using Equation 5

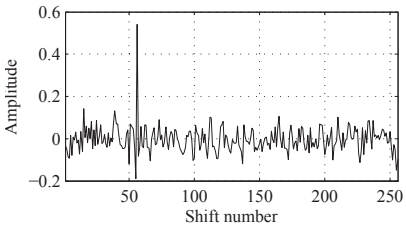

Figure 13: Normalized phase correlation of the signals $\boldsymbol{d}_1(n)$ and $\boldsymbol{d}_2(n)$, after projection onto the orthogonal complement of a truncated Gram polynomial basis of degree $d = 2$.

The second test is with the images shown in Figure 10, it has been chosen since it is freely available online [1] and results from other research groups are available for this image pair. Correct registration has been achieved with the new method and required in a MATLAB implementation: this compares with required by Suarez et. al [22] and with a "Fast entropy" method [21]. The results are for the same data set. The new method delivers a speed improvement in the range of two orders of magnitude.

The results shown in Figure 14 for the case where data was acquired directly in the production line and an unrealistically large pin-cushion distortion has been synthetically applied. The aim being to show that the method can deal with very large distortions. The method has successfully registered the images and identified the correct distortion.

The last test involved registration of images during the automatic inspection process, see Figure 15. The production samples demonstrated only a very low distortion. All production samples were successfully registered, i.e. the registration enables the comparison of the local colour patterns.

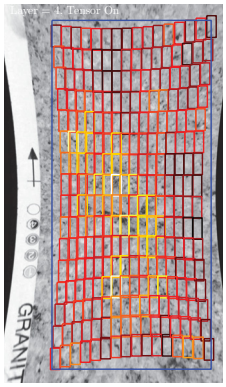

Figure 14: The above test patterns have been acquired with the production instrument, whereby the pin-cushion and barrel distortion has been applied artificially. The aim was to determine the limits of the algorithm.

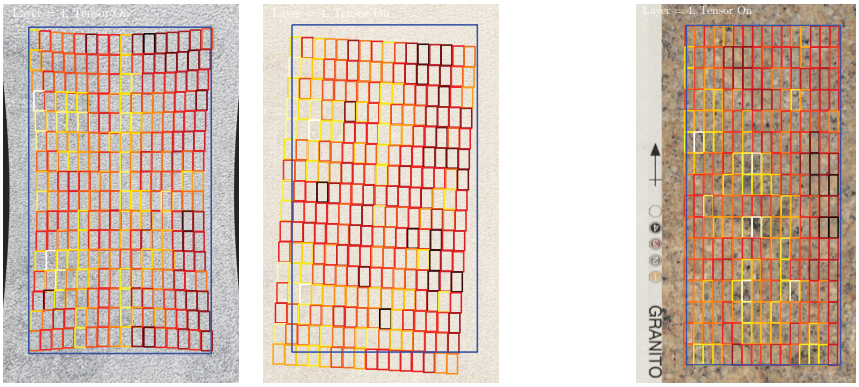

Figure 15: The above patterns were measured with the production instrument. The comparison is between two samples produced in different batches.

5 Conclusions

This paper has presented a new solution to non-rigid elastic registration of hyper spectral data. The method has been applied to hyper spectral data for the automatic quality control of decorative foils which are subject to deformation during lamination. Local polynomial approximation offers a successful method of implementing simultaneous filtering and image decimation as required for multi-resolution pyramids.

Modified Fourier basis functions implemented by projection onto the orthogonal complement of a truncated Gram polynomial basis are presented. The modified functions are used to compute spectra whereby the Gibbs error associated with local gradients in the image are reduced. This improves the statistical consistency across the subdivision tree. The improvement associated with this method are demonstrated for a one dimensional data set.

The paper also presents the first direct linear solution to weighted tensor product polynomial approximation. This method is used to regularize the patch coordinates, the solution is equivalent to a Galerkin type solution to a partial differential equation. The new solution is applied to test samples and compared with other methods. The speed of the new solution justifies explicit reference: the present solution implemented in MATLAB requires approximately 1.3 second to register an image of size 800×500 pixels. The is approximately a factor 10 to 100 faster than previously published results for the same data set.

References

[1] *http://www.mathworks.com/matlabcentral/fileexchange/20057.*

[2] A. Andronache, M. von Siebenthal, G. Szekely, and Ph. Cattin. Non-rigid registration of multi-modal images using both mutual information and cross-correlation. *Medical Image Analysis*, 12(1):3–15,, 2008.

[3] Amir Badshah, Paul O'Leary, and Matthew Harker. Gram polynomial image decimation and its application to non-rigid registration. volume 7877, pages 787–707. SPIE, 2011.

[4] Chein Chang. *Hyperspectral Imaging: Techniques for Spectral Detection and Classification*. Springer, 2003.

[5] Bernd Fischer, Benoit M.Dawant, and Cristian Lorenz. Biomedical image registration 4th international workshop, WBIR 2010, Lübeck, July 11-13, proceedings. In *Image Processing, Computer Vision, Pattern Recognition, and Graphics*, volume 6204 of *Lecture Notes in Computer Science*, page Approx. 280 p.

[6] E. Gladilin, V. Pekar, K. Rohr, and H. S. Stiehl. A comparison between BEM and FEM for elastic registration of medical images. *Image and Vision Computing*, 24(4):375–379, April 2006.

[7] R. W. Hamming. *Digital filters (3rd ed.)*. Prentice Hall International Ltd., Hertfordshire, UK, 1989.

[8] Roger Horn and Charles R. Johnson. *Topics in matrix analysis*. Cambridge University Press, Cambridge, 1991.

[9] Abdul Jerri. *The Gibbs Phenomenon in Fourier Analysis, Splines and Wavelet Approximations*. Kluver Academic Publishers, Dordrecht, Netherlands, 1998.

[10] Helmut Kipphan. *Handbook of Print Media*. Springer, berlin, 2001.

[11] E. Kofidis and P. Regalia. Tensor approximation and signal processing applications. In *in AMS Conf. on Structured Matrices in Operator theory, Numerical Analysis, Control, Signal and Image Processing*, 2000.

[12] P.J. Kostelec, J.B. Weaver, and D.M. Healy Jr. Multiresolution elastic image registration. *Medical physics*, 19(1-2):1593–1604,, 1998.

[13] Hava Lester and Simon R. Arridge. A survey of hierarchical non-linear medical image registration. *Pattern Recognition society*, 32:129 – 149, 1999.

[14] B. Likar and F. Pernu. A hierarchical approach to elastic registration based on mutual information. *Image and Vision Computing*, 19(1-2):33 – 44, 2001.

[15] Tony Lindeberg. Scale-space theory: a basic tool for analyzing structures at different scales. *Journal of Applied Statistics*, 21:225–270, 1994.

[16] M. Mellor and M. Brady. Non-rigid multimodal image registration using local phase. *MICCAI. LNCS*, 3216:789–796, 2004.

[17] P. O'Leary and M. Harker. Discrete polynomial moments and savitzky-golay smoothing. In *World Academy of Science, Engineering and Technology 2010*, 2010.

[18] Paul O'Leary and Matther Harker. Polynomial approximation: An alternative to windowing in fourier analysis. *Instrumentation and Measurement Technology Conference (I2MTC), 2011 IEEE*, pages 1–6, May 2011.

[19] S. Periaswamy and H. Farid. Elastic registration in the presence of intensity variations. *Medical Imaging, IEEE Transactions on*, 22(7), July 2003.

[20] A. Savitzky and M. Golay. Smoothing and differentiation of data by simplified least squares procedures. *Analytical Chemistry*, 36 (8):1627–1639, 1964.

[21] E. Suarez, J. A. Santana, Eduardo Rovaris, C.-F.Westin, and J. Ruiz-Alzola. Fast entropy-based nonrigid registration. In *Computer Aided Systems Theory (EUROCAST'03), Lecture Notes in Computer Science 2809*, pages 607–615. Springer Verlag, February 24–28 2003.

[22] Eduardo Suarez, Carl-Fredrik Westin, Eduardo Rovaris, and Juan Ruiz-Alzola. Nonrigid registration using regularized matching weighted by local structure. In *Medical Image Computing and Computer-Assisted Intervention MICCAI 2002*, volume 2489 of *Lecture Notes in Computer Science*, pages 581–589. 2002.

[23] C. F. van Loan. The ubiquitous Kronecker product. *Journal of Computational and Applied Mathematics*, 123:85–100, 2000.

[24] Yongmei Wang and Lawrence H. Staib. Physical model-based non-rigid registration incorporating statistical shape information. *Medical Image Analysis*, 1:35–51, 2000.

[25] G. Wollny and F. Kruggel. Computational cost of nonrigid registration algorithms based on fluid dynamics [MRI time series application]. *Medical Imaging, IEEE Transactions on*, 21(8):946–952, 2002.

[26] Stefan Wrz and Karl Rohr. Physics-based elastic registration using non-radial basis functions and including landmark localization uncertainties. *Computer Vision and Image Understanding*, 111(3):263 – 274, 2008.

[27] Bin Zhou, Zhao-Yan Li, Guang-Ren Duan, and Yong Wang. Weighted least squares solutions to general coupled sylvester matrix equations. *J. Comput. Appl. Math.*, 224:759–776, February 2009.

[28] Barbara Zitov and Jan Flusser. Image registration methods: a survey. *Image and Vision Computing*, 21:977–1000, 2003.

Strain Analysis by Regularized Non-Rigid Registration[1]

Amir Badshah[1], Paul O'Leary[1], Matthew Harker[1] and Daniel Tscharnuter[2]
[1] University of Leoben, A-8700 Leoben, Austria
[2] Polymer Competence Center Leoben GmbH, Roseggerstrasse 12, 8700 Leoben, Austria

Abstract

This paper presents a new approach to optical material stress analysis, which eliminates the need to apply a random dot pattern to the surface of the sample being tested. A multi-resolution hierarchical sub-division is implemented, with a consistent polynomial decimation applied at each layer of the tree. The degree of decimation must be selected depending on the nature of the structure of the surface of the sample being At each layer the individual patches are registered using a modied normalized phase correlation, whereby the Fourier basis functions are projected onto the orthogonal complement of a low degree Gram polynomial basis. This reduces the effect of the Gibbs error on the local registration. The registration positions are then subjected to a regularization via an entropy weighted tensor-polynomial approximation. The Gibbs polynomial basis is used for the tensor product, since they are orthonormal and model the continuous deformation associated with an elastic deformation. The stability of the proposed method is demonstrated in real measurements and the results with and without the application of the random pattern are compared.

1 Introduction

The problem of optical strain analysis can be regarded as being fundamentally the same task as non-rigid registration [2][1]: a sequence of images of the sample is acquired during the tensile of compressive testing. The deformation of the sample is a continuous process of elastic and plastic deformation up the point when the sample ruptures. Consequently, a nonrigid registering of the individual images will yield the deformation of the sample at the time point when the image was acquired.

Numerous papers have been written on the topic of strain measurement by digital image correlation and grid method,i.e, [5, 7, 3, 8]. In general these methods require a stochastic pattern on the surface of the material so as to enable a reliable registration. Commercial

[1]This paper presented in SPIE Electrnic Imaging conference 22 - 26 February 2012 Hyatt Regency San Francisco Airport Burlingame, California, USA.

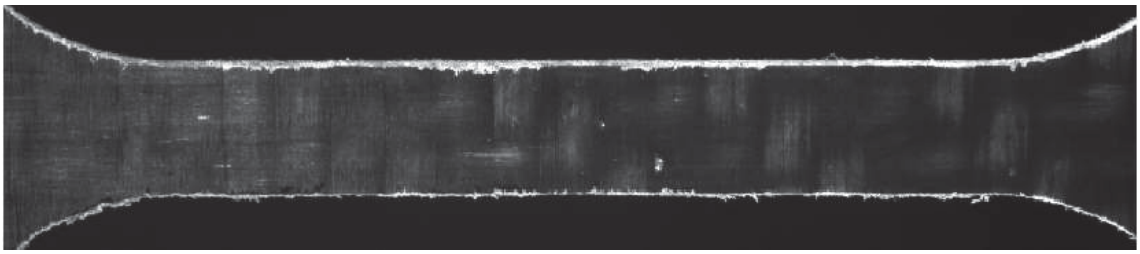

Figure 1: Test sample of a composite material which is to be tested. The surface exhibits a texture associated with the weaving pattern of the reenforcing material. (The material used here is Tepex Dynalite 102-RG600C3 from Board Laminates GmbH)

systems require a random dot pattern on the surface to ensure good registration of the sequence of images. The application of the pattern is performed in two steps: a white coating is applied as a base; then the black dots are generated using a graphite spray[2]. However, particularly in the testing of polymer material [6] the application of a coating containing solvents can have serious undesirable side effects. The solvents penetrate deep into small cracks and may have a chemical interaction with the material being tested. During testing a parallel evaluation with a commercial system was performed. The system failed without application of the dot pattern. Consequently there is justification for the development of a new evaluation scheme which can deal with both globally and locally structured surfaces. This is particularly important for the measurement of composite materials which may have a repetitive weaving pattern associated with the reinforcing material. The material being tested in this paper is a perfect example of such a case, a sample without coating can be seen in Figure 1.

There are two main reasons which lead to the need to apply the stochastic pattern: the registration methods used in optical strain measurement are rudimentary and no systematic analysis of this issue is provided; for example, Haile and Ifuj [5] use a locally weighted mean transform. This is in no way related to the physics of the problem at hand. Koljonen et al. [8] investigated different measures for confidence and adapted the template size to achieve a higher degree of confidence. More advances methods of entropy based regularization, as used in medical imaging, were too slow for application in strain analysis, see for example Suarez et. al [15] require and with a "Fast entropy" method [14] they required for a single regularization; secondly, registration via normalized phase correlation (NPC) is subject to Gibbs error, since the stochastic pattern is not periodic. Recently the authors introduced a new real time nonrigid registration method which addresses this issues and provides solutions applicable to strain analysis, details of their work can be found in [2][1], consequently only the salient points relevant to strain analysis are dealt with in this paper in more detail.

[2]In this application a U89 Developer from a dye penetrant inspection system by Helling is used as the base white coating and a graphite spray 33 from Kontakt Chemie is used to generate the dot pattern.

2 Experimental setup

A universal testing machine is used to perform all the measurements presented in this paper, the machine is shown in Figure 2 and the sample mounted for testing in Figure 3. The technical specification of the universal materials testing machine are given in Table 2. This machine can be used for tension, compression and bending tests up to 250kN. The image sequences were acquired with a commercial video extensometer system from the company GOM mbH.: ARAMIS HS system with Basler 504k cameras, equipped with 50mm lenses for the tensile testing and a S5LPJ0625 telecentric lens for the compression test.

Table 1: Technical Specification of the Universal Testing Machine.

Type	UPM Zwick/Roell Z 250
Load Range	1 kN to 250 kN
Working space	800mm max
Test speed	max. 600 mm/min
Equipment:	laser extensometer, max. 400 mm with 0.1 micron resolution
Grips	Hydraulic
Application	Tension, compression, bending and elasticity tests

3 Principle of operation of elastic registration

A hierarchial decomposition [10] of the image, also called multiresolution [9] pyramids[3] is performed. This type of decomposition ensures that structures with a combination of stochastic and repetitive patterns can be reliably registered. At each level in the decomposition the image is subdivided into four sub-images, see Figures 4 and 5: this results in a quad-tree structure. As the tree is traversed the resolution of the patches is reduced via Savitzky-Golay [13, 11] approximation combined with a consistent decimation. The decimation rate must be selected prudently: since, a higher degree of decimation will improve the speed of computation, however, for stochastic patterns sufficient local information must be maintained to enable global registration. Registration of the individual patches is performed at each layer using a modified FFT based normalized phase correlation. The patch is projected onto the orthogonal complement of a low degree Gram polynomial basis prior to computation of the normalized phase correlation. This eliminates the predominant a-periodic portion of the data and with this reduces the Gibbs error significantly.

Then the coordinates of the registered patches are regularized by weighted least squares approximation by a sum of a tensor products of Gram polynomials [4, 12]. The weighted tensor product of two sets of truncated Gram polynomial basis functions of maximum degree n ensures that the solution lies on a $C(n)$ continuous grid. This is consistent with the elastic deformations of the sample which are also $C(n)$ continuous up to the

[3]The term pyramids emerged in parallel to the term hierarchical subdivision.

point of rupture. The entropy of the data contained in each patch is used as a weighting factor during the least squares tensor approximation. This ensures that patches with low information content do not contribute so strongly to the functional as do the patches with a strong information content.

4 Testing

The first test is on a standard sample to which a random dot pattern has been applied, Figure 6(a) shows the specimen prior to loading, 6(b) the final image from which the deformation is to be measured, 6(c) and 6(d) show the third and fourth layers of the quad-tree registration. It can be seen that the registration has performed correctly.

In the second test a porous compressible medium is compressed, see Figure 7 and 8. The typical barrel distortion with flat tops and bottoms can be observer. The area of the original grid can be compared with the area of the compressed grid to determine the volumetric compression of the material, it should be noted that two cameras mounted at 90 to each other are require to perform a precise volumetric measurement.

The third test shows a sample which has been specially prepared: one half of the sample has been coated with a stochastic dot pattern, while the second half is left in its original form. The commercial system fails to function of the surface which has not been prepared. The results of three evaluations are presented in Figure 9: (left) registration only on the prepared portion of the surface; (center) registration on the whole sample and (right) registration on the unprepared surface. All three measurements are consistent, demonstrating that the method has functioned correctly on the unprepared surface.

5 Conclusions

This work has demonstrated a non-rigid registration techniques based on hierarchical decomposition together with entropy weighted regulatization is suitable for the measurement of mechanical strain on composite materials. The advance achieved in this paper is that the surface of the sample need not be prepared prior to measurement. The weaving structure associated with composite materials does not affect the quality of the results.

The weighted tensor polynomial approximation is consistent with the solutions of the Navier-Stokes differential equation, i.e. that is the equation describing the flow of viscous materials. This is a suitable model when measuring composite plastics.

6 Acknowledgements

D. Tscharnuter is funded by the COMET-program of the Austrian Ministry of Traffic, Innovation and Technology with contributions by the University of Leoben. The PCCL

is funded by the Austrian Government and the State Governments of Styria and Upper Austria.

7 Appendix I: A note on the Gram Polynomials

There is considerable confusion in the literature on the Tchebychev and discrete Tchebychev polynomials. We choose the term Gram [4] since in his original work from 1883 he also considered the issue of weighted polynomial approximations. The Gram polynomials are continuous polynomials which are orthonormal on a set of discrete sample points. The recurrence relationship for the Gram polynomials is,

$$g_n(x) = 2\ \alpha_{n-1}\ x\ g_{n-1}(x) - \frac{\alpha_{n-1}}{\alpha_{n-2}}\ g_{n-2}(x), \tag{1}$$

whereby,

$$\alpha_{n-1} = \frac{m}{n}\left(\frac{n^2 - 1/2}{m^2 - n^2}\right)^{1/2} \tag{2}$$

and

$$g_0(x) = 1, \quad g_{-1}(x) = 0 \quad \text{and} \quad \alpha_{-1} = 1, \tag{3}$$

for x on equidistant points,

$$x = -1 + \frac{(2k-1)}{m}, \quad 1 \leq k \leq m, \tag{4}$$

note these points do not span the full range $[-1, 1]$. The bases functions are scaled by $\sqrt{m}$ yielding a unitary bases set. It should be noted that the coefficients α_n are also a function of m the number of nodes.

References

[1] A. Badshah, P. O'Leary, M. Harker, and C. Sallinger. Non-rigid registration for qualitiy control of printed materials. In *10th SPIE International Conference on Quality Control by Artificial Vision (QCAV)*, Saint-Etienne, France, June 2011.

[2] Amir Badshah, Paul O'Leary, and Matthew Harker. Gram polynomial image decimation and its application to non-rigid registration. volume 7877, pages 787–707. SPIE, 2011.

[3] H. T. Goldrein, S. J. P. Palmer, and J. M. Huntley. Automated fine grid technique for measurement of large-strain deformation maps. *Optics and Lasers in Engineering*, 23(5):305 – 318, 1995. Interferogram Analysis.

[4] J. Gram. Uber die entwickelung reeler functionen in reihen mittest der methode der kleinsten quadrate,. In *jOURNAL FR DIE REINE UND ANGEWANDTE mATHEMATIK;*, volume 94, pages 41–73., 1883.

[5] M. A. Haile and P. G. Ifju. Application of elastic image registration and refraction correction for non-contact underwater strain measurement. *Strain*, 2011.

[6] M Jerabek, Z Major, and R W Lang. Uniaxial compression testing of polymeric materials. *Polymer Testing*, 29(3):302–309, 2010.

[7] H. Jin, S. Haldar, H. Bruck, and W.-Y. Lu. Grid method for microscale discontinuous deformation measurement. *Experimental Mechanics*, 51:565–574, 2011. 10.1007/s11340-010-9459-7.

[8] Janne. Koljonen, Olli. Kanniainen, and Jarmo T. Alander. Dynamic template size control in digital image correlation based strain measurements. *Proceedings of SPIE, Vol. 6764,*, pages 67640L–112, 2007. 911 Sept. 2007.

[9] P.J. Kostelec, J.B. Weaver, and D.M. Healy Jr. Multiresolution elastic image registration. *Medical physics*, 19(1-2):1593–1604,, 1998.

[10] B. Likar and F. Pernu. A hierarchical approach to elastic registration based on mutual information. *Image and Vision Computing*, 19(1-2):33 – 44, 2001.

[11] P. O'Leary and M. Harker. Discrete polynomial moments and savitzky-golay smoothing. In *World Academy of Science, Engineering and Technology 2010*, 2010.

[12] Paul O'Leary and Matther Harker. An algebraic framework for discrete basis functions in computer vision. *Indian Conference on Computer Vision, Graphics and Image Processing*, 0:150–157, 2008.

[13] A. Savitzky and M. Golay. Smoothing and differentiation of data by simplified least squares procedures. *Analytical Chemistry*, 36 (8):1627–1639, 1964.

[14] E. Suarez, J. A. Santana, Eduardo Rovaris, C.-F.Westin, and J. Ruiz-Alzola. Fast entropy-based nonrigid registration. In *Computer Aided Systems Theory (EUROCAST'03), Lecture Notes in Computer Science 2809*, pages 607–615. Springer Verlag, February 24–28 2003.

[15] Eduardo Suarez, Carl-Fredrik Westin, Eduardo Rovaris, and Juan Ruiz-Alzola. Nonrigid registration using regularized matching weighted by local structure. In *Medical Image Computing and Computer-Assisted Intervention MICCAI 2002*, volume 2489 of *Lecture Notes in Computer Science*, pages 581–589. 2002.

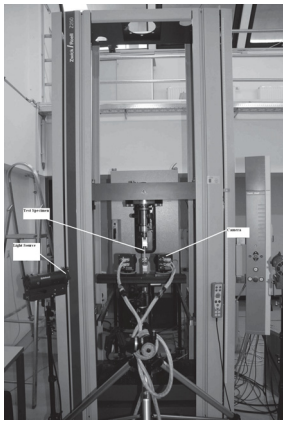

Figure 2: The universal testing machine used: UPM Zwick/Roell Z 250.

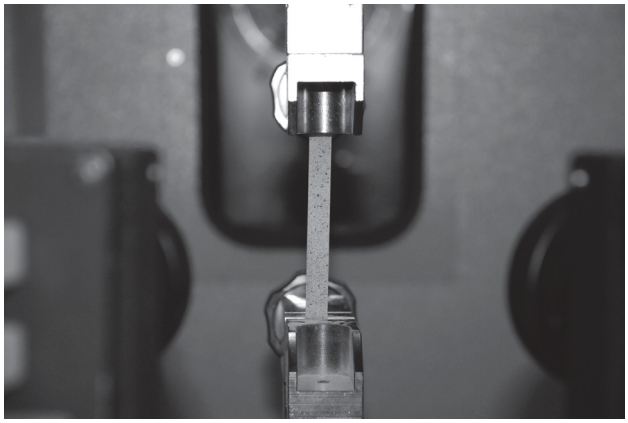

Figure 3: Specimen held in the jaws ready for testing, this sample has been coated with the random dot pattern.

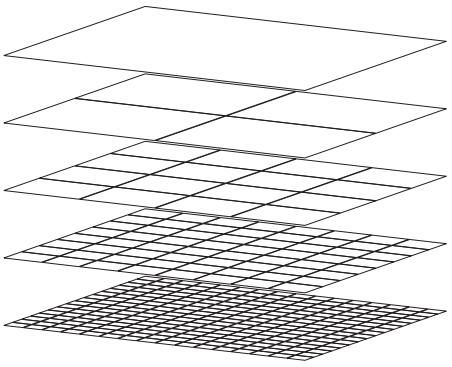

Figure 4: Reference decomposition tree, with five layers. The reference tree is generated on the first image of the sample prior to applying force.

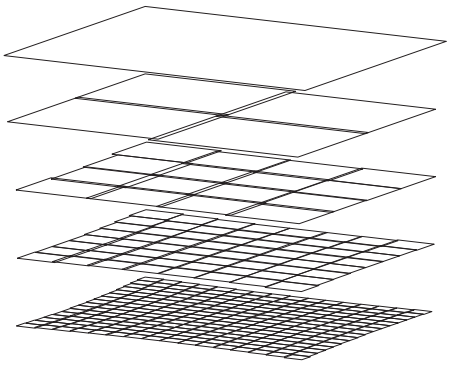

Figure 5: Registered decomposition tree, with five layers, the modified position of each patch can be seen. The registration is performed for each subsequent image as required.

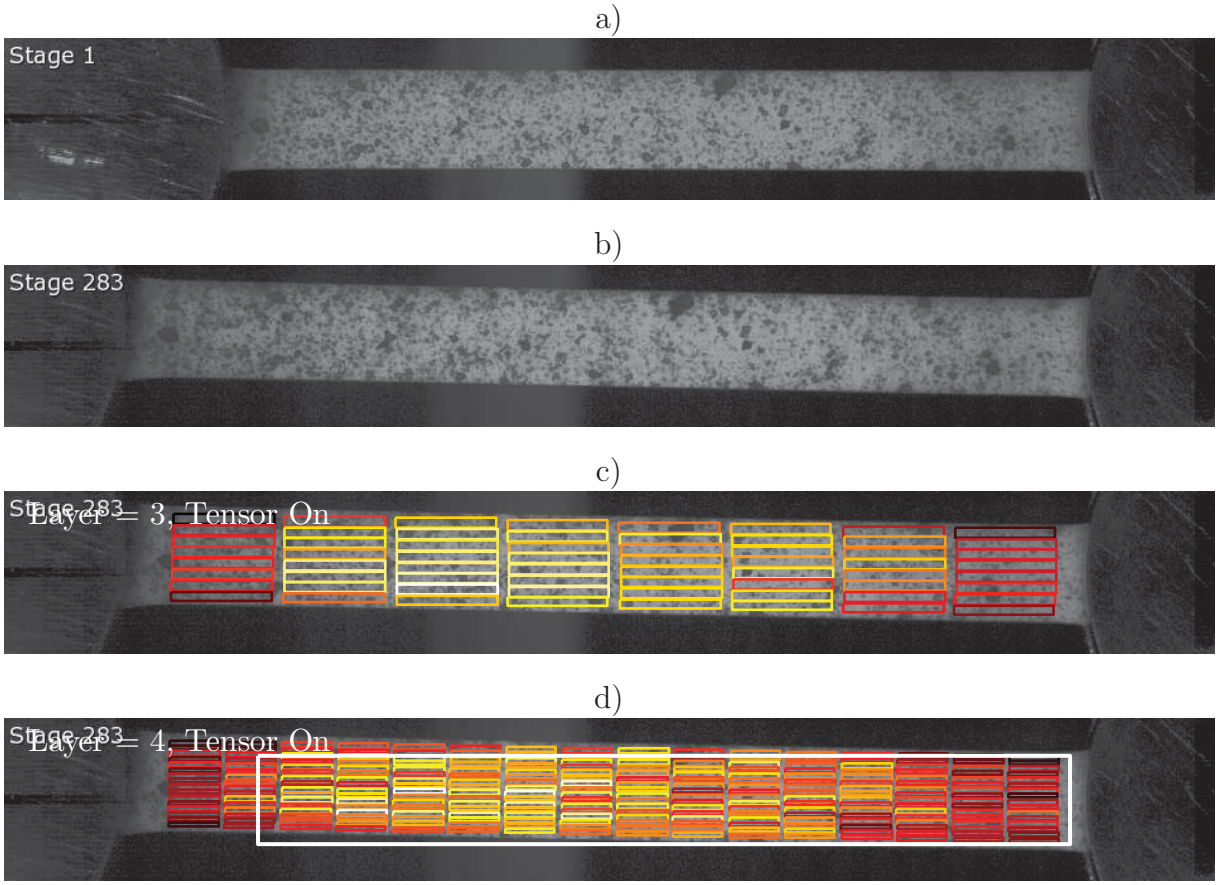

Figure 6: Specimen being measured: a) prior to extension; b) after extension; c) the distortion map relating the specimen prior and post extension at level 3 of the hierarchical decomposition; d) the distortion map as the final result. The colors of the grid are proportional to the entropy in the corresponding image tile. The white rectangle corresponds to the position of the grid prior to extension.

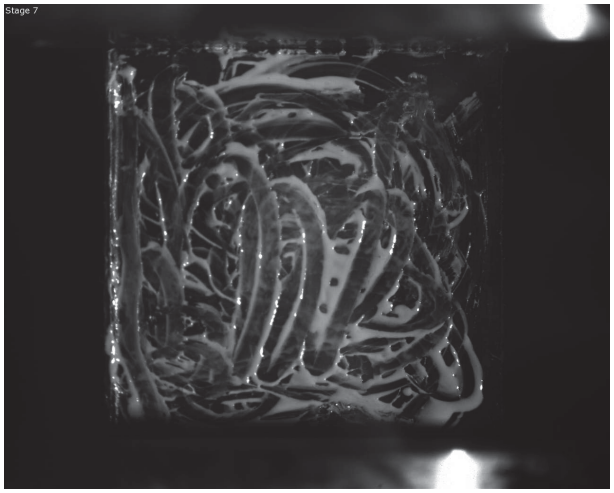

Figure 7: Test specimen for compression testing. This is a porous compressible medium.

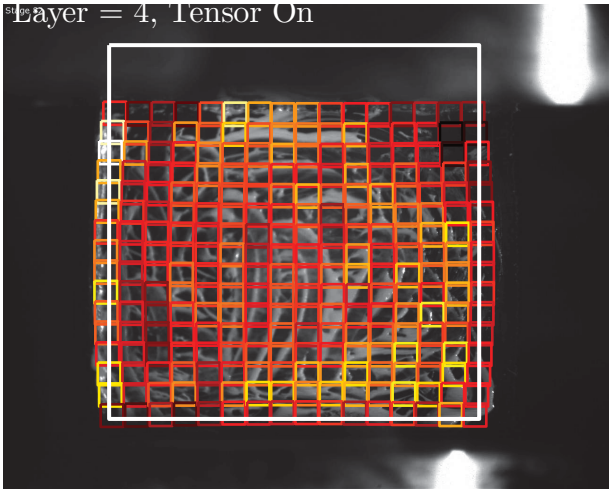

Figure 8: The sample under compression and the distortion mat relating it to the uncompressed state. The colors of the grid ar proportional to the entropy in the corresponding image tile. The white rectangle corresponds to the position of the grid prior to compression.

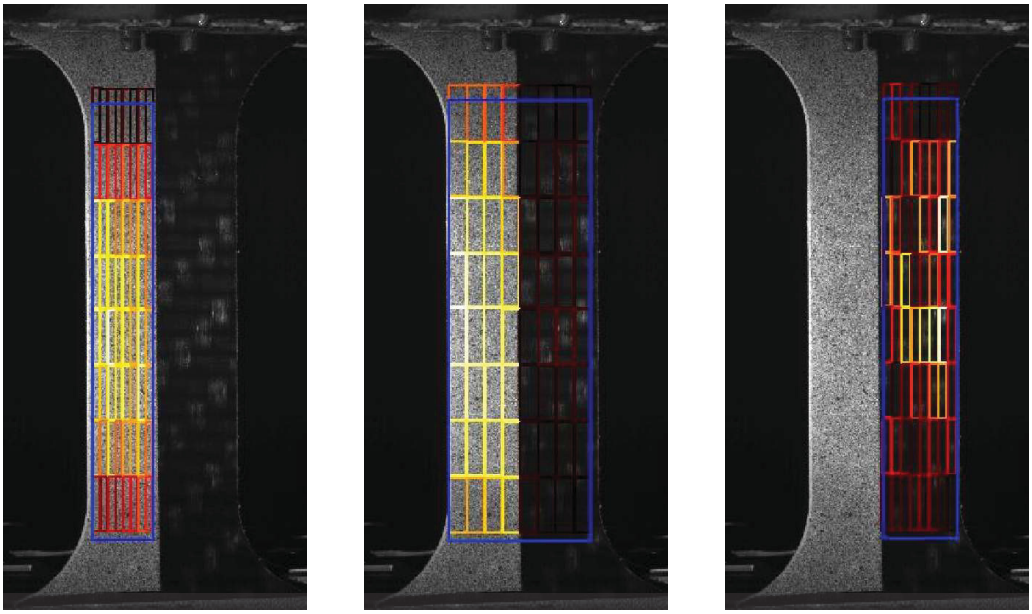

Figure 9: Three test of the elastic registration method: (left); (center); (right).

Tunnel inspection by non-rigid registration[1]

Amir Badshah, Paul O'Leary, and Matthew Harker
University of Leoben, Leoben, Austria

Abstract

Machine vision play major rule in the filed of quality control by inspecting the in line product using image processing tools. These automatic inspection methods are contactless and more accurate compared to the other manual procedures inspection methods either by sensor or human being. Yearly or quarterly inspection of tunnels are recommended for safety purposes. Presently the inspection of tunnels are mostly done by human being physically. Some long tunnels of length of few kilometers are challenging for such methods. An automatic method could enhance the quality of inspection and less effort is required in short time. Initially series of images are taken at different position in the tunnel and saved. When the time of inspection comes again images are taken at the exact same positions. These old and new images are registered with each other by non-rigid regularized registration method. Any displacement at any position of the tunnel is pointed out.

1 PROBLEM STATEMENT

The infrastructure manager belong to road safety and tunnel inspection evaluate how to commit the human and financial resources for the work of tunnel inspection and other clearances for stringent safety and tunnel accessibility standards. In the most cases, these measurement and inspection are carried out by manually-operated measuring devices at very low speed, during this measurement and inspection process time all the line is closed for traffic which could otherwise be used by revenue-earning. On lines with a high traffic density, finding the time to carry out such inspections safely and without disruption to traffic is a perennial challenge. But recent technological advances mean a new generation of more compact measuring systems is now emerging, offering the opportunity to fit such equipment to normal service. In the proposed inspection procedures first establish an initial data images, which will serve as baseline for future inspections. The inspections cover structural elements i.e. rocks movements, tunnel wall displacement, and other systems appurtenances. Ideally all data collected during the initial and follow-up inspections should be gathered in an electronic database. The new data images are registered with the previous data. Maintenance remains the key in preserving the operational status of all underground structures.

[1]This paper is in process and to be submitted in tunnelling conference

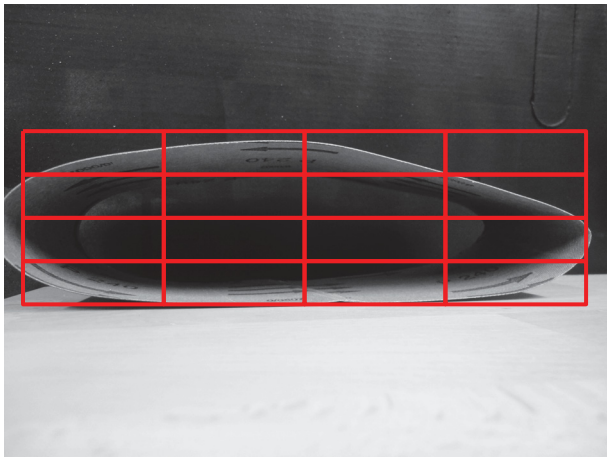

Figure 1: Test tunnel before deformation

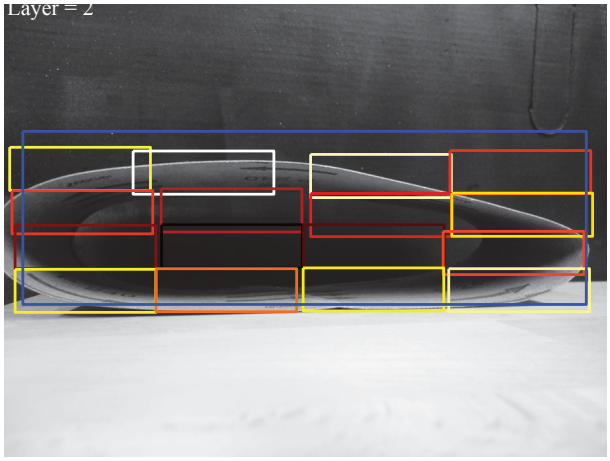

Figure 2: Test tunnel after deformation.

.

2 Introduction

Tunnel inspection by machine vision could be studied in the papers,i.e, [5] [7] [6] [8]. To find the deformation in the tunnels methods are used differently by different researchers ,i.e, holography, spot center tracking, grid tracking, spectral method and Fourier transformation of the grid pattern. There are many advantages of these methods against the measurement by some mechanical instruments, of those the most important is the reliability and accuracy of the measurements. Moreover the simplicity of the procedure is also valuable. In order to find displacement, movement of each grid block is followed on the test specimen from frame to frame.

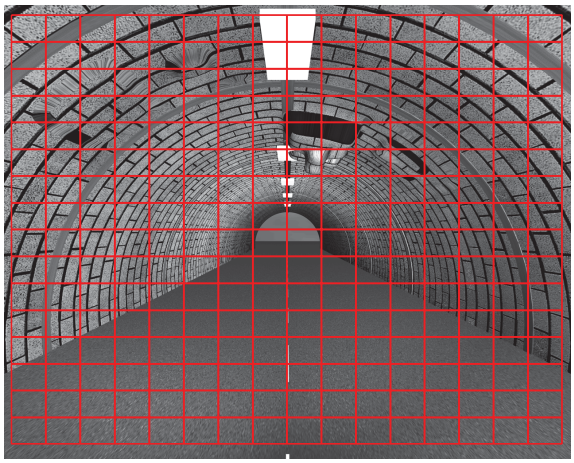

Figure 3: Tunnel before distortion.

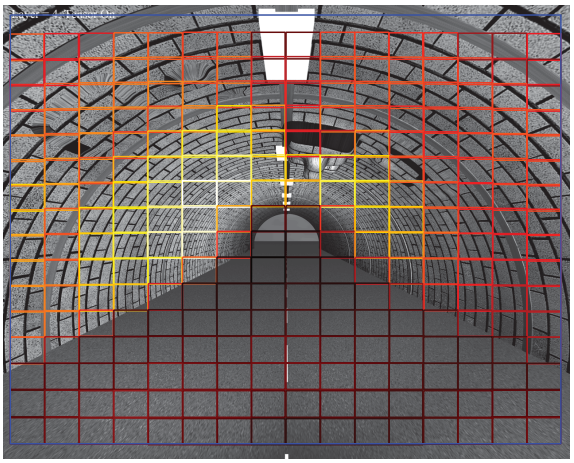

Figure 4: Tunnel registered after distortion.

.

All these strain measurement methods are direct observation of the grid patterns or positions of spots in the data images stored during the test process. These approaches need more attention and time to process. Also the grid lines may disappear during the test

process. A low cost machine vision system is required to increase the accuracy and decrease processing time. A new method is introduced for the measurement of the strain of an object, in which no marking of grid lines, grid spots or laser pointer is need as a pre-process of the test sample.

The main contributions of this paper are:

1. tunnel inspection by non-rigid registration has been presented;
2. on line tunnel inspection could be carried out without stoping the road traffic;
3. a simple method has been proposed for tunnel inspection ;
4. the method is robust to noise and ambient lighting;
5. a significant speed improvement has been achieved.
6. results are presented which demonstrate the functionality of the complete non-rigid registration method.

3 Experimental Setup

A panoramic vision system is introduced in [3] that improves the geotechnical data acquisition and analysis at tunnel construction sites. It consists of two rotating colour CCD line-scan cameras in a stereoscopic arrangement and software components that allow different kinds of image analyses. The system can acquire panoramic images up to 360 angular coverage with 27000x6000 pixels. A radiometric calibration procedure ensures high image quality. The special image formation is described by a mathematical sensor model leading to a geometrical camera calibration. The cameras are absolutely oriented in relation to the tunnel, thus enabling three-dimensional (3D) measurements from the images. The image analyses can be performed directly at the tunnel site and are separated into: (i) interactive annotations on single images supported by (ii) an interactive binocular vision system that allows a 3D navigation through a virtual tunnel face model, (iii) automatic edge extraction from single images, (iv) automatic 3D surface reconstruction; (v) by overlaying the resulting 2D discontinuity maps from (i) or (iii) onto the reconstructed surface from (iv) brings the structural data into 3D. Besides, the system delivers comprehensive documentations of a rock mass.

3.1 Calibration of the setup

An accurate calibration of the external and internal parameters of the system is required, if the displacement measurement is needed in millimeters. Determination of the projection matrices is the main idea from calibration of a system. Fauster et al. in [2] described in detail the evaluation and calibration method for the video-extensometer. In which a calibration target with a grid of bore is used, where the center positions of all bores are

known with in a planar real-world coordinate frame. The authors will follow the same method to calibrate the system.

3.2 Displacement Measurements

This method is based on the quad-tree structure, for which the indices of the grid are known. By subtracting the old indices position from the new one the distortion map is obtained. A detail description has been given in [1] for the distortion mapping. The same method is followed to find the strain distribution in the x and y directions.

$$s_x(u,v) = \nabla_x(u,v) - \nabla_x^*(u,v) \tag{1}$$

$$s_y(u,v) = \nabla_y(u,v) - \nabla_y^*(u,v) \tag{2}$$

After solving the displacement components, the field of the strain is evaluated by numerical matrix algebra. Harker and O'Leary [4] solved the surface reconstruction by a matrix based approach; by the derivative matrices of proper size, D_x and D_y, the partial derivatives of a surface Z are given as

$$\frac{\partial Z}{\partial x} = Z D_x^T \tag{3}$$

$$\frac{\partial Z}{\partial y} = D_y Z \tag{4}$$

The above equations give us the approximate strain distribution(ε_{xx},ε_{yy}) at any point in the deformed surface.

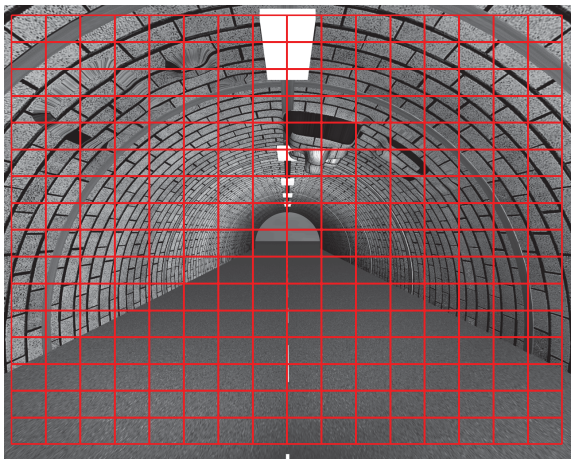

Figure 5: Tunnel before distortion.

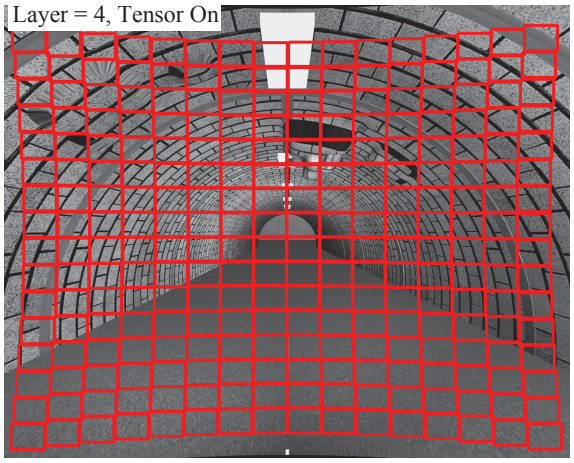

Figure 6: Tunnel registered after distortion.

.

4 Conclusions

The above proposed method provides a new and efficient method for the tunnel inspection. Complete shutdown of the tunnel is required for the tunnel observation, used by the previous methods. The time for the process is saved on one side, the efficiency is also improved. The exact place of the distortion could be pointed out where the rocks changes their position.

References

[1] S Barone, M Berghini, and L Bertini. Grid pattern for in-plane strain measurements by digital image processing. *The Journal of Strain Analysis for Engineering Design*, 36(1):51–59, 2001.

[2] Fauster. Ewald, Schalk. Peter, and Tratnig. Mark. Calibration method for light sectioning measurement systems. *2nd WSEAS International Conference on Signal Speech and Image Processing ICOSSIP 2002 WSEAS Press Skiathos Greece*, pages 1891–1898, 2002.

[3] Andreas Gaich, Alfred Fasching, and Wulf Schubert. Geotechnical data collection supported by computer vision. *EUROCH Conference Finland*, 36(1):65–70, 2001.

[4] Matthew Harker and Paul O'Leary. Least squares surface reconstruction from measured gradient fields. In *Computer Vision and Pattern Recognition*, 23-28 June, Anchorage, AK.

[5] Michael J. Kavvadas. Monitoring ground deformation in tunnelling current practice in transportation tunnels. *Engineering Geology*, 79(1-2):93– 113, 2005.

[6] X. Pan, T. J. Ellis, and T. A. Clarke. Robust tracking of circular features. In *Proceedings of the 6th British conference on Machine vision (Vol. 2)*, BMVC '95, pages 553–562, Surrey, UK, UK, 1995. BMVA Press.

[7] Masato UKAI. Advanced inspection system of tunnel wall deformation using image processing. *Quarterly Report of RTRI*, 48(2):94–98, 2007.

[8] Fenghui Yao., Guifeng Shao., Ryoichi Takaue., and Akikazu Tamaki. Automatic concrete tunnel inspection robot system. *Advanced Robotics*, 17(4):319–337, 2003.

Chapter 9

Conclusions and Future Work

9.1 Contributions of the Thesis

This work has presented a novel approach to non-rigid or elastic registration. It has been shown that consistent decimation during hierarchical subdivision enables non-rigid registration of two images. In particular the use of Gram polynomial basis is more suitable than the Fourier basis for this task. This results from the general nature of the image data. Gradients in images do not result in a Gibbs error when polynomial bases are used during decimation. Further more a new solution to non-rigid elastic registration of hyper spectral data has been presented. The method has been applied to hyper spectral data for which the other methods i.e. Fourier decimation and Gram basis globally has been failed to register. The use of global versus local polynomial approximation is a trade off between noise suppression and Gibbs error. Local polynomial approximation offers a successful method of implementing simultaneous filtering and image decimation as required for multi-resolution pyramids. It has been demonstrated on real data that the modified normalized phase correlation procedure performs better than past Fourier methods. Modified Fourier basis functions implemented by projection onto the orthogonal complement of a truncated Gram polynomial basis are presented. The modified functions are used to compute spectra whereby the Gibbs error associated with local gradients in the image are reduced. This improves the statistical consistency across the subdivision tree. The improvement associated with this method are demonstrated for a one dimensional and two dimensional data set.

9.2 Open Problems

There are some practical and theoretical issues that need to be addressed. The concept of local polynomial approximation for decimation was introduced. The use of Savitzky-Golay type smoothing for decimation requires further investigation. In particular, there are still no clear rules for the selection of the support length a tradeoff between local features and noise suppression — and degree of approximation, i.e., the number of bases functions used.

The analysis of the registration of the present approach is rather bounded to cartesian coordinate system. Much remains to be done in this regard, especially when applying in polar coordinate. Images with different type of distortion i.e. rigid, non-rigid and elastic, are registered successfully. The method is tested only in cartesian coordinate system. Additional work will be required to adapt the current procedure to suit for both cartesian and polar coordinate system both. Which will be a generalized system of registration.

References

[1] A. Andronache, M. von Siebenthal, G. Szekely, and Ph. Cattin. Non-rigid registration of multi-modal images using both mutual information and cross-correlation. *Medical Image Analysis*, 12(1):3–15,, 2008.

[2] A. Badshah, P. O'Leary, M. Harker, and C. Sallinger. Non-rigid registration for qualitiy control of printed materials. In *10th SPIE International Conference on Quality Control by Artificial Vision (QCAV)*, Saint-Etienne, France, June 2011.

[3] Amir Badshah, Paul O'Leary, and Matthew Harker. Gram polynomial image decimation and its application to non-rigid registration. volume 7877, pages 787–707. SPIE, 2011.

[4] R.W Barnard, G Dahlquist, K Pearce, L Reichel, and K.C Richards. Gram polynomials and the kummer function. *Journal of Approximation Theory*, 94(1):128 – 143, 1998.

[5] S Barone, M Berghini, and L Bertini. Grid pattern for in-plane strain measurements by digital image processing. *The Journal of Strain Analysis for Engineering Design*, 36(1):51–59, 2001.

[6] John Boyd. *Chebyschev and Fourier Spectral Methods*. Dover Publications Inc., Mineola, New York, 2001.

[7] C. Canuto, M. Y. Hussaini, A. Quarteroni, and T. A. Zang. *Spectral methods in Fluid Dynamics*. Springer-Verlag, 1988.

[8] Laurent Demaret, Laurent Demaret, Armin Iske, and Armin Iske. Scattered data coding in digital image compression. In *in Curve and Surface Fitting: Saint-Malo 2002*, pages 107–117. Nashboro Press, 2002.

[9] H. Dirilten and T. G. Newman. Pattern matching under affine transformations. *IEEE Trans. Comput.*, 26:314–317, March 1977.

[10] Kroon Dirk Jan. http:www.mathworks.com. May 2008.

[11] Sahibsingh A. Dudani, Kenneth J. Breeding, and Robert B. McGhee. Aircraft identification by moment invariants. *IEEE Trans. Comput.*, 26:39–46, January 1977.

[12] Murray. Eden, Michael. Unser, and Riccardo Leonardi. Polynomial representation of pictures. *Signal Processing*, 10:385–393, 1986.

[13] Fauster. Ewald, Schalk. Peter, and Tratnig. Mark. Calibration method for light sectioning measurement systems. *2nd WSEAS International Conference on Signal Speech and Image Processing ICOSSIP 2002 WSEAS Press Skiathos Greece*, pages 1891–1898, 2002.

[14] Bernd Fischer, Benoit M.Dawant, and Cristian Lorenz. Biomedical image registration 4th international workshop, WBIR 2010, Lübeck, July 11-13, proceedings. In *Image Processing, Computer Vision, Pattern Recognition, and Graphics*, volume 6204 of *Lecture Notes in Computer Science*, page Approx. 280 p.

[15] G. Forsythe. Generation and use of orthogonal polynomials for data-fitting with a digital computer. *Journal of the Society for Industrial and Applied Mathematics*, 5(2):74–88, 1957.

[16] Andreas Gaich, Alfred Fasching, and Wulf Schubert. Geotechnical data collection supported by computer vision. *EUROCH Conference Finland*, 36(1):65–70, 2001.

[17] E. Gladilin, V. Pekar, K. Rohr, and H. S. Stiehl. A comparison between BEM and FEM for elastic registration of medical images. *Image and Vision Computing*, 24(4):375–379, April 2006.

[18] Gene H. Golub and Charles F. Van Loan. *Matrix computations (3rd ed.)*. Johns Hopkins University Press, Baltimore, MD, USA, 1996.

[19] Ardeshir Goshtasby. Image registration by local approximation methods. *Image Vision Comput.*, 6(4):255–261, 1988.

[20] Ardeshir Goshtasby. Registration of images with geometric distortion. *IEEE Trans. on Geosciences and Remote Sensing*, 26(1):60–64, 1988.

[21] D. Gottlieb and J. S. Hesthaven. Spectral methods for hyperbolic problems. *Journal of Computational and Applied Mathematics*, 128(1-2):83–131, 2001.

[22] J. Gram. Uber die entwickelung reeler functionen in reihen mittest der methode der kleinsten quadrate,. In *jOURNAL FR DIE REINE UND ANGEWANDTE mATHEMATIK;*, volume 94, pages 41–73., 1883.

[23] R. Gray. Toeplitz and circulant matrices: A review, 1977.

[24] R. W. Hamming. *Digital filters (3rd ed.)*. Prentice Hall International Ltd., Hertfordshire, UK, 1989.

[25] Matthew Harker and Paul O'Leary. Least-squares polynomial approximation for the reduction of frequency spreading and gibbs error in fourier analysis. *Submitted for publication to: IEEE TIM*, Feb 2012.

[26] Martin Held, Werner Weiser, and Franz Wilhelmsttter. Fully automatic elastic registration of MR images with statistical feature extraction. *Journal of WSCG*, 12:153–160, 2004.

[27] Roger Horn and Charles R. Johnson. *Topics in matrix analysis*. Cambridge University Press, Cambridge, 1991.

[28] Khalid Hosny. Exact Legendre moment computation for gray level images. *Pattern Recognition*, doi:10.1016/j.patcog.2007.04.014, 2007.

[29] Ming-Kuei Hu. Visual pattern recognition by moment invariants. *IEEE Transactions on Information Theory*, 8(2):179–187, February 1962.

[30] O. Hunt and R. Mukundan. A comparison of discrete orthogonal basis functions for image compression. In *In Proc. of Conf. on Image and Vision Computing IVCNZ04 New Zealand*, pages 53–58, 2004.

[31] Atsushi Imiya. Formal polynomials for image processing. volume 101 of *Advances in Imaging and Electron Physics*, pages 99 – 142. Elsevier, 1997.

[32] Anil K. Jain, Mrio Figueiredo, and Josiane Zerubia. Energy minimization methods in computer vision and pattern recognition. *Springer*, (1), 2001.

[33] Abdul Jerri. *The Gibbs Phenomenon in Fourier Analysis, Splines and Wavelet Approximations*. Kluver Academic Publishers, Dordrecht, Netherlands, 1998.

[34] E. Kofidis and P. Regalia. Tensor approximation and signal processing applications. In *in AMS Conf. on Structured Matrices in Operator theory, Numerical Analysis, Control, Signal and Image Processing*, 2000.

[35] E. Kofidis and P. A. Regalia. Tensor approximation and signal processing applications. *Structured Matrices in Mathematics, Computer Science, and Engineering I, V. Olshevsky (Ed.), Contemporary Mathematics Series, American Mathematical Society.*, 2001.

[36] Tamara G. Kolda and Brett W. Bader. Tensor Decompositions and Applications. *SIAM Review*, 51(3):455–500, 2009.

[37] P.J. Kostelec, J.B. Weaver, and D.M. Healy Jr. Multiresolution elastic image registration. *Medical physics*, 19(1-2):1593–1604,, 1998.

[38] L. Kotoulas and I. Andreadis. Image analysis using moments. *5th Int. Conf. on Technology and Automation, Thessaloniki, Greece,.*, pages 360–364, 2005.

[39] Hava Lester and Simon R. Arridge. A survey of hierarchical non-linear medical image registration. *Pattern Recognition society*, 32:129 – 149, 1999.

[40] B. Likar and F. Pernu. A hierarchical approach to elastic registration based on mutual information. *Image and Vision Computing*, 19(1-2):33 – 44, 2001.

[41] Tony Lindeberg. Scale-space theory: a basic tool for analyzing structures at different scales. *Journal of Applied Statistics*, 21:225–270, 1994.

[42] Huafeng Liu and Pengcheng Shi. Meshfree particle method. In *Proceedings of the Ninth IEEE International Conference on Computer Vision - Volume 2*, ICCV '03, pages 289–, Washington, DC, USA, 2003. IEEE Computer Society.

[43] C Loan. The ubiquitous kronecker product. *Journal of Computational and Applied Mathematics*, 123(1-2):85–100, 2000.

[44] P. Meer and I. Weiss. Smoothed differentiation filters for images. In *IEEE I10th International Conference on Pattern Recognition*, volume 2, June 1990, page 121..126, Atlantic City, NJ, USA, 1990.

[45] M. Mellor and M. Brady. Non-rigid multimodal image registration using local phase. *MICCAI. LNCS*, 3216:789–796, 2004.

[46] R Mukundan. Some computational aspects of discrete orthonormal moments. *IEEE Transactions on Image Processing*, 13(8):1055–1059, 2004.

[47] R Mukundan. Transform coding using discrete tchebichef polynomials. In *UProc. Intnl. Conf. on Visualization Imaging and Image Processing VIIP*, pages 270–275., Aug 2006.

[48] R. Mukundan, S. Ong, and P. Lee. Image analysis by Tchebichef moments. *IEEE Transactions on Image Processing*, 10(9):1357–1363, 2001.

[49] R Mukundan, S H Ong, and P A Lee. Image analysis by tchebichef moments. *IEEE Transactions on Image Processing*, (9):1357–1364, 2001.

[50] P. O'Leary and M. Harker. Discrete polynomial moments and savitzky-golay smoothing. In *World Academy of Science, Engineering and Technology 2010*, 2010.

[51] Paul O'Leary and Matthew Harker. An algebraic framework for discrete basis functions in computer vision. *Indian Conference on Computer Vision, Graphics and Image Processing*, 0:150–157, 2008.

[52] Paul O'Leary and Matthew Harker. Discrete polynomial moments for real-time geometric surface inspection. *Journal of Electronic Imaging*, 18(1):013015, 2009.

[53] Paul O'Leary and Matthew Harker. Polynomial approximation: An alternative to windowing in fourier analysis. *Instrumentation and Measurement Technology Conference (I2MTC), 2011 IEEE*, pages 1–6, May 2011.

[54] J A Parker, R V Kenyon, and D E Troxel. Comparison of interpolation methods for image resampling. *IEEE Transactions on Medical Imaging*, 2(1):31–39, 1983.

[55] S. Periaswamy and H. Farid. Elastic registration in the presence of intensity variations. *Medical Imaging, IEEE Transactions on*, 22(7), July 2003.

[56] A. Savitzky and M. Golay. Smoothing and differentiation of data by simplified least squares procedures. *Analytical Chemistry*, 36 (8):1627–1639, 1964.

[57] F. W. Smith and M. H. Wright. Automatic ship photo interpretation by the method of moments. *IEEE Trans. Comput.*, 20:1089–1095, September 1971.

[58] E. Suarez, J. A. Santana, Eduardo Rovaris, C.-F.Westin, and J. Ruiz-Alzola. Fast entropy-based nonrigid registration. In *Computer Aided Systems Theory (EUROCAST'03), Lecture Notes in Computer Science 2809*, pages 607–615. Springer Verlag, February 24–28 2003.

[59] Eduardo Suarez, Carl-Fredrik Westin, Eduardo Rovaris, and Juan Ruiz-Alzola. Nonrigid registration using regularized matching weighted by local structure. In *Medical Image Computing and Computer-Assisted Intervention MICCAI 2002*, volume 2489 of *Lecture Notes in Computer Science*, pages 581–589. 2002.

[60] M.R Teague. Image analysis via the general theory of moments. Technical report, 1980.

[61] Panagiotis Tsanakas. Algorithms and data structures for hierarchical image processing. In *Master Thesis, ohio university*, 1985.

[62] C. F. van Loan. The ubiquitous Kronecker product. *Journal of Computational and Applied Mathematics*, 123:85–100, 2000.

[63] Gregory K. Wallace. The jpeg still picture compression standard. *Commun. ACM*, 34:30–44, April 1991.

[64] Yongmei Wang and Lawrence H. Staib. Physical model-based non-rigid registration incorporating statistical shape information. *Medical Image Analysis*, 1:35–51, 2000.

[65] Andrew P. Witkin. Scale-space filtering. In *Proceedings of the Eighth international joint conference on Artificial intelligence - Volume 2*, pages 1019–1022, San Francisco, CA, USA, 1983. Morgan Kaufmann Publishers Inc.

[66] G. Wollny and F. Kruggel. Computational cost of nonrigid registration algorithms based on fluid dynamics [MRI time series application]. *Medical Imaging, IEEE Transactions on*, 21(8):946–952, 2002.

[67] Robert Y. Wong and Ernest L. Hall. Scene matching with invariant moments. *Computer Graphics and Image Processing*, 8(1):16 – 24, 1978.

[68] Qing Wu, Tian Xia, Chun Chen, Hsueh-Yi Sean Lin, Hongcheng Wang, and Yizhou Yu. Hierarchical tensor approximation of multi-dimensional visual data. *IEEE Transactions on Visualization and Computer Graphics*, 14:186–199, January 2008.

[69] Jun Xu, Lei Yang, and Dapeng Wu. Ripplet: A new transform for image processing. *J. Vis. Comun. Image Represent.*, 21:627–639, October 2010.

[70] G.Y. Yang, H.Z. Shu, G.N. C. Han, and L.M. Luo. Efficient Legendre moment computation for grey level images. *Pattern Recognition*, 39:74–80, 2006.

[71] Pew-Thian Yap and Raveendran Paramesran. An efficient method for the computation of legendre moments. *IEEE Transactions on Pattern Analysis and Machine Intelligence*, 27:1996–2002, 2005.

[72] Pew-Thian Yap and Paramesran Raveendren. Image analysis by Krawtchouk moments. *IEEE Transactions on Image Processing*, 12(11):1367–1377, 2003.

[73] Xie Zhiyong and Gerald E. Farin. Image registration using hierarchical b-splines. *IEEE Transactions on Visualization and Computer Graphics*, 10(1):85–94, 2004.

[74] Bin Zhou, Zhao-Yan Li, Guang-Ren Duan, and Yong Wang. Weighted least squares solutions to general coupled sylvester matrix equations. *J. Comput. Appl. Math.*, 224:759–776, February 2009.

[75] Barbara Zitov and Jan Flusser. Image registration methods: a survey. *Image and Vision Computing*, 21:977–1000, 2003.